Contents

Chapter 1

Atomic Structure and B-splines

1.1 Introduction

In its general form the problem of the determination of the eigenstates of a many-electron atom with atomic number Z is impossible without drastic, physically justified approximations. Present day quantum mechanical theory offers the machinery and the mathematical formulation for the systematic and rigorous analysis of phenomena occurring at the atomic level. The calculation and understanding of atomic observables are simplified considerably through a sequence of approximations. The task of finding suitable approximations for the problem at hand is by itself part of the art, guided by physical intuition as well as experience. The definitive criterion for the succes, of a method, is the comparison with experimental observations. Although, from the point of view of physics, many methods have been suggested and implemented succesfully, the computational part of each method will be in continous in development taking the full advantage of evolution of the modern computer hard- and software.

1.2 Many-Electron Atomic Systems

Since the basic constituents of the nucleus (neutron and proton) are much heavier than the electron (ratio $\sim 10^{-3}$) and the volume occupied by the nucleus is much smaller than that of the electronic cloud (ratio $\sim 10^{-5}$), considered the nucleus of the atom can be considered infinitely massive and motionless. Interacting with the orbital electrons through a static Coulomb

potential ($\sim Ze^2/r^2$). The nucleus has a finite volume, in size and shape, intimately connected with its charge distribution. The static Coulombic approximation of the nucleus-electrons interaction is adequate only for light atoms where the electron velocities are low ($\sim Z\alpha c \ll c$), with α being the fine stucture constant ($\sim 1/137$). In this limit the radiation part of the interaction is neglected. For the same reasons, we also approximate the electron-electron interaction with the static Coulomb part ($\sim e^2/r_{ij}$), where r_{ij} is the distance between the i-th and j-th electron.

For an N-electron atom, the Hamiltonian is written as[1]:

$$H = \sum_{i=1}^{N} h_i(\mathbf{r}_i) + \sum_{i<j}^{N} g(\mathbf{r}_i, \mathbf{r}_j)\,, \tag{1.1}$$

where $h_i(\mathbf{r_i}) = T(\mathbf{p}_i) - Z/r_i$ is the one-particle Hamiltonian operator for the motion of a single electron in the field of a nucleus of charge Z, located at the origin of the coordinate system and $T(\mathbf{p}_i)$ is the kinetic energy operator[2],

$$T(\mathbf{p}_i) = \begin{cases} \mathbf{p}_i^2/2, & \text{Schrödinger} \\ c\alpha_i \mathbf{p}_i + \beta_i c^2, & \text{Dirac} \end{cases} \tag{1.2}$$

where $\mathbf{p_i}$ is the momentum of the i-electron and $\alpha_\mathbf{i}, \beta_i$ are operators connected with the spin of the i-electron (see equation (1.8)). The two-particle operator $g(\mathbf{r}_i, \mathbf{r}_j)$ represents the interaction energy of a pair of electrons, which reads:

$$g(\mathbf{r}_i, \mathbf{r}_j) = \begin{cases} 1/r_{ij} & \text{Schrödinger}\,, \\ 1/r_{ij} + B(\mathbf{r}_i, \mathbf{r}_j), & \text{Dirac} \end{cases} \tag{1.3}$$

with $B(\mathbf{r}_i, \mathbf{r}_j)$ being the Breit interaction representing the spin-spin interaction between two electrons [68]. The Dirac Hamiltonian $h_D(\mathbf{r}) \equiv c\alpha\mathbf{p} + \beta c^2 - Z/r$ through a perturbation expansion of α^2 leads to the

[1] Note that in general $Z \neq N$ except for the case of neutral atoms.

[2] In nonrelativistic quantum mechanics, the notion of the potential is introduced in order to represent the interaction between the particles. This allows the use of the potential in conjunction with the Schrödinger equation. On the other hand, in the relativistic quantum theory the number of particles is not conserved, and interactions arise from the exchange of quanta. Therefore, a consistent relativistic theory of the atomic structure requires the formalism of second quantization. However, an effective potential representing the interactions, can be constructed by taking the Fourier transform of the lowest-order interaction matrix elements (page 258 [68]). In that sense, the present Hamiltonian should be understood as a model Hamiltonian, sufficient for most purposes in relativistic atomic stucture calculations.

Schrödinger Hamiltonian $h_S(\mathbf{r}) \equiv \mathbf{p}^2/2 - Z/r$ plus the relativistic corrections in first order of α^2.

$$h_D - c^2 \rightarrow h_S + \alpha^2 \left[\frac{Z}{r^3}\mathbf{ls} - p^4/4 - \frac{Z}{4}\nabla^2(1/r)\right] + O(\alpha^4). \qquad (1.4)$$

The Schrödinger Hamiltonian therefore neglects terms of the order[3] $\sim \alpha^2 Z^4$ such as, the spin-orbit interaction $V_{so} = \alpha^2(Z/r^3)\mathbf{ls}$, the mass correction $V_m = -\alpha^2 p^4/4$ and the Darwin interaction $V_d = -\alpha^2 Z\nabla^2(1/r)/4$.

One-electron Schrödinger Equation. Concentrating now to the non-relativistic equation, $H_S\phi(\mathbf{r}) = \varepsilon\phi(\mathbf{r})$, where $H_S \equiv \mathbf{p}^2/2 + U(r)$ and noting that it represents the motion of an electron in a central field, the eigenstates $\phi(\mathbf{r})$ (omitting the subscript i) are written in terms of spherical harmonics,

$$\phi_{nlmm_s}(\mathbf{r}) = \frac{1}{r}P_{nl}(r)Y_{lm}(\theta,\phi)\sigma(m_s)\,, \qquad (1.5)$$

where Y_{lm} are the spherical harmonics as defined in [69], thus satisfying the eigenvalue equations $\mathbf{l}^2 Y_{lm} = l(l+1)Y_{lm}$, $l_z Y_{lm} = mY_{lm}$ and the orthonormality condition $\int d\Omega_r Y^*_{lm} Y_{l'm'} = \delta_{ll'}\delta_{mm'}$. The spin-1/2 eigenfunctions σ_{m_s} satisfy the eigenvalue equations, $\mathbf{S}^2\sigma(m_s) = (3/4)\sigma(m_s)$ and $S_z\sigma(m_s) = m_s\sigma(m_s)$. The radial functions P_{nl}, which satisfy the boundary conditions $P_{nl}(r \rightarrow 0, \infty) \rightarrow 0$, and the energy eigenvalues ε_{nl} are the unknown quantities to be determined. Indexing by n should be understood as involving discrete and continuous energy eigenvalues of the equation. Since $H_S = \mathbf{p}^2/2 + U(r) = r^{-1}\partial^2(r)/\partial r^2 - \mathbf{l}^2/2r^2 + U(r)$ the Schrödinger equation leads to the following radial equation for the $P_l(r)$ functions :

$$-\frac{d^2P_l}{dr} + \left(U(r) + \frac{\hbar^2 l(l+1)}{r^2}\right)P_l(r) = \varepsilon_l P_l(r). \qquad (1.6)$$

One-electron Dirac Equation. The field-free Dirac Hamiltonian is of the type:

$$H_D = c\alpha\mathbf{p} + \beta mc^2 + U(r) \qquad (1.7)$$

where the α, β matrices are defined by:

$$\alpha = \begin{bmatrix} 0 & \sigma \\ \sigma & 0 \end{bmatrix}, \qquad \beta = \begin{bmatrix} 1 & 0 \\ 0 & -1 \end{bmatrix}, \qquad (1.8)$$

[3]Other first-order terms of α^2, scaling as $\alpha^2 Z^3$, come from the two-particle Dirac operator $g_D(\mathbf{r}_i, \mathbf{r}_i) = 1/r_{ij} + B(\mathbf{r}_i, \mathbf{r}_j)$ [35]

and σ is the 2×2 Pauli matrix and $\mathbf{1}$ the diagonal matrix. Since we are dealing with isolated atoms the static potential 'seen' by the electron has spherical symmetry and is t a function therefore only of the distance of the electron from the nucleus. The potential $U(r)$ is of the type $U(r) = -Ze^2/r + V(r)$, with $-Ze^2/r$ being the nuclear potential and $V(r)$ the 'screening' potential which is either a model potential or a Dirac-Fock potential determined self-consistenly.

The time-independent Dirac equation is written as:

$$H_D\psi_E(\mathbf{r}) = E\psi_E(\mathbf{r}), \tag{1.9}$$

where $\psi_E(\mathbf{r}), E$ are the eigenfunctions and the respective eigenenergies. Note that the wavefunction $\psi_E(\mathbf{r})$ is a four-component vector $\psi^\dagger = (\psi_1^\star, \psi_2^\star, \psi_3^\star, \psi_4^\star) = (\psi_A^\dagger, \psi_B^\dagger)$. The Hamiltonian H_D commutes with the total angular momentum defined by $\mathbf{j} = \mathbf{l} + \mathbf{s}$ with $\mathbf{l}$ being the orbital angular momentum and $\mathbf{s}$ the spin of the electron. The Hamiltonian of the atom commutes also with the z-component of $\mathbf{j}$. It is then possible to write the eigenfunction in a $\mathbf{j}^2$ form as :

$$\psi_{k_i m_{j_i}}(\hat{\mathbf{r}}) = \frac{1}{r}\begin{bmatrix} iG_{k_i}(r)\chi_{k_i m_{j_i}}(\hat{\mathbf{r}}) \\ F_{k_i}(r)\chi_{-k_i m_{j_i}}(\hat{\mathbf{r}}) \end{bmatrix} \tag{1.10}$$

where χ_{km_j} are the 2×2 spinors defined in terms of the Glebsch-Gordan coefficients and the spherical Harmonics. The quantum numbers k and m_j have their origin to the eigenvalue equations of the operators $\mathcal{K} = -2\mathbf{ls} - \mathbf{1}$ and J_z. The quantum number k is the relativistic analog of the l quantum number in the classification of the states in the Schrödinger approximation. Knowledge of k is therefore equivalent to knowledge of the quantum nubers j, l of the $\mathbf{j}^2, \mathbf{l}^2$ operators.

Keeping in mind the above relations, and with the help of the orthonormality condition $\int d\Omega_r \chi^\dagger_{km_j}\chi_{k'm'_j} = \delta_{kk'}\delta_{mm'}$, the 3-D Dirac equation can be reduced to an one-dimensional radial eigenvalue equation, from the solution of which, we can determine the radial wavefunctions and the corresponding eigenenergies:

$$h_D(r)\mathbf{u}_\varepsilon(r) = \varepsilon\mathbf{u}_\varepsilon(r) \qquad \mathbf{u} = \begin{bmatrix} G(r) \\ F(r) \end{bmatrix} \tag{1.11}$$

with $\varepsilon = E - mc^2$ the 'transformed' energy and h_D given by:

$$h_D(r) = \begin{bmatrix} U(r) & \hbar c\left(-\frac{d}{dr} + \frac{k}{r}\right) \\ \hbar c\left(\frac{d}{dr} + \frac{k}{r}\right) & -2mc^2 + U(r) \end{bmatrix} \tag{1.12}$$

The above radial equations including the boundary conditions for the $G(r), F(r)$ at the points $r = 0$ and $r = \infty$ and the orthonormality condition, $\int_0^\infty dr\,[G_{nk}(r)G_{n'k}(r) + F_{nk}(r)F_{n'k}(r)] = \delta_{nn'}$ are solved numerically for the determination of the radial functions $G(r), F(r)$.

Central field approximation[4]. One of the most succesful methods for the solution of the eigenvalue equation $H\,\Psi(\mathbf{r}_1, \mathbf{r}_2, ..\mathbf{r}_N) = E\,\Psi(\mathbf{r}_1, \mathbf{r}_2, ..\mathbf{r}_N)$ is the central field approximation originally proposed by Hartree and Slater. This is based on an independent particle model, where each electron moves in an effective potential representing the attractive nuclear potential and the repulsive interaction originating from the remaining N-1 electrons. Hamiltonian (1.1) is written as :

$$\begin{aligned} H &= H_0 + H_p = \sum_i^N H(\mathbf{r}_i) + H_p \\ &= \underbrace{\sum_{i=1}^N [T(\mathbf{p}_i) + U(r_i)]}_{H_0} + \underbrace{\sum_{i=1}^N \left[-U(r_i) - \frac{Z}{r_i}\right] + \sum_{i<j}^N g(\mathbf{r}_i, \mathbf{r}_j)}_{H_p} \end{aligned} \quad (1.13)$$

At this stage, $H(\mathbf{r}_i) \equiv T(\mathbf{p}_i) + U(\mathbf{r}_i)$ is the one-electron Hamiltonian which stands for the independent motion of the electron in the "screened" potential $U(r)$ originating from nucleus-e and $(N-1)e - e$ interactions. The Hamiltonian H is written as a sum of the central field Hamiltonian H_0 and the "perturbative" H_p. The Hamiltonian H_p is treated as a perturbation since $\langle H_p \rangle \ll \langle H_0 \rangle$. Neglecting, the perturbative term H_p we must solve the eigenvalue equation $H_0\,\psi(\mathbf{r}_1, \mathbf{r}_2, ..., \mathbf{r}_N) = E_0\,\psi(\mathbf{r}_1, \mathbf{r}_2, ..., \mathbf{r}_N)$. The solution of that eigenvalue equation, $\psi(\mathbf{r}_1, \mathbf{r}_2, ..., \mathbf{r}_N)$, should be determined in combination with the Pauli exclusion principle. According to this principle the wavefunction of a system consisting of identical fermion particles (electrons in the present case) changes sign after the mutual commutation of any pair of electrons (spatial and spin) coordinates, $\psi(\mathbf{r}_1, .., \mathbf{r}_i, ...\mathbf{r}_j ...) = -\psi(\mathbf{r}_1, ..., \mathbf{r}_j, ...\mathbf{r}_i ....)$. The simplest wavefunction satisfying this principle is the Slater determinant given by:

$$\begin{aligned} \psi_s(\mathbf{r}_1, \mathbf{r}_2, ...\mathbf{r}_N) &= \mathcal{A}\psi(\mathbf{r}_1, \mathbf{r}_2, ...\mathbf{r}_N) \\ &= \frac{1}{\sqrt{N!}} \begin{vmatrix} \phi_\alpha(\mathbf{r}_1), & \phi_\beta(\mathbf{r}_1), & .., \phi_\nu(\mathbf{r}_1) \\ \phi_\alpha(\mathbf{r}_2), & \phi_\beta(\mathbf{r}_2), & .., \phi_\nu(\mathbf{r}_2) \\ ... & ... & ... \\ \phi_\alpha(\mathbf{r}_N), & \phi_\beta(\mathbf{r}_N), & .., \phi_\nu(\mathbf{r}_N) \end{vmatrix}, \end{aligned} \quad (1.14)$$

where, the states $\phi(\mathbf{r})$ are solutions of the one-electron eigenvalue equa-

tion, $H(\mathbf{r}_i)\phi(\mathbf{r}_i) = \varepsilon_i\phi(\mathbf{r}_i)$. $\mathcal{A}$ is the antisymmetrization operator and $s \equiv (\alpha, \beta, ..., \nu)$. Each of the $\alpha, \beta, ..., \nu$ specifies the quantum numbers[5] describing the one-electron orbitals.

Defining the total angular momentum of the N-electron atomic system as $\mathbf{L} = \sum \mathbf{l}_i = \sum \mathbf{r}_i \times \mathbf{p}_i$, it is straightforward to prove that the Hamiltonian H_0 commutes with $\mathbf{L}$ and $\mathbf{L}^2$. Also, since H_0 does not contain any spin-operators, it commutes with $\mathbf{S}$ and $\mathbf{S}^2$, where $\mathbf{S} = \sum \mathbf{s}_i$ is the total spin of the atomic system. At the same time, the obvious Hamiltonian invariance under the replacement $\mathbf{r} \to -\mathbf{r}$ suggests that the eigenstates have a well defined parity Π, the eigenvalue of the parity operator $\mathcal{P}$. From the above discussion, it follows that in general the eigenstates of the Hamiltonian H_0 labelled as $|E\,\Pi\,L\,S\,M_L\,M_S\rangle$ can be determined as simultaneous eigenstates of the $H, \mathcal{P}, \mathbf{L}^2, \mathbf{S}^2, L_z, S_z$ operators with eigenvalues E, $(-1)^{\sum l_i}$, $L(L+1)$, $S(S+1)$, M_L, M_S correspondigly, where l_i is the angular quantum number of the i-electron.

The wavefunction ψ_s (Slater determinant) is an eigenfunction of the operators H_0, L_z, S_z but not in general an eigenstate of the operators $\mathbf{L}^2, \mathbf{S}^2$. These functions are constructed by taking a suitable linear combination of Slater determinants ψ_{sl}, summing up over all magnetic quantum numbers [9] m_{l_i}, m_{s_i} for $i = 1, 2, ..N$.

$$\psi^{\Lambda} = \sum_{all\, m_l, m_s} C(m_l, m_s)\, \psi_0, \tag{1.15}$$

where $\Lambda \equiv (LSM_LM_S)$. A more detailed description of such a construction is presented in later sections, concerned with the description of two-electron atoms. The following sections present some theoretical approaches we have followed for the description of the atomic systems in combination with the finite basis method and the B-splines technique [23].

1.3 Schrödinger Equation and B-splines method.

Although the method we use has been presented in detail in [43, 9, 73] for various atoms like H,H^-,He etc.., for completeness and later reference we describe here the essentials of the method and emphasize specific subtle points in order to make clear the underlying physics clear.

Finite basis method. In this paragraph, we give a brief presentation of the finite basis method and its connection with the variatonal technique

[5] For the Schrödinger Hamiltonian these numbers are the (n, l, m_l, m_s) while for the Dirac Hamiltonian are the $(n, j, l, m_j) \equiv (n, k, m_j)$.

for the non-relativistic case. As a starting point consider the Hamiltonian H, the spectrum of which we are seeking to approximate. Consider also the wavefunctions $\psi^{(n)} = \sum_i^N c_i^{(n)} f_i$, with $i = 1, 2...N$ as the candidate eigenstates of H, in terms of an orthonormal set of functions $f_i, i = 1, 2...N$. The eigenvalue equation is $H\psi_n = \varepsilon_n \psi_n$ where n represents both bound ($\varepsilon_n \leq 0$) and continuum ($\varepsilon_n \geq 0$) solutions. The spectrum of H contains an infinitely number of bound states and a denumerable number of infinite extended in space states. Inserting the expansion for ψ_n in the eigenvalue equation for H, we obtain for the unknown coefficients $c_i^{(n)}$:

$$\sum_{i=1}^{N} c_i^{(n)} \left[H_{ij} - E^{(n)} \delta_{ij} \right] = 0 \qquad\qquad n = 1, 2...N \tag{1.16}$$

where $H_{ij} = \langle f_i | H | f_j \rangle$. We have used the property $\langle f_i | f_j \rangle = \delta_{ij}$ for f_i. The gain of the finite basis method is the transformation of the eigenvalue equation to a matrix eigenvalue problem through an approximation of the real Hamiltonian H with its "finite" matrix representation (H_{ij}). The accuracy of the method is intimately connected with the "size" of the basis in the sense that,

$$\mathbf{1} \approx \sum_{i=1}^{N} |\psi_i^{(n)}\rangle\langle\psi_i^{(n)}| \overset{N\to\infty}{\to} \mathbf{1}. \tag{1.17}$$

Diagonalization of the matrix (H_{ij}) in equation (1.16), results to N eigenvectors $c^{(n)}, n = 1, 2...N$ with the corresponding eigenvalues $E^{(n)}$. Each of these eigenvectors gives rise to a variatonal state through the relation $\psi^{(n)} = \sum_i^N c_i^{(n)} f_i$. The eigenvalues $E^{(n)}$, according to the Hylleraas-Undheim theorem [42], are upper bounds to the first N exact eigenvalues of H ($\varepsilon_n \leq E^{(n)}, n = 1, 2....N$). The equality is satisfied when N approaches infinity. As the final result of the above procedure, we have at hand a set of states $\psi^{(n)}, n = 1, 2...N$ which approximate the first N-exact eigenstates of H and the corresponding N energies (upper bound of the first N exact eigenenergies[6]).

The transformation of the infinite spectrum of H into a discretized pseudospectrum has as a consequence the transformation of the continuum integrals to a summation over the discrete states and energies i.e. $\int dE \psi^\star H \psi \approx \sum_n \psi_n^\star \hat{H} \psi_n$. This discrete representation of integrals has been

[6] In the relativistic limit, the Hamiltonian of the system is the Dirac operator H_D (equation (1.7)) and a generalization of the Hylleraas-Undheim is necessary [27]. This complication has its origin to the unbound nature of the spectrum of H_D from below ($\varepsilon_n \to \pm\infty$).

studied and understood [67] throughout the years and calculations relevant to this technique have proved to give very accurate results, depending on the choice of the basis-set ($\mathbf{L}^2$-expansions, STO, GTO, B-splines,Sturmian) and its size($\sim N$).

Action principle and SE in a box. One of the basic assumptions is that the atom is considered confined inside a sphere ("box") of radius R, with the boundary conditions at $r = 0$ and $r = R$ instead of $r = \infty$. Therefore the incorporation of the boundary conditions in the formalism should be achieved through a systematic procedure. We work with the action ($\mathcal{S}$) of an electron inside a central potential $U(r)$, where applying the variatonal principle $\delta\mathcal{S} = 0$, under certain constraints (i.e.$\delta P_l(0) = \delta P_l(0) = 0$) we obtain the differential equation for the radial wavefunction $P_l(r)$ functions. In quantum mechanics it is well-known that the time-dependent equation for the wavefunction of a quantum-mechanical system $\Psi(\mathbf{r}, t)$ can be derived, independently from the specific form of the Hamiltonian, through the Langragian formalism. To be more specific, the Langragian $\mathcal{L}$ of the system in the state Ψ is defined to be the quantity:

$$\mathcal{L}[\Psi] = \Psi^{\dagger}(i\partial_t - H)\Psi \tag{1.18}$$

with H the energy operator being the sum of kinetic and potential operators. Requiring the action $\mathcal{S}[\Psi] = \int dt d^3\mathbf{r}\mathcal{L}[\Psi]$ of the system to have an extremum ($\delta\mathcal{S}[\Psi] = 0$), we obtain the usual time-dependent Shrodinger equation. The above definitions are valid in general. In the case where the state function Ψ has only one component however, as in the non-relativistic limit, the Langragian is defined in analogy as $\mathcal{L}[\Psi] = \Psi^*(i\hbar\partial_t - H)\Psi$. For the time-independent case, the action of the system in the state ψ can be written as [46], $\mathcal{S}[\psi] = \int d^3\mathbf{r}\mathcal{L}[\psi] = \langle\psi|(\varepsilon - H)|\psi\rangle$. Here, we assume as H the Schrödinger Hamiltonian of an electron moving in a central potential $U(r)$ and ε the corresponding energy eigenvalue. The $\psi(\mathbf{r})$ wavefunction is written as $r^{-1}P_l(r)Y_{lm}(\theta, \phi)$ and the action is expressed now as :

$$\mathcal{S}[\psi] = \int d^3\mathbf{r}\psi^*(\mathbf{r}) \left[\varepsilon - \left(-\frac{\hbar^2}{2m}\nabla_{\mathbf{r}}{}^2 + U(r)\right)\right] \psi(\mathbf{r}). \tag{1.19}$$

Expanding the operator $\nabla^2_{\mathbf{r}}$ in spherical coordinates (r, θ, ϕ) and using the equation $\mathbf{L}^2 Y_{lm} = \hbar^2 l(l+1)Y_{lm}$ in combination with the orthonormality of the spherical harmonics we get $\langle\psi|\psi\rangle = \int_0^R dr P_l^2(r)$. Combining all of the above, we obtain for the action:

$$\mathcal{S}[P_l] = \frac{1}{2}\int_0^R dr \left\{\frac{1}{2}\left(\frac{dP_l}{dr}\right)^2 + \left[U(r) + \frac{\hbar^2 l(l+1)}{r^2}\right] P_l(r) - \varepsilon_l P_l^2(r)\right\}$$

$$- \quad \frac{1}{2}\left[P_l(R)P_l'(R) - P_l(0)P_l'(0)\right] \tag{1.20}$$

where $P_l'(r) = dP_l(r)/dr$. The last term of the right-hand-side (RHS) of equation (1.20) is the surface term which represents the effect of the finiteness of the space on the wavefunctions. Note here the mathematical meaning of the eigenvalue ε_l which plays the role of Langrage multiplier, in order to ensure the physical requirement of normalization. The variation of the action under small variation of the undetermined yet $P_l(r)$ is the following :

$$\begin{aligned} \delta\mathcal{S}\left[P_l\right] &= \frac{1}{2}\int_0^R dr \left\{ -\frac{d^2P_l}{dr} + \left[U(r) + \frac{\hbar^2 l(l+1)}{r^2}\right] P_l(r) - \varepsilon_l P_l(r) \right\} \\ &- \frac{1}{2}\left[\delta P_l(R)P_l'(R) - \delta P_l(0)P_l'(0)\right]. \end{aligned} \tag{1.21}$$

From the variatonal principle for the $\mathcal{S}$ with the constraints $\delta P_l(0) = \delta P_l(R) = 0$ we obtain the radial Schrödinger equation for the $P_l's$:

$$\left[-\frac{d^2P_l}{dr} + \left(U(r) + \frac{\hbar^2 l(l+1)}{r^2} \right) P_l(r) \right] = \varepsilon_l P_l(r). \tag{1.22}$$

ns	Analytical	B-splines
1	-0.5	-0.49999999999401
2	-0.125	-0.125
3	-0.05555555555556	-0.055555555555557
4	-0.03125	-0.03125
5	-0.02	-0.02
6	-0.01388888888889	-0.013888888888887
7	-0.01020408163265	-0.010204081566722
8	-0.00782125	-0.0078123810887326
9	-0.00617283950617	-0.0061572727152837
10	-0.005	-0.004760808277328
11	-0.004132231204096	-0.0031194774936659
12	-0.003472222222222	-0.0011044353071858

Table 1.1: Energies of the ns states of the Hydrogen, obtained with the Schödinger Hamiltonian H_S analytically and computationally. The B-splines parameter are, $k = 9, n = 200, R = 200a.u.$ and linear grid.

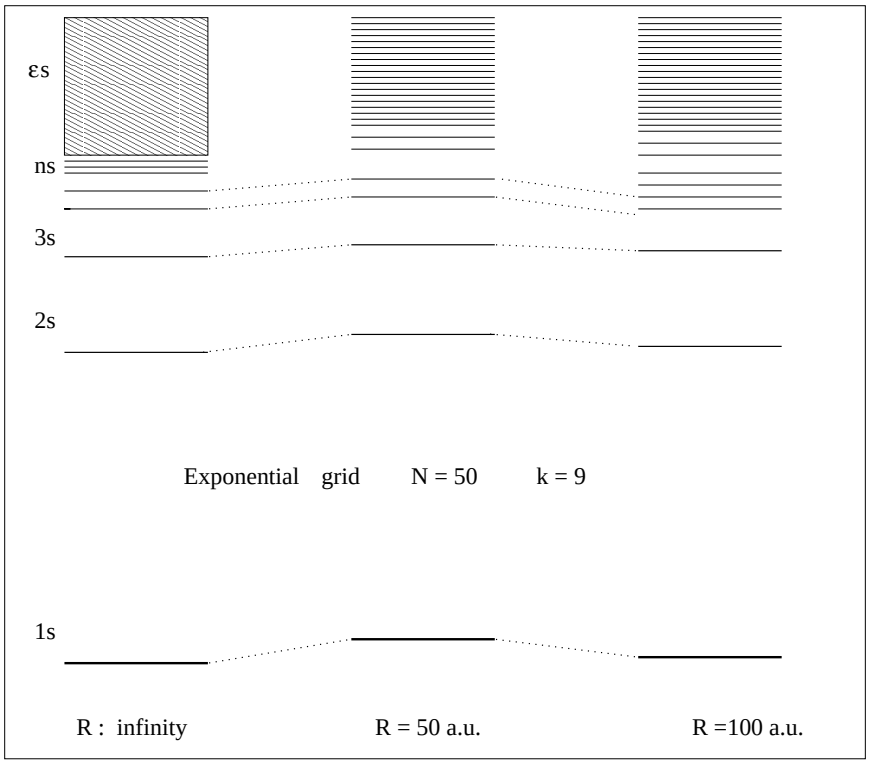

Figure 1.1: The finite-basis spectrum obtained for the Hydrogen for two different boxes. For box radius $R = 50a.u.$ the bound states of the spectrum are five, while for $R = 100a.u.$ (with the number of B-splines fixed) the bound states increase to seven. The last members of the bound spectrum fail to represent the Rydberg states for this choice of the B-spline parameters.

B-splines method We expand the radial function in a set of B-splines[7] of total number n and order k, defined inside the interval $[0, R]$ from which we have excluded the first B_1 and the last B-spline B_n in order to ensure the boundary condition at the interval edges ($P_l(0) = P_l(R) = 0$).

$$P_l(r) = \sum_{i=2}^{n-1} c_i^{(l)} B_i(r). \tag{1.23}$$

Variatonal principle $\delta\mathcal{S} = 0$ is equivalent to the equations $\partial\mathcal{S}/\partial c_i = 0$, $i = 1, 2, ..n-1$ which in matrix form leads to a $(n-2 \times n-2)$ symmetric

[7] For a summary of B-splines definition and properties see the relevant appendix at the end of this chapter

generalized eigenvalue equation:

$$A_l \vec{v}^{(l)} = \varepsilon_l B \vec{v}^{(l)} \quad \vec{v}^{(l)} = (c_1^{(l)}, c_2^{(l)}, ..., c_{n-1}^{(l)}). \tag{1.24}$$

The elements of matrices A, B are calculated through the finite integrals :

$$\begin{aligned} A_{ij} &= \int_0^R dr \left\{ \frac{1}{2} \frac{dB_i}{dr} \frac{dB_j}{dr} + B_i(r) \left[U(r) + \frac{\hbar^2 l(l+1)}{r^2} \right] B_j(r), \right\} \\ B_{ij} &= \int_0^R dr B_i(r) B_j(r). \end{aligned}$$

Solution of equation (1.24) gives $n-2$ vectors $\vec{v}^{(l)}$ which through equation (1.23) correspond to the eigenstates of the system. Simultaneously, $n-2$ eigenenergies are obtained. A finite number of states (n_b) with energies $\varepsilon_{nl} \leq 0$ represent bound states of the atomic system. The positive energy solutions $\varepsilon \geq 0$ corresponds to the continuum states exhibiting an oscillatory behavior at large r. The number of the bound states depends strongly on the box size and this number increases with increasing box radius, while the true spectrum corresponds to $\lim_{R\to\infty} n_b \to \infty$. The bound solutions just below the threshold $\varepsilon = 0$, does not correspond to any of the true bound states of the atomic system. This is due to the large space extension of these states (although bound), thus making the boundary effects dominant, with the consequence of making the spectrum at this energy range not reliable. The numerical representation of high Rydberg states using this method, in general demands large box radius. In figure 1.1 the finite-basis spectrum is plotted for Hydrogen for two different boxes. For box radius $R = 50 a.u.$ the bound states of the spectrum are five, while for $R = 100 a.u.$ (with the number of B-splines fixed) the bound states increases to seven. The last members of the bound spectrum fail to represent the Rydberg states for this choice of the B-spline parameters but correspond to pseudostates which, however, do contain the necessary oscillator strength.

Integration and diagonalization with B-splines. B-spline functions are piecewise polynomials, depending on the knot distribution. When integration is needed for a calculation, full advantage of their properties is taken. Integrals involving wavefunctions, lead to integrals containing only B-spline polynomials. Integrals of the type $M(a,b,q) = \int_0^R P_a(r) q(r) P_b(r)$, through an expansion of the type (1.23) can be written as:

$$M(a,b,q) = \sum_{i,j=1}^{n-1} c_i^{(a)} c_j^{(b)} M_{ij}(q) \tag{1.25}$$

$$M_{ij}(q) = \int_0^R B_i(r) q(r) B_j(r) \; . \tag{1.26}$$

In the general case, the quantity $q(r)$ is considered to be a differential operator. The most frequent types of $q(r)$ are: $q(r) = 1, r, 1/r, d/dr, d^2/dr^2$. As an illustration of the technical details arising in the integration process of B-splines, the special case $q(r) = 1$ is considered. Then the integral $\langle B_i|B_j\rangle \equiv \int_0^R B_i(r)B_j(r)$ needs to be calculated. Half of the calculation is avoided when the property $B_i(r)B_j(r) = B_i(r)B_j(r)$ is used. When, $|i-j| > k$ the integral vanishes automatically because of the local nature of the B-spline polynomials. The relevant B-splines do not overlap. When $|i-j| < k$, the integration over the interval is reduced to an integration over an interval of the order $r(t_{i+k}) - r(t_i)$. Finally, this interval is separated to k intervals $r(t_{i+1}) - r(t_i), i = 1, 2, ..k$, where a k-order Gaussian integration [67] takes place. Improvement of the efficiency of the code is possible, when a uniform knot sequence is used. For this case B-splines keep their form constant over the interval $[0, R]$. In other words, the integrals $\langle B_i|B_j\rangle = \langle B_{i+k}|B_{j+k}\rangle$ are equal. From the B-splines properties, one can verify the relations $\langle B_i|B_j''\rangle = \langle B_i''|B_j\rangle = -\langle B_i'|B_j'\rangle$ and $\langle B_i|B_j'\rangle = -\langle B_i'|B_j\rangle$. If $q(r)$ is a polynomial up to the order $2k-1$, then the integrals calculated with kth order Gaussian quadrature are exact. Obviously, when $q(r)$ contains negative powers of r (i.e. 1/r) the integrals are approximations of the exact value with a degree of accuracy depending on the order k of the Gaussian quadrature used. Improvement of the necessary code for the diagonalization, necessary for the solution of the eigenvalue equation (1.24), can be achieved. The origin of these improvements derives again from the localization of the B-splines polynomials. The matrices A, B involved have the banded stucture of figure 1.2. Ordinary matrices A, B demand a $\sim (n-2)\times(n-2)$ disc space storage and $\sim n^3$ computing time. Because of the banded structure and symmetry of the matrices A, B, methods requiring $\sim k \times (n-2)$ disc space storage and $\sim k \times n^2$ computing time can be implemented.

For $i \neq 1, n$ and $q(r)$ a function of r, the relations $\langle B_i'|B_j'\rangle = -\langle B_i'|B_j'\rangle$ and $\langle B_i|q|B_j\rangle = \langle B_j|q|B_j\rangle$, are true hold which means that the resulting A, B matrices are symmetric[8].

Continuum states and normalization. In atomic quantum theory, bound states are normalized to unity while the continuum eigenstates are energy normalizable.

$$\langle \phi_a|\phi_b\rangle = \begin{cases} \sim \delta_{ab}, \\ \sim \delta(\varepsilon_a - \varepsilon_b)\,. \end{cases} \tag{1.27}$$

[8]Note that, inclusion of the last B-spline (boundary conditions where, $P_l(R) \neq 0$) has the effect of leading to non-hermitian matrices.

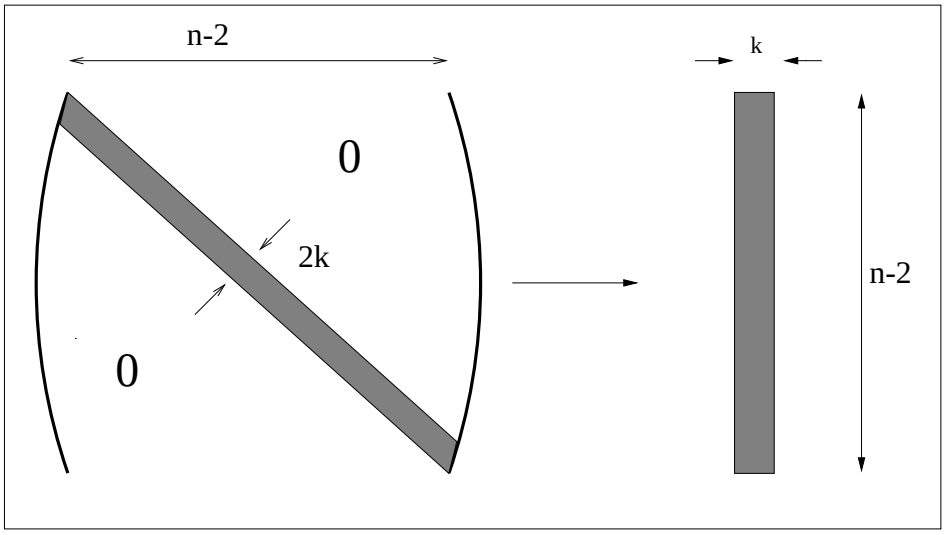

Figure 1.2: Ordinary matrices A, B demand a $\sim (n-2) \times (n-2)$ storage of disc space and $\sim n^3$ computing time is needed. Because of the banded structure of the matrices A, B, methods requiring $\sim k \times (n-2)$ storage of disc space and $\sim n^2$ computing time can be implemented.

Thus, bound states have the dimension $\sim 1/\sqrt{volume}$ while continuum states have the dimension $\sim 1/\sqrt{energy}$. In a finite basis method, the entire spectrum is represented by a discretized one inside a box of radius R, with normalization to unity for both negative and positive energy eigenfunctions. Although for the bound solutions $\varepsilon \leq 0$ no problem arises about their normalization and physical meaning, for the positive energy solutions it is not evident what they represent. The spectral decomposition of the true Hamiltonian is given by:

$$H = \sum_n |\phi_n\rangle E_n \langle\phi_n| + \int dE |\phi(E)\rangle E \langle\phi(E)|. \tag{1.28}$$

The finite representation of the H operator, $\hat{H}$ is writen as:

$$\hat{H} = \sum_{E_i \leq 0} |\chi_n\rangle E_i \rangle \chi_i| + \sum_{E_i \geq 0} |\chi_i\rangle E_i \langle\chi_i| \,. \tag{1.29}$$

The numerical evaluation of the continuum integral is approximated as $\int dE|\phi(E)\rangle E\langle\phi(E)| \approx \sum_i w_i |\phi(E_i)\rangle E_i \langle\phi(E_i)|$, where w_i is the weight of the equivalent quadrature. Requiring the operator $\hat{H}$ to be the finite representation of the Hamiltonian H leads to the equality, $\sum_{E_i \geq 0} |\chi_i\rangle E_i \langle\chi_i| =$

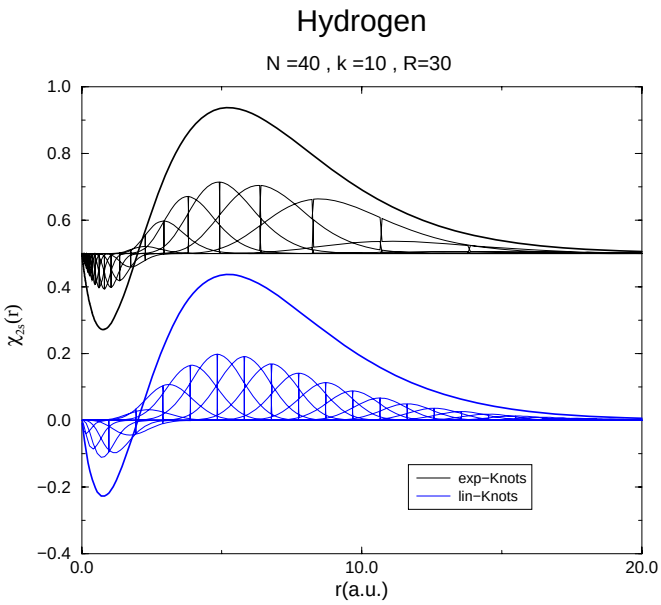

Figure 1.3: B-spline expansion of the 2s radial function of Hydrogen for two different knot sequences.

$\sum_i w_i|\phi(E_i)\rangle E_i\langle\phi(E_i)|$, with the result of,

$$\phi(E_i) = \frac{1}{w_i}\chi(E_i). \tag{1.30}$$

The physical meaning of the calculated positive-energy wavefunctions $\chi(E_i)$ within the basis-set framework is now clear: The positive-energy solutions $\chi(E_i)$ (normalized in unity), when divided by the weight w_i which allows integration over the continuum, represent the actual continuum Coulomb function, of energy E_i, *inside the box*. The determination of the correct weight of the equivalent quadrature for the evaluation of the integrals is not a-priori known. A thorough analysis of that subject has been discussed by Reinhardt [67].

One of the consequences of the adoption of boundary conditions at finite radius has to do with the spacing of consecutive energy eigenvalues. The density of states $\rho(E)$ instead of the δ-function form takes now finite values, $\rho(E_i) = 2/(E_i - E_{i+1})$. Choosing as $w_i = \sqrt{\rho(E_i)}$ for the normalization of the discrete positive-energy states we obtain, $\langle\phi_i|\phi_j\rangle = \rho(E_i) \overset{R\to\infty}{\to} \delta(E-E')$. The limit of that normalization when $R \to \infty$ goes to δ-function as it should.

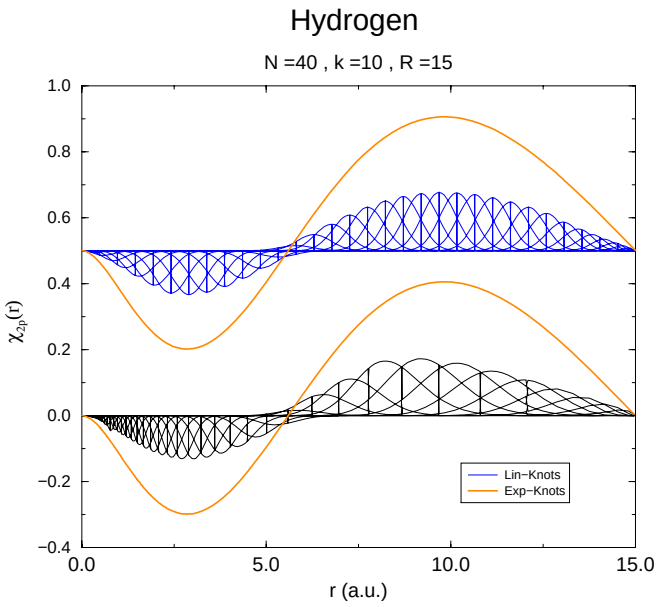

Figure 1.4: B-spline expansion of the 2p radial function of Hydrogen for two different knot sequences.

For typical atomic potentials where $(\lim_{r\to 0}(r^2U(r)) \to 0)$ and $(\lim_{r\to\infty}(rU(r)) \to -Z_{eff})$, the energy spectrum includes a discrete part of negative energy bound states, and a continuum of positive energy states. The asymptotic behavior of these states satisfy the relation [78]:

$$\phi_{kl} \to \begin{cases} C_{\varepsilon l} r^{l+1}, & r \to 0 \\ A_{\varepsilon l} e^{-\sqrt{-2\varepsilon}\, r}, & r \to \infty \end{cases} \tag{1.31}$$

for the bound states and

$$\phi_{kl} \to \begin{cases} C_{kl} r^{l+1}, & r \to 0 \\ A_{kl} \sin(\phi_{nl}(r) + k_{nl} r + \delta_{kl}), & r \to \infty \end{cases} \tag{1.32}$$

for the continuum states, where $\varepsilon = k^2/2$. In the above relation, $\phi_{kl}(r) = (Z_{eff}/k_{nl}) ln(2k_{nl}R) - l\pi/2 + \Gamma(l+1-i)$ where Z_{eff} is the effective nuclear charge, $\Gamma(x)$ is the Gamma function and δ_l is the scattering phase shift which carries information about the distortion potential $(U(r) - [l(l+1)/2r^2 - Z_{eff}/r])$ "seen" by the outgoing electron. It is worthwhile to note here that for attractive potentials, the phase shift δ_l has an

Figure 1.5: Phase shifts of continuum states in H^- corresponding to single ionization with total angular momentum S,P,D and F. Note the smallness of the P,D,F channels phase shifts comparing to that of the S-channel.

negative-energy extension to region (below the ionization threshold) extension related to the quantum defect $\mu_{nl} = \delta_{nl}/\pi$. The quantum defect μ_{nl} is defined through the negative-energy eigenvalues as $\varepsilon_n = -(Z_{eff})^2/2(n - \mu_{nl})^2$. In practice, because of the boundary conditions $P_l(R) = 0$, only the continuum states of the system with momentum $\hbar k_{nl} = \sqrt{2\varepsilon_{nl}}$ (in order to satisfy the relation $k_{nl}R + (Z/K_{nl})ln(2k_{nl}R) - l\pi/2 + \delta_c + \delta_l = \rho\pi, \rho = 1, 2...$) are obtained.

For the higher continuum states, where the scattering phase shift is expected to be small, the term kR dominates ($kR = \rho\pi$), thus giving rise to the square discretization of continuum ($E = k^2/2 = \rho^2\pi^2/2R^2$). Methods exist for the determination of the scattering phase shift[8, 12, 9]. In the next section, we present such a calculation for the case of a singly ionized two-electron continuum state. In figures 1.3, 1.4, we have shown the radial part of the hydrogen bound states $2s, 2p$. In the same figures, we also plot the B-splines on which the radial functions are expanded. The phase shifts for the continuum states with total angular momentum $L = 0, 1, 2, 3$ are shown in figure 1.5. The phase shift of the channel S is considerably different from zero, exhibiting a strong non-plane-wave behavior up to a rather large photoelectron energy range. As expected, the value of the phase shift decreases with the energy of the outgoing electron.

Grid selection Particular attention should be given to the numerical radial grid selection, since its specification is critical for the reliability of the calculations. The radial function, because of the singularity at the origin, changes rapidly for $r \to 0$. In order to describe this behavior accurately, a dense grid is needed for the region near the nucleus (small r). On the other hand, a good representation of the continuum (which extends up to R) requires a dense number of grid points (knots) even for large values of r. In principle, there are many kinds of grids, but in practice some are used more often than others, depending on the context. We have used three types of grids, a linear-like, an exponential-like and a sine-like :

Linear-like grid:

$$r_i = H \cdot (i - 1), \qquad H = \frac{R}{n - 1}, \tag{1.33}$$

Sine-like grid:

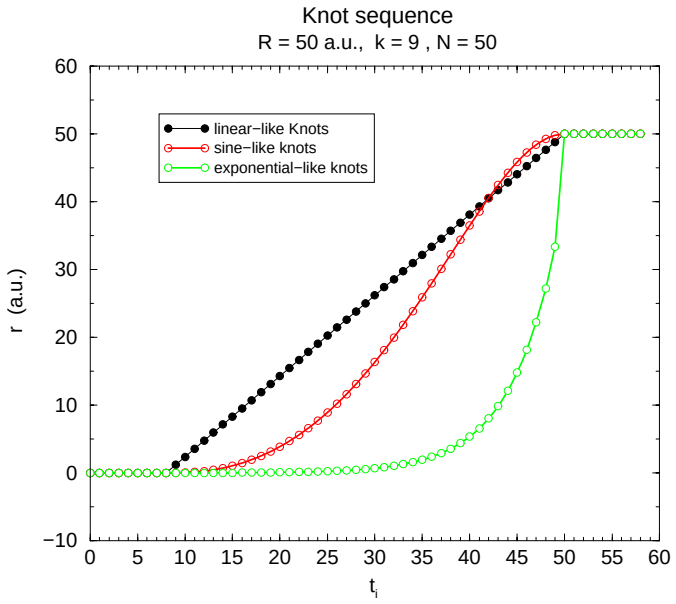

Figure 1.6: Knots distribution for three types of grid. Linear,sine and exponential-like distributions are plotted.

$$H = R \sin\left[\frac{\pi}{2}\left(\frac{(i-1)H}{R}\right)^{p}\right] \qquad H = \frac{R}{n-k+1} \tag{1.34}$$

Exponential grid:

$$r_i = H \cdot \left[e^{(i-1)/n} - 1\right], \qquad H = \frac{R}{e^{(i-1)/n} - 1} \tag{1.35}$$

The variable i takes the integer values $i = 1, 2, ...n - k + 2$ for all grid types. Specification of the sine-like grid is made through the position of the first knot point. In figure 1.6 the knot sequence of the three types of grid are plotted.The other B-splines parameters have the values $k = 9, R = 50a.u., n = 50$. Depending on the problem we are interested in, the selection of the grid type may be is essential for the results. For example, if we aim at for a very accurate determination of the ground state of an atomic system, an exponential grid around the nucleus is probably the most appropriate. Obviously, the reason for this is the dense sequence of knot points near the origin, where the ground state is expected to have non-vanishing values (see Fig.1.3). Another example, is the calculation of the two-photon ionization cross section (3.2) or the static polarizability of a bound state (equation

5.14). For such calculations it is important to have a good description of the continuum states since the entire spectrum of states is needed. Then, a linear knot sequence (with respect to $kr \sim r/\lambda$) is suitable. In order to keep constant the number of knots inside an interval of size λ for all continuum states (characterized by the momentum $\hbar k$), one has to take into account the variation of λ while increasing the energy ($\sim \hbar k$). Fischer and Idrees have used a composite grid [32] where near the nucleus, the knot points are distribuded exponentially while the outer region a linear distribution is used. Decleva et all [24] in a careful study of the Helium ground state have used a parametrized grid which they optimize in a systematic manner. In the same work, a quantitative comparison between different grid selections, has been made.

Of equal importance, for the reliability of the calculation, is the box size R in combination with the total number of B-splines. Calculation of the energies of bound states is possible even in a small box, but for Rydberg or continuum states (which extend to large r) a large box is necessary. The number of B-splines set is chosen so that a reasonable density of grid points is obtained. Stability of the results with respect to the magnitude of R is a criterion for the convergence of the calculations. Note that it is necessary to have the same basis-set for all calculations, otherwise orthonormality between eigenstates which originating from different basis-sets is not satisfied.

1.4 Dirac equation and B-splines method

Assumming that we consider the boundaries of space at infinite distance from the atom, the equations for the Dirac radial functions $G(r), F(r)$ are given by equations (1.11,1.12). As in the analogous non-relativistic problem we obtain a different set of equations, for finite boundaries, using the concept of action.

The use of the finite basis method in the Dirac equation (DE) has certain problems that do not appear in the case of the SE. The main reason is that the spectrum of the DE is not bound from below (the negative eigenenergies decrease indefinitely to $-\infty$ (see figure 1.7), thus making the variatonal method inappropriate for relativistic calculations.

Boundary conditions. Solution of the DE of a particle in a repulsive potential leads to the Klein paradox [68](1930) when the potential has strength of the order $\sim 2mc^2$. The electron, belonging initially to the positive continuum ($\varepsilon > 0$), because of the tunneling effect, jumps to a degenerate state which belongs to the negative continuum region of the space

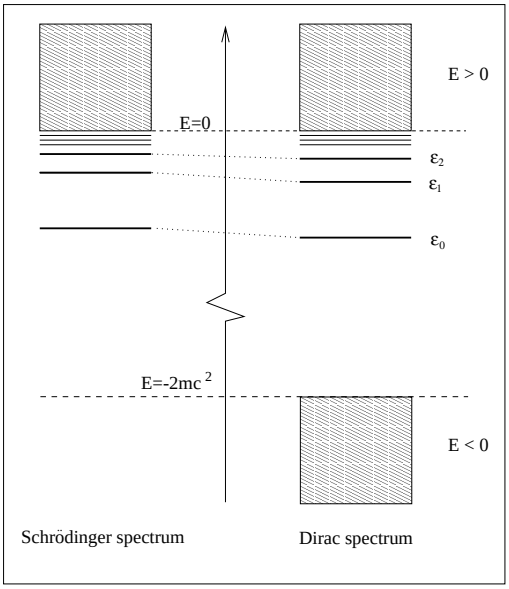

Figure 1.7: The finite-basis spectrum obtained as solution of the Dirac relativistic equation for one-electron atoms.

such that relation $\varepsilon < U(r) - 2mc^2$ is satisfied, with the unphysical result of a non-decaying wavefunction at infinite distance (oscillatory wavefunction). The strong confinement of the electron in a box leads to the opposite result. This means that we cannot put as a boundary condition $\psi(R, \theta, \phi) = 0$, because it is equivalent to an infinitely high ($U(R) = \infty$) potential at this point. In order to avoid this problem, we follow the MIT-bag model [28] which makes the cavity wall an infinitely steep scalar potential gradient, equivalent to assumming the mass of electron infinite outside the box. The resulting boundary condition for $r = R$ reads:

$$\left(1 - i\gamma\hat{r}\right)\psi(\mathbf{r})\big|_{r=R} = 0 \tag{1.36}$$

which, noticing that $\sigma\hat{r}\chi_{km_j} = i\chi_{km}$ and $\sigma\hat{r}\chi_{km_j} = \chi_{-km}$, and expanding the $\psi(\mathbf{r})$ as in equation (1.10) gives for the radial components $G(R) = F(R)$.

Action principle and boundary conditions. The action of a particle moving in a central potential $U(r)$ is given by $\mathcal{S}[\psi] = \langle\psi|(\varepsilon - H_D)|\psi\rangle$, with ψ being the four-component wavefunction.

Our objective is to derive the radial differential equations for $G(r), F(r)$, for an atom inside a box of radius R. We need to separate the Hamiltonian

H_D in a radial part and a part containing only angle variables. Defining as $\alpha_r = \alpha\hat{r}$ and $p_r = -i\hbar(\partial/\partial r + 1/r)$ the radial parts of the α and $\mathbf{p}$ operators, we write :

$$\alpha\mathbf{p} = \alpha_r \left(p_r + i\frac{\sigma\mathbf{L} + \hbar}{r} \right) \qquad \hbar\mathbf{k} = \beta\left(\sigma\mathbf{L} + \hbar\right) \tag{1.37}$$

$$\alpha_r = \begin{bmatrix} 0 & -i \\ i & 0 \end{bmatrix}, \qquad \alpha_r = \begin{bmatrix} 0 & i \\ i & 0 \end{bmatrix}. \tag{1.38}$$

With the above relations, we rewrite the Hamiltonian of the system, as $H_D = c\hat{\alpha}_r\hat{p}_r + i(\hbar c/r)\alpha_r\beta\hat{\mathcal{K}} + \beta mc^2 - U(r)$, and for the action $\mathcal{S}$ we obtain:

$$\begin{aligned} \mathcal{S}[\psi] &= \int d^3\mathbf{r}\psi^\dagger_{nkm_j}(\varepsilon - H_D)\psi_{nkm_j} \\ &= -\hbar c \int d^3\mathbf{r}\psi^\dagger_{nkm_j} \begin{bmatrix} \frac{mc^2 - U(r)}{\hbar c} & \left(-\frac{\partial}{\partial r} + \frac{\hat{k}}{r} + \frac{1}{r}\right) \\ \left(\frac{\partial}{\partial r} + \frac{\hat{k}}{r} + \frac{1}{r}\right) & -\frac{mc^2 + U(r)}{\hbar c} \end{bmatrix} \psi_{nkm_j} \\ &- E\int d^3\mathbf{r}\psi^\dagger_{nkm_j}\psi_{nkm_j}. \end{aligned}$$

From the orthonormalization condition of the angular part of the ψ_{nkm_j} wavefunction, $\int d\Omega_r \chi^\dagger_{km_j}\chi_{k'm'_j} = \delta_{kk'}\delta_{mm'}$, we find
$\int d^3\mathbf{r}\psi^\dagger_{nkm_j}\psi_{nkm_j} = \int_0^R dr(G^2_{nk} + F^2_{nk})$, and finally, after some algebra, we have for the action, in terms of the radial functions $G(r), F(r)$:

$$\begin{aligned} \mathcal{S}[G,F] &= \frac{1}{2}\int_0^R dr \left\{ \hbar c G_{nk}\left(\frac{\partial}{\partial r} - \frac{k}{r}\right)F_{nk} - \hbar c F_{nk}\left(\frac{\partial}{\partial r} + \frac{k}{r}\right)G_{nk} \right. \\ &+ \left. U(r)\left[G^2_{nk}(r) + F^2_{nk}(r)\right] - 2mc^2F^2_{nk}(r)\right\} \\ &- \frac{\varepsilon}{2}\int_0^R dr\left[G^2_{nk}(r) + F^2_{nk}(r)\right]. \end{aligned} \tag{1.39}$$

where $\varepsilon = E - mc^2$. As in the non-relativistic case, the quantity ε plays the role of a Langrage multiplier, ensuring the normalization of the radial wavefunctions. Now by varying the unknown functions G, F we obtain the variation in action $\delta\mathcal{S}$:

$$\begin{aligned} \delta\mathcal{S}[G,F] &= \frac{\partial\mathcal{S}}{\partial F}\delta F + \frac{\partial\mathcal{S}}{\partial(\frac{\partial\mathcal{S}}{\partial F})}\delta\left(\frac{\partial\mathcal{S}}{\partial F}\right) + \frac{\partial\mathcal{S}}{\partial G}\delta G + \frac{\partial\mathcal{S}}{\partial(\frac{\partial\mathcal{S}}{\partial G})}\delta\left(\frac{\partial\mathcal{S}}{\partial G}\right) \\ &= \int_0^R dr\hbar c\left\{\left[\left(\frac{\partial}{\partial r} - \frac{k}{r}\right)F_{nk}(r) + U(r)G_{nk}(r) - \varepsilon G_{nk}\right]\delta F_{nk}(r)\right. \end{aligned}$$

$$- \quad \left[\left(\frac{\partial}{\partial r}+\frac{k}{r}\right)G_{nk}(r)+(2mc^2-U(r))F_{nk}(r)-\varepsilon F_{nk}(r)\right]\delta G_{nk}\Big\}$$

$$+ \quad \frac{c}{2}\left[G_{nk}(r)\delta F_{nk}(r)-F_{nk}(r)\delta G_{nk}(r)\right]_0^R .$$

From the above equations, we obtain the radial eigenvalue equation (1.11) by stipulating $\delta\mathcal{S}=0$ under the variation of G,F with the constraint $\delta G(R)=\delta G(0)=\delta F(R)=\delta F(0)=0$. Following this method, the resulting equation will lead to unphysical solutions for the radial functions $G(r),F(r)$, because of the boundary conditions[9].

In order to ensure $G(R)=F(R)$, the boundary conditions adopted from the MIT-bug model, we add to the action a boundary term, $\mathcal{S}_b'$, given by:

$$\mathcal{S}_b'=\frac{c}{4}\left[G_{nk}^2(R)-F_{nk}^2(R)\right]-\frac{c}{2}G_{nk}(0)F_{nk}(0)+\begin{pmatrix} c/2, \text{ if } k<0 \\ c^2, \text{ if } k>0 \end{pmatrix}G_{nk}^2(0). \tag{1.40}$$

Note here the difference between the formulas for $k>0$ and $k<0$, which is connected with the appeareance of spurious states in the spectrum[10] of h_D for $k>0$. Including the variation of this term with respect to variation of $G(r),F(r)$ we obtain for the total variation of the action on the surface:

$$\begin{aligned}\mathcal{S}_b &= \frac{c}{2}\left[G_{nk}(R)-F_{nk}(R)\right]\left[\delta G_{nk}(R)+\delta G_{nk}(R)\right] \\ &- \frac{c}{2}G_{nk}(0)\delta F_{nk}(0)+\begin{pmatrix} c, \text{ if } k<0 \\ 2c^2, \text{ if } k>0 \end{pmatrix}G_{nk}(0)\delta G_{nk}(0). \end{aligned} \tag{1.41}$$

At this point, the arbitrary addition of the boundary term $\mathcal{S}_b'$ is becoming more obvious. Since, asking for variations of $\mathcal{S}$ without constraints in variations $\delta G(r),\delta F(r)$ we have $\delta\mathcal{S}=0$ only when $G(R)=F(R)$ and $G(0)=0$[11], which are the boundary conditions being satisfied.

We should emphasize the crucial difference in the way we stipulate the boundary conditions between the relativistic and the non-relativistic Hamiltonian. For the non-relativistic Hamiltonian, where the radial functions

[9] This problem is connected with the Klein paradox, appearing when a particle is trapped in an attractive potential of height $V_0\sim mc^2$.

[10] Spurious states are states that are not physical and their appearance is an inherent problem of the finite basis method. [27]

[11] In the non-relativistic limit of $G(r),F(r)$ this condition leads to the correct behavior for the corresponding radial function.

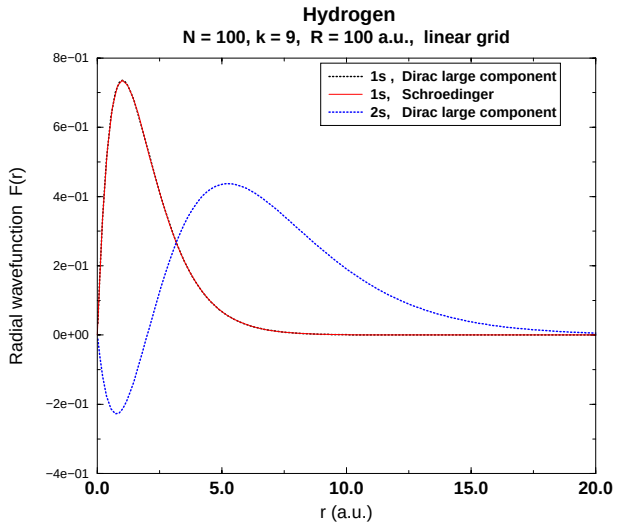

Figure 1.8: The large components of the Dirac $1s, 2s$ states of the Hydrogen are plotted. In the same figure the 1s radial function obtained from the Schrödinger equation is plotted.

$P_l(r)$ should satisfy $P_l(R) = P_l(0) = 0$, we work with the radial equations corresponding to an infinite box and we expand the $P_l(r)$ in a basis set which does not include the first and the last member, ensuring that way the vanishing of the radial functions at the boundaries. On the other hand, in the relativistic Hamiltonian, we are imposing the boundary conditions via the addition 'by hand' of a surface term in the action, which is chosen so that the radial functions $G(r), F(r)$ satisfy the specific boundary conditions. Within this approach we do not remove any member of the B-spline set.

B-spline method. Detailed presentation and application of the method has been given by Johnson and Sapirstein in a pioneering paper [43] and in a recent review [73].

The basic idea is the same as in the non-relativistic case, which is the confinement of the atom in a sphere (box) of radius R. This has the effect of the finiteness of the number of the bound states (for $R \to \infty$ this number is infinite) and the dicretization of the continuum spectrum, while the number of the continuum states remains infinite. For a central potential $U(r)$, the states are written as in equation (1.10) with the unknown radial equations G, F satisfying $G(R) = F(R)$. We try to represent the infinite spectrum of solutions for this problem. through a finite spectrum (pseudospectrum)

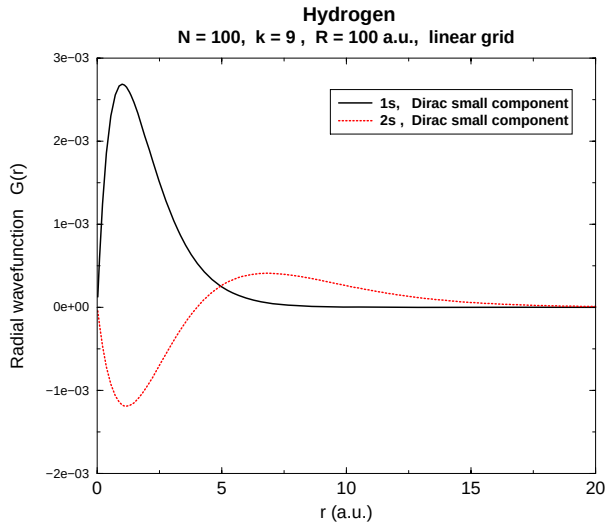

Figure 1.9: The small components of the Dirac $1s, 2s$ states of the Hydrogen are plotted. Note the $Z\alpha \sim 10^{-2}$ ratio of the amplitudes between the small and large component (see Fig. 1.8).

just expanding the radial functions in a finite basis set, which in the present case is the B-splines set. The equations to be solved, are derived using the action, which as we have already discussed has the advantage of introducing the boundary condition into the radial equations in a systematical manner.

Expanding therefore the radial equations in a B-spline set of order k, total number N, defined in a region $[0, R]$ as:

$$G_k(r) = \sum_{n=1}^{N} p_i^{(k)} B_i(r) \qquad F_k(r) = \sum_{n=1}^{N} q_i^{(k)} B_i(r), \tag{1.42}$$

we obtain the $2N \times 2N$ generalized eigenvalue equation, from $\partial S/\partial p_i = 0, \partial S/\partial q_i = 0$:

$$A\mathbf{u}^{(k)} = \varepsilon_k B\mathbf{u}^k, \qquad \mathbf{u}^k = (p_1^k, p_2^k, ..., p_N^k, q_1^k, q_2^k, ...q_N^k), \tag{1.43}$$

where the A, B matrices are given by:

$$A = \begin{bmatrix} M(U) & \hbar c \left(M(\frac{d}{dr}) - M(\frac{k}{r}) \right) \\ -c \left(M(\frac{d}{dr} + M(\frac{k}{r}) \right) & -2c^2 M(1) + M(U) \end{bmatrix} + A' \tag{1.44}$$

	ω_n	
$ns_{1/2}$	Analytical	B-splines
1	-0.50000665656957	-0.5000066565997
2	-0.12500208019145	-0.12500208018833
3	-0.055556295171932	-0.05555629517705
4	-0.031250338036512	-0.031250338031454
5	-0.020000181052151	-0.020000181060167
6	-0.01388899674244	-0.013888996751446
7	-0.010204150879325	-0.010204150944494
8	-0.0078124283017605	-0.0078125471281836
9	-0.0061573131021036	-0.0061728729874227
10	-0.0047608935306592	-0.0050000246263673
11	-0.0031196540796009	-0.0041322500461132
12	-0.0011047159880257	-0.0034722366697655

Table 1.2: Energies of the ns states of the Hydrogen, obtained with the Dirac Hamiltonian H_D analytically and computationally. The B-splines parameter are, $k = 9, n = 200, R = 200a.u.$ and linear grid.

and

$$B = \begin{bmatrix} M(1) & 0 \\ 0 & M(1) \end{bmatrix} \tag{1.45}$$

and where the elements of the matrix M are given by (equation 1.26) $M_{ij}(q) = \int_0^R B_i(r)q(r)B_j(r)$. The elements of the "boundary" matrix A' are derived straightforward by from the equations $\partial S_b/\partial p_i = 0, \partial S/\partial q_i = 0$.

The solution of the above system gives N states with $\varepsilon > 0$ (positive states) and N states with $\varepsilon < 0$ (negative states). Figure 1.7 gives schematically the spectrum obtained after the diagonalization. The first bound states of the pseudospectrum approach (from above) the corresponding states of the real spectrum, with accuracy depending mainly on the radius R and the total number N of the B-splines set. As in the non-relativistic case, the higher the bound state is the more innacurate is its representation. In figure 1.8 the small and large components of the 1s,2s radial functions are plotted.

Finite-size nucleus. The hydrogenic Dirac wavefunctions for $j = 1/2$ diverges near the origin $r \to 0$, in contrast to those of the hydrogenic Schrödinger wavefunctions, which remains finite for $l = 0$. Although the divergence is quite weak, it becomes more serious when Z increases. For

	ω_n	
ns	H_S	H_D
1	-0.49999999999401	-0.5000066565997
2	-0.125	-0.12500208018833
3	-0.055555555555557	-0.05555629517705
4	-0.03125	-0.031250338031454
5	-0.02	-0.020000181060167
6	-0.013888888888887	-0.013888996751446
7	-0.010204081566722	-0.010204150944494
8	-0.0078123810887326	-0.0078125471281836
9	-0.0061572727152837	-0.0061728729874227
10	-0.004760808277328	-0.0050000246263673
11	-0.0031194774936659	-0.0041322500461132
12	-0.0011044353071858	-0.0034722366697655

Table 1.3: Energies of the ns states of the Hydrogen, obtained with the Dirac Hamiltonian H_D and the Schrödinger Hamiltonian. The B-splines parameter are, $k = 9, n = 200, R = 200a.u.$ and linear grid.

$Z\alpha > 137$ the formation of the $j = 1/2$ states is impossible. The wavefunction inside a heavy nucleus (with finite extension) is rather different from that of a point-like charge. To avoid this problem, one should take into account the finite charge distribution of the nucleus, which in principle, is not well-known. A uniform distribution[12] gives for the potential the form,

$$U_n(r) = \begin{cases} -\frac{3Z}{2r_c}\left[1 - \frac{1}{3}\left(\frac{r}{r_c}\right)^2\right], & 0 \le r \le r_c\,, \\ U(r) & r \ge r_c\,, \end{cases} \tag{1.46}$$

where r_c corresponds to the nuclear charge extension, and its specific value depends on the atomic system.

1.5 One-electron atoms: Model potential method

Consider an atomic system (atom or ion) consisting of a spherically symmetric core with N_c electrons plus a number of (N_v) of outer electrons (valence

[12] Another, more sophisticated charge distribution for the nucleus is the Fermi distribution $\rho(r) = r_0/1 + exp((r - R)/r_c)$. Details of that form can be found in [44].

electrons). When $N_v = 1$, we call this atomic system the "one-electron" system and when $N_v = 2$ the "two-electron" system, respectively.

The basic idea of the model potential method is to approximate the SE depending on the $N_c + N_v$ electron coordinates with a SE for the valence electron(s) coordinates thus reducing the number of the independent variables. The model SE will contain the core-valence electron interaction through an effective potential $U(r)$, known as model potential. Although the core-valence interaction term is in general a complicated function of the electron position (r), in the asymptotic region $(r_c \ll r)$ a simple analytical formula can be derived [53]. The quantity r_c is an estimation of the core extension.

Long-range formula of model potential. The exact many-electron Hamiltonian is written as $H = H_c + T^{(v)} + V_{cv}$ where H_c depends on the core-electrons' coordinates, $T^{(v)} = \sum^{N_v} \mathbf{p}_i^2/2m$ represents the kinetic energy operator of the valence electrons and V_{cv} denotes the core-valence interaction term. Since we are interested in the long-range behaviour of the V_{cv} term, we are able to make an approximation reducing the problem to an alternative form. Consider a model potential $U(r)$ with the valence Hamiltonian given by $H^{(v)} = T^{(v)} + U$, having as eigenvalues the Rydberg energies E_R of the exact Hamiltonian :

$$H_v\psi_v = (T_v + U)\psi_v = E_R\psi_v \tag{1.47}$$

Using a projection-operator method [53] simple asymptotic formulas are derived, where for the simplest cases of one- and two- electron atomic systems (neglecting dynamical terms) are given by :

One-electron atomic system:

$$U_1(r) = -\frac{Z - N_c}{r} - \frac{a_d}{2r^4} - \frac{a_q - 6b_1}{2r^6} + O(r^{-7}), \tag{1.48}$$

Two-electron atomic system:

$$\begin{aligned} U_2(r) &= -\frac{1}{r_{12}} \\ &- (Z - N_c)\left(\frac{1}{r_1} + \frac{1}{r_2}\right) - \frac{a_d}{2}\left(\frac{1}{r_1^4} + \frac{1}{r_2^4}\right) - \frac{a_q - 6b_1}{2}\left(\frac{1}{r_1^6} + \frac{1}{r_2^6}\right) \\ &- \frac{a_d}{r_1^2 r_2^2} P(\hat{r}_1\hat{r}_2) + O(r^{-8}). \\ &= -\frac{1}{r_{12}} + U_1(r_1) + U_1(r_2) - \frac{a_d}{r_1^2 r_2^2} P(\hat{r}_1\hat{r}_2). \end{aligned} \tag{1.49}$$

In the above relations a_d, a_q are the dipole and quadrapole core polarizabilities and b_1 is the dynamical dipole polarizability of the core, playing the role of a correction to a_d because of the delayed response of the core to the motion of the valence electron (equation 5.14). Finally, $P_1(x)$ is the first-order Legendre polynomial. The term that contains the Legendre polynomial is called "dielectric" term.

Corrections of U(r). Since formulas (1.48,1.49) have been derived as asymptotic limits of the core-valence interaction terms, certain modifications should be introduced to make them more reliable at the short-range limit. Since all terms of the above formulae are strongly singular at the origin, cut-off functions $W(r/r_c)$ are introduced. The r_c parameter is varied, in a semi-empirical method, in order to reproduce experimental data (usually the first lower energy eigenvalues). It is necessary to emphasize the possible eigenvalue solutions of the model potential method. The lower eigensolutions correspond to occupied (by the core electrons) states, thus violating the Pauli exclusion principle. Considering, therefore the allowed valence electron states, we should exclude from the spectrum of H_v the first n-lower eigenstates with n being the principal number of the highest occupied core state. For example, in the case of Caesium (Cs, Z=55), an one-electron atom according to our terminology, the electron configuration is of the type $[...5d^{10}]\ 6s$. Thus, solving the model potential Hamiltonian for this atom, whatever is the explicit form of $U(r)$, from the spectrum we obtain, we have to exclude the first 4 states. At this point, it might be useful to make a point regarding, the similar in spirit pseudopotential method. In this method, the orthogonality property of the core-valence electron states (required as mentioned by the Pauli exclusion principle) is taken into account from the very begining by introducing an additional repulsive short-range term into the potential $U(r)$. In the pseudopotential approach therefore all solutions (eigenstates) correspond to allowed valence states and consequently there is no need to exclude part of them. This is the main distinction between a model potential and a pseudopotential approach.

Until now, we have adopted a "frozen" core in the sense that the existence of the outer electron(s), or equivalently the dynamics of the valence electron(s), does not have any influence on the core-electrons. This allows of the use the ground state of an isolated core (the core without the outer electron(s)). Although in many situations this is a good approximation, there are certain cases where this approach is inadequate and an additional modification (taking into account the the influence of the valence electron on the core state) must be introduced. In many cases this modifications is implemented through the addition of a term known as "core-polarization".

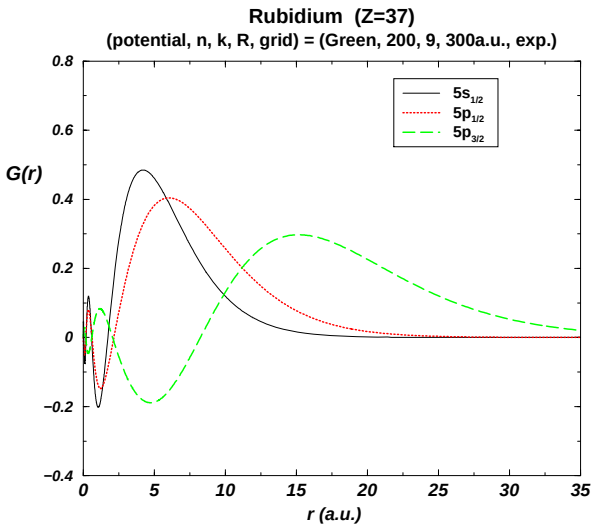

Figure 1.10: The large radial component of the three lower states of Rb.

As expected, the name originates from the polarization of the core-electrons by the influence of the outer-electron. Usually this term gives rise to an angular momentum dependent potential (l-dependent), with l the orbital angular quantum number of the outer electron(s). The l-dependence complicates somewhat the calculation of certain atomic properties.

H^- **: model potentials.** We have used two different kinds of model potentials for the negative hydrogen. The simplest one is the so-called Yukawa potential $U(r) = \mu \exp(-\lambda r)/r$. In order to derive the ground state of H^-, as accurately as possible, the choice $\mu = 1.1$ and $\lambda = 1$ is necessary. This model potential has been used by many authors for the study of the photodetachment properties of H^- [77, 22, 15]. Using $k = 9, R = 300a.u., n = 200$ and linear grid, we find for the ground state energy $E_g = -0.52775a.u$, measured from the double ionization threshold. In Figure 1.12 we plot the radial part of the ground state wavefunction of H^-. Note the large extension of the "outer" electron $r \sim 10a.u.$ in contrast to that of the homonuclear $Z = 1$ hydrogen $r \sim 0.5a.u.$. This is reasonable since the "inner" electron screens the nucleus, thus making the effective charge "seen" by the "outer " electron less than $Z = 1$. The outer electron is therefore expected to be loosely bound, as the small ionization energy and the large radial extension imply. Another, more sophisticated potential, has also been used, introduced by Laughlin and Chu [52] in their study of multiphoton detachment of

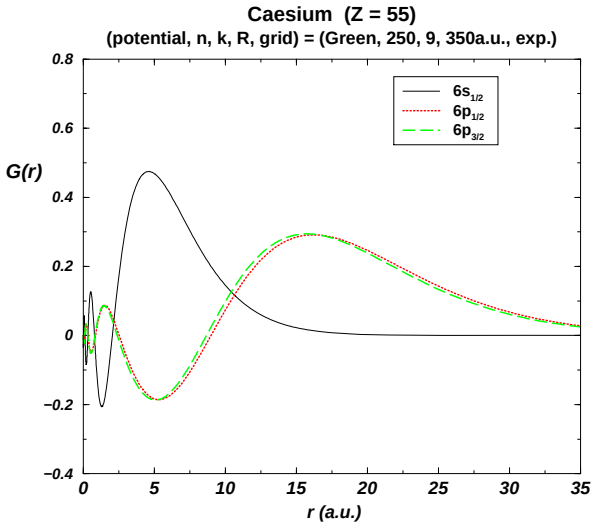

Figure 1.11: The large radial component of the three lower states of Cs.

H^-, within lowest-order perturbation theory (LOPT). This model potential reads:

$$U_l(r) = -\left(1+\frac{1}{r}\right)e^{-2r} - \frac{a_d}{2r^4}W_6(\frac{r}{r_c}) + u_l(r)\,, \qquad (1.50)$$

$$u_l(r) = \left(c_0 + c_1 r + c_2 r^2\right)e^{-\beta r}\,, \qquad (1.51)$$

where $a_d = 9/2$ is the static polarizability of the core (hydrogen). The function $W_i(x) = 1 - exp(-x^i)$ and the quantity r_c are the cut-off parameters The parameters $r_c, c_0, c_1, c_2, \beta$ are choosen so as to produce the negative hydrogen ground state energy and the low-energy phase shifts, simultaneously, as accurately as possible. The parameters are presented in table 1.5. This type of model potential takes into acount the polarization of the core, due to the outer electron. Furthermore this polarization is l-dependent. This complicates somewhat, the calculation of the transition matrix elements. For more details see the next section. For $k = 9, R = 300a.u., n = 200$ and linear grid the ground state energy obtained is $E_g = -0.5277a.u.$ measured from the double ionization threshold.

Finally in figure 1.12 we plot the Yukawa and Laughlin-Chu model potentials. Note the similarity of the Yukawa potential with that of Laughlin and Chu for $l \geq 1$.

Cs, Rb : model potentials. Two types of model potentials have been used for the study of Caesium ($Z = 55$) and Rubidium ($Z = 37$). These

Table 1.4: Energies of Cs and Rb from various model potential and HF potential.

(n, k, R, grid) = (100, 9, 50$a.u.$, expon.)				
Caesium, $Z = 55$, H_D				
	$-\omega_{njl}$(a.u.)[1]			
State	Tietz	Green	Exp.[2]	HF[2]
$6s_{1/2}$	0.143 424	0.143 088	0.143 10	0.127 37
$6p_{1/2}$	0.092 474	0.092 231	0.092 17	0.085 62
$6p_{3/2}$	0.088 918	0.089 148	0.089 64	0.083 79
$7s_{1/2}$	0.058 265	0.059 011	0.058 65	0.055 19
$7p_{1/2}$	0.043 784	0.044 239	0.043 93	0.042 02
$7p_{3/2}$	0.042 698	0.043 228	0.043 10	0.041 37
Rubidium, $Z = 37$, H_D				
	$-\omega_{njl}$[1](a.u.)			
State	Tietz	Green	Exp.	HF
$5s_{1/2}$	0.154 143	0.153 477	0.153 51	0.139 29
$5p_{1/2}$	0.095 565	0.096 146	0.096 19	0.090 82
$5p_{3/2}$	0.093 984	0.094 801	0.095 11	0.089 99
$6s_{1/2}$	0.061 401	0.062 150	0.061 77	0.058 70
$6s_{1/2}$	0.045 047	0.045 703	0.045 45	0.043 89
$6s_{3/2}$	0.044 563	0.045 261	0.045 10	0.032 44

[a] Compared with the table I of reference [44].
[b] [59]

potentials have been used previously by Jonhson et al [44] in order to investigate P-violating electric dipole matrix elements in heavy alkali-like atoms, Rb,Cs,Au and Th. The specific forms of those potentials read:

Tietz:

$$U(r) = -\frac{1}{r}\left[1 + \frac{Z-1}{(1+tr)^2}\right] e^{-\gamma r} \tag{1.52}$$

Green:

$$U(r) = -\frac{1}{r}\left[1 + \frac{Z-1}{H(e^{r/d}-1)+1}\right] e^{-\gamma r} \tag{1.53}$$

where $H = d(Z-1)^{1/3}$. The parameters involved in these potentials are chosen as in the reference [44]. In table 1.4 we present the energies of the lower states of Cs and Rb obtained for various model potentials. In the same

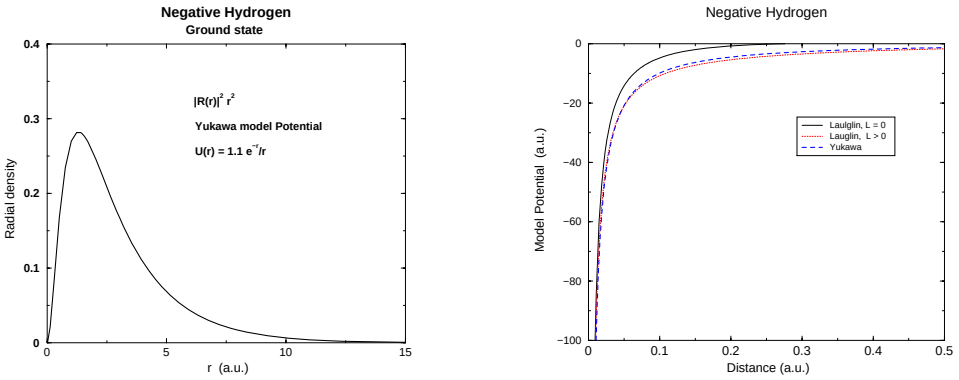

Figure 1.12: Ground state of negative hydrogen obtained by the Yukawa model potential.

H^- : Laughlin potential , H_S						
$l = 0$	4.5	4.0	5.332 1766	-5.254 3795	0.420086	1.4
$l \geq 1$	4.5	4.0	-2.3020310	2.2276939	-0.2776939	1.4

Table 1.5: Laughlin model potential parameters for the negative hydrogen.

table, we also present the Hartree-Fock (HF) results, for direct comparison. The B-splines parameters for these calculations are $n = 100, k = 9, R = 50a.u.$ and an exponential-like grid has been used.

1.6 Radial dipole matrix elements

In photoionization studies the accurate determination of the dipole matrix elements $\langle\phi_a|\mathbf{D}|\phi_b\rangle$ and the eigenenergies E_a, E_b, for each pair of the eigenfunctions $\phi_a(\mathbf{r}), \phi_b(\mathbf{r})$, are of essential importance. For one-electron atoms, the dipole operator is $\mathbf{D} = -i\nabla = \mathbf{p}$, where $\mathbf{p}$ is the momentum operator of the valence electron. Elementary operator algebra gives the relation $\langle\phi_a|\mathbf{p}|\phi_b\rangle = i(\omega_a - \omega_b)\langle\phi_a|\mathbf{r}|\phi_b\rangle$, thus providing an equivalent form for the dipole matrix elements.

Schrödinger equation. In the non-relativistic case, the states are characterized by (n, l, m_l, m_s). Taking the explicit form of the $\phi(\mathbf{r})$ and performing the angular momentum algebra we obtain the following relation for the

Hydrogen, $Z = 1$, H_S		
np	$M_l(1s, np)$	$M_v(1s, np)$
1	1.29026620195449e+00	1.29026620195549e+00
2	5.16689242613434e-01	5.16689242613670e-01
3	3.04583803889118e-01	3.04583803889207e-01
4	2.08703916132692e-01	2.08703916132757e-01
5	1.55135444380143e-01	1.55135444380167e-01
6	1.21419631093697e-01	1.21419631093733e-01
7	9.85139728054122e-02	9.85139728054480e-02
8	8.36039866656059e-02	8.36039866656444e-02
9	8.37676356568420e-02	8.37676356569791e-02

Table 1.6: Non-relativistic dipole radial matrix elements in the length and velocity form from the ground state of Hydrogen to the first 9 states of the np symmetry. The B-splines parameter used for the calculation are $k = 9, n = 200, R = 200 a.u.$ and linear grid. Compared with the table (1.7).

radial part of the matrix elements,

$$\int_0^R dr r P_a(r) P_b(r) = \frac{1}{\omega_{ab}} \int_0^R dr\, P_a(r) \left[\frac{d}{dr} + \frac{l_b}{r} \right] P_b(r)\,, \tag{1.54}$$

where, $\omega_{ab} = \omega_a - \omega_b$ and $l_b = l_a + 1$. Using the notation of the previous section for radial integrals, the same relation is written as, $M(a, b; r) = M(a, b; d/dr + l_b/r)/\omega_{ab}$. The first form of dipole radial matrix elements $M_l(a, b) \equiv M(a, b; r)$ is called the "length" form, while the second form $M_v(a, b) \equiv M(a, b; d/dr + l_b/r)$ is the "velocity" form. Another equivalent form, the "acceleration" form can be derived as $M_a \equiv (Z/\omega_{ab}) M(a, b; 1/r^2)$.

When exact eigenfunctions are used, the above equality is valid in all cases. In atomic structure calculations, this property is used for the evaluation of the quality of the wavefunctions and energies. Both forms are calculated and the results are compared. In numerical studies, the wavefunctions are approximations, either because of the model Hamiltonian used for the calculations or because of the finite representation of the numbers in a computer. Therefore for all cases we should have $M_l \approx M_v$. Note here, that $M_l = M_v$ does not guarante reliable wavefunctions and energies. The functions $q(r) = r, d/dr + l/r, 1/r^2$ inside the three forms of the integrals, emphasize different regions of r inside the box. The length form $q_l(r) = r$ emphasizes large values of r while the velocity form $q_v(r) = d/dr + l/r$ weights intermediate regions. If we have calculated the wavefunctions with

greatest accuracy at intermediate regions of r, then the best results for the radial matrix elements will be obtained through the velocity form. The $1/r^2$ term in the accelerator form emphasizes small values of r, which demands the accurate knowledge of the wavefunctions near the nucleus. For many-electron atoms, such a calculation is difficult, thus making use of this form inconvenient[13]. Turning now to the present numerical approach it should be

Hydrogen, $Z = 1$, H_D			
$np_{1/2}$	$M_l(1s, np_{1/2})$	$M_v(1s, np_{1/2})$	$\Delta M_{lv}/M_v$
1	1.29026380654502e+00	1.29026165971940e+00	1.66e-06
2	5.16681353450675e-01	5.16682882349402e-01	2.96e-06
3	3.04577547214437e-01	3.04578941278759e-01	4.58e-06
4	2.08699050414195e-01	2.08700161925750e-01	5.33e-06
5	1.55131562913682e-01	1.55132452237668e-01	5.73e-06
6	1.21416452948795e-01	1.21417178776176e-01	5.98e-06
7	9.85113016007058e-02	9.85119061839450e-02	6.14e-06
8	8.36010689889997e-02	8.36015912653121e-02	6.25e-06
9	8.37628281312041e-02	8.37633591445413e-02	6.34e-06
$np_{3/2}$	$M_l(1s, np_{3/2})$	$M_v(1s, np_{3/2})$	$\Delta M_{lv}/M_v$
1	1.29024109639367e+00	1.29024109640016e+00	5.03e-12
2	5.16682700078259e-01	5.16682700102513e-01	4.69e-11
3	3.04580320234872e-01	3.04580320242094e-01	2.37e-11
4	2.08701587659982e-01	2.08701587663778e-01	1.82e-11
5	1.55133717259505e-01	1.55133717260954e-01	9.34e-12
6	1.21418272006356e-01	1.21418272007822e-01	1.21e-11
7	9.85128523989615e-02	9.85128523997500e-02	8.00e-12
8	8.36025009813833e-02	8.36025009812263e-02	1.88e-12
9	8.37645038783856e-02	8.37645038821564e-02	4.50e-11

Table 1.7: Relativistic dipole radial matrix elements in the length and velocity form from the ground state of Hydrogen to the first 10 states of the $p_{1/2}\, p_{3/2}$ symmetries. The B-splines parameter used for the calculation are $k = 9, n = 200, R = 200 a.u.$ and linear grid. Compared with table (1.6).

[13]For single-photon double-ionization of a two-electron atom, however, the acceleration form is of particular usefulness. The reason is that double ejection with one-photon is impossible without the inter-electronic interaction $1/r_{12}$ [49]. Then, not only the initial but also the final states are strongly correlated but the final also. And since correlation takes place when electrons are close to the nucleus the usefulness of the acceleration form becomes obvious. It gives the best results compared to the velocity and lentgh form.

emphasized that when evaluating the relevant integrals it should be taken into account that we represent the continuum states as discrete. When at least one of the states belongs to the positive-energy finite basis spectrum then the integrals are box-size dependent. Furthemore, because of the different normalization between bound and continuum states, integrals involving BB, BC and CC states are not directly comparable, unless the normalization factor for the positive-energy finite-basis states is taken into account.

Dirac equation. In the relativistic case the states ϕ_a, ϕ_b, given by the equation (1.10) are characterized by the quantum numbers $(n, j, l, m_j) \equiv (n, k, m_j)$. They decompose into the large and small component (smaller by the factor $\sim (Z\alpha)^2$). The relativistic dipole operator now is of the form $\mathbf{D} = -c\alpha$, where α is given by equation (1.8) . After carrying out the angular momentum algebra, the radial part of the matrix element $\langle\phi_a|\mathbf{D}|\phi_b\rangle$ in the "velocity" and the length form is:

$$M_l(a,b) = \int_0^R dr\, r\,[G_a(r)G_b(r) + F_a(r)F_b(r)] \tag{1.55}$$

$$M_v(a,b) = \frac{1}{\omega_{ab}}\int_0^R dr\,[(k_b - k_a + 1)G_a(r)F_b(r) + (k_b - k_a - 1)G_b(r)F_a(r)]$$

In order to investigate the reliability of the calculations we compare with experimental oscillator strengths, which are available in the literature. The partial and the multiplet oscillator strentghs of a transition between states $a \equiv (n,l), b = (n,l+1)$ for one-electron atoms are given by:

$$f(nlj \to nl+1j) = \frac{2\omega}{3}\frac{1}{4j(j+1)}|M(nlj; nl+1j)|^2 \tag{1.56}$$

$$f(nlj \to nl+1j+1) = \frac{2\omega}{3}\frac{2j+3}{4(j+1)}|M(nlj; nl+1j+1)|^2 \tag{1.57}$$

$$f(nl \to nl+1) = \frac{2\omega}{3}\frac{l+1}{4(2l+1)}|M(nl; nl+1)|^2 \tag{1.58}$$

Note that $f(nlj \to nl+1j+1)/f(nlj \to nl+1j) = j(2j+3)|M(nlj; nl+1j+1)|^2/|M(nlj; nl+1j)|^2$. When the spin-orbit coupling is not significant $|M(nlj; nl+1j+1)|^2 \sim |M(nlj; nl+1j)|^2$, and the value of the ratio is close to 2 for j =1/2. Any deviation from that value implies strong spin-orbit coupling influence in the formation of the wavefunction of the state. The extreme example of such transitions is the Cs atom. The correct treatment of such atoms demands the incorporation of the core polarization due to the valence electron [62]. Introduction of the polarization term in the central potential, however, introduces a correction in the dipole matrix elements. In

table 1.8, we present partial and multiplet oscillator strengths for Rubidium using the Green model potential. Core polarization effects are not taken into account. Sufficient agreement is found with the experimental data. This means that polarization of the core is not a strong effect in Rubidium in contrast with the Caesium. Similar calculations in Caesium (not presented here) give only qualitative agreement with the experimental data.

Table 1.8: Green model potential oscillator strengths for Rubidium. Core polarization effects are not taken into account.For all transitions the agreement of length - velocity forms is excellent.

Rubidium, $Z = 37$, H_D								
	$f_l(5s_{1/2} \rightarrow np_{1/2})$		$f_l(5s_{1/2} \rightarrow np_{3/2})$		$\rho \equiv f_{3/2}/f_{1/2}$		$f_l(5s \rightarrow np)$	
np	Green[1]	Exp.[2]	Green[1]	Exp[2]	Green	Exp.	Green	Exp.
5	3.69(-1)	3.32(-1)	7.50(-1)	6.68(-1)	2.03	2.01	1.12	1.00
6	5.81(-3)	3.73(-3)	1.53(-2)	9.54(-3)	2.64	2.56	2.11(-2)	1.33(-2)
7	1.02(-3)	4.87(-4)	3.03(-3)	1.48(-3)	2.98	3.04	4.05(-3)	1.97(-3)
8	3.47(-4)	1.38(-4)	1.11(-3)	4.68(-4)	3.19	3.39	1.45(-3)	6.06(-4)
9	1.61(-4)	5.22(-5)	5.35(-4)	1.97(-4)	3.33	3.77	6.95(-4)	2.49(-4)
10	8.83(-5)	2.61(-5)	3.03(-4)	1.08(-4)	3.43	4.14	3.91(-4)	1.34(-4)
11	5.42(-5)	1.46(-5)	1.89(-4)	6.38(-5)	3.49	4.37	2.44(-4)	7.84(-5)
12	3.59(-5)	9.00(-6)	1.27(-4)	4.09(-5)	3.54	4.54	1.63(-4)	4.99(-5)
13	2.51(-5)	5.82(-6)	8.99(-5)	2.86(-5)	3.58	4.91	1.15(-4)	3.44(-5)
14	1.93(-5)	3.97(-6)	7.00(-5)	2.00(-5)	3.62	5.04	8.93(-5)	2.40(-5)

[a] Calculations can be compared with the Table 2 of reference [58].
[b] [76]

Core-polarization and *l*-dependent model potentials. For model potentials which include the core-polarization term, every one-body operator should be modified, in order to take into account the contribution of the dipole moment induced by the core polarization [53].The general form of the length dipole operator now is $\mathbf{D} = \mathbf{r} + \mathbf{G}(\mathbf{r})$. Furthermore, for an l-dependent model potential the relation, $\langle\phi_a|\mathbf{p}|\phi_b\rangle = i\omega_{ab}\langle\phi_a|\mathbf{r}|\phi_b\rangle$ is no longer valid, making thus the values of the velocity and the length form unequal. For the length form, the corrected dipole-operator is given by [62]:

$$\mathbf{G}(\mathbf{r}) = -\frac{a_d}{r^3} W_3(\frac{r}{r_c})\mathbf{r}, \tag{1.59}$$

where, $W_3(x) = 1 - exp(-x^3)$ is a cut-off function, with the parameter r_c

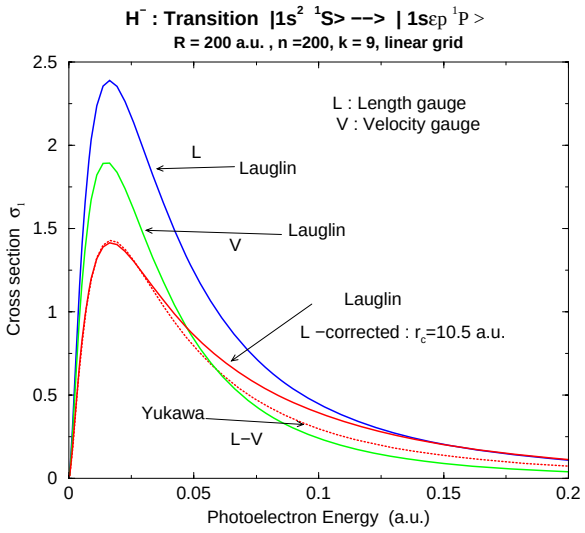

Figure 1.13: One-photon cross sections for the negative hydrogen, calculated with different potentials.

determining its radial extension and a_d the static polarizability of the core. Provided that the calculated wavefunctions are correct asymptotically, the appropriate dipole operator is that of the length form, given by equation (1.59).

1.7 Two-electron atomic systems : CI method

Configuration Interaction (CI). The Hamiltonian of a two-electron atomic system is written as :

$$H = H_0(\mathbf{r}_1) + H_0(\mathbf{r}_2) + \frac{1}{|\mathbf{r}_1 - \mathbf{r}_2|} \tag{1.60}$$

where $H_0 = \mathbf{p}^2/2m + U(r)$. The central potential $U(r)$ is determined either through an Hartree-Fock procedure [6] or modelled by a model potential. The simplest two-electron systems are the Negative Hydrogen (H^-) and Helium (He), where the total number of electrons are two. For these systems, $U(r)$ is pure Coulombic potential, allowing thus H_0 to be written as $H_0 = \mathbf{p}^2/2m - Ze^2/r$ ($Z = 1$ for H^- and $Z = 2$ for He).

The eigenstates of isolated atomic systems can be written as simultaneous eigenfunctions of the $\mathbf{L}^2, \mathbf{S}^2, L_z, S_z$, operators. Solutions of the Hamiltonian H_0 are hydrogenic orbitals of the type (1.5). The Slater determinant

$\psi^{m,m'}_{nl,n'l'}$ is given by:

$$\psi^{m,m'}_{nl,n'l'}(\mathbf{r}_1,\mathbf{r}_2) = \frac{1}{\sqrt{2}} \begin{vmatrix} \phi_{nlm}(\mathbf{r}_1), & \phi_{n'l'm'}(\mathbf{r}_1) \\ \phi_{nlm}(\mathbf{r}_2), & \phi_{n'l'm'}(\mathbf{r}_2) \end{vmatrix} \tag{1.61}$$

In the above notation, we consider $m \equiv (m_l, m_s)$ the magnetic quantum number of orbital angular momentum and spin. The two-electron orbitals are constructed as a sum over all magnetic quantum numbers:

$$\Psi^{\Lambda}_{nl,n'l'}(\mathbf{r}_1,\mathbf{r}_2) = \sum_{all\ m} (-)^{l-l'} \left[(2L+1)(2S+1)\right]^{1/2}$$
$$\begin{pmatrix} l & l' & L \\ m_l & m'_l & -M_L \end{pmatrix} \begin{pmatrix} 1/2 & 1/2 & S \\ m_s & m'_s & -M_S \end{pmatrix} \psi^{m,m'}_{nl,n'l'}(\mathbf{r}_1,\mathbf{r}_2) \tag{1.62}$$

The eigenvalue equation to be solved is $H\Phi = E\Phi$. Expanding the states Φ on the two-electron orbitals:

$$\Phi^{\Lambda}_{n(E)} = \sum_{nl,n'l'} C^{\Lambda}_{n(E)}(nl,n'l')\Psi^{\Lambda}_{nl,n'l'}(\mathbf{r}_1,\mathbf{r}_2)\ , \tag{1.63}$$

and inserting in the eigenvalue equation, we are to a matrix diagonalization problem which gives the unknown coefficients $C^{\Lambda}_{n(E)}(nl,n'l')$. The quantity $|C^{\Lambda}_{n(E)}(nl,n'l')|^2$ gives the contribution of the configuration $(nl,n'l')$ in the state $\Phi^{\Lambda}_{n(E)}$. Diagonalization gives N_c states, where N_c is the total number of configurations $(nl,n'l')$. This procedure is repeated for different sets of quantum numbers S, L, M_L, M_S. A detailed discussion for the diagonalization of the H_0 matrix has been given by Chang [9]. The most intricate part of the relevant codes, developed by Tang X., Chang T-N and co-workers, concerns the computation of the configuration matrix elements $1/r_{12}$.

The eigenstates $\Phi^{\Lambda}_{n(E)} \equiv \Phi_{nLM}$, satisfy the eigenvalue equation:

$$H\Phi_{nlm} = E_{nL}\Phi_{nlm}. \tag{1.64}$$

When $E \leq 0$, Φ_{nLM} represents a bound state of energy E, indexed by the integer $n \equiv n(E)$, while $E < 0$ corresponds to a continnum states of the system. In two-electron atomic systems, the continnum has a more complex meaning, in comparison with that of a one-electron atom since there are various types of continuum, depending on the state of the residual ion or atom. One category of continnua is obtained when one of the electrons remains bound to the nucleus (in the ground state or an excited) and the other electron moves away the nucleus region. The other category of continuua corresponds to both electrons being ionized (double ionization).

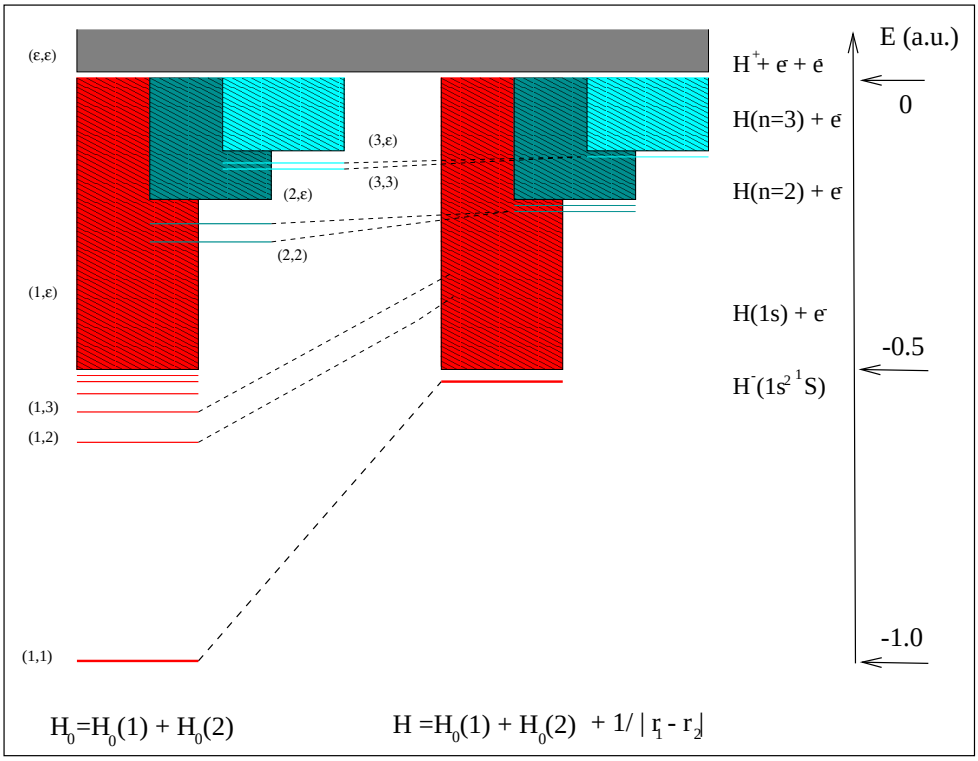

Figure 1.14: The influence of the CI in the states of the Negative Hydrogen is sketched.

Autoionizing states: Position (E_a) and widths (Γ_a). An important feature of the structure of two-electron atomic systems, such as He, H^- and the alkaline earths, is the existence of the so-called autoionizing states. These states corresponds to doubly excited states with energy above at least the first ionization threshold (see figure 1.14). Ignoring, the term $1/r_{12}$, the two-electron orbital $\Psi_{2s,2p} \equiv |2s2p\rangle$ has total energy larger than the lowest-energy orbital $|1s\varepsilon p\rangle$. The term $1/r_{12}$ introduces the so-called configuration interaction (CI) between the doubly-excited orbital $|2s2p\rangle$ and the entire continnum $|1s\varepsilon p\rangle$, leading thus to a strongly, energy-dependent continuum structure. In the CI spirit, the physical state of the system is a superposition over the discrete state $|2s2p\rangle$, the continuum $|1s\varepsilon p\rangle$ and any other configuration that gives rise to the ^1P two-electron continuum (restricted by selection rules).

$$|2s2p^1P\rangle = C(2s2p)|2s2p\rangle + \sum_{\varepsilon} C(\varepsilon)|1s\varepsilon p\rangle + ... \qquad (1.65)$$

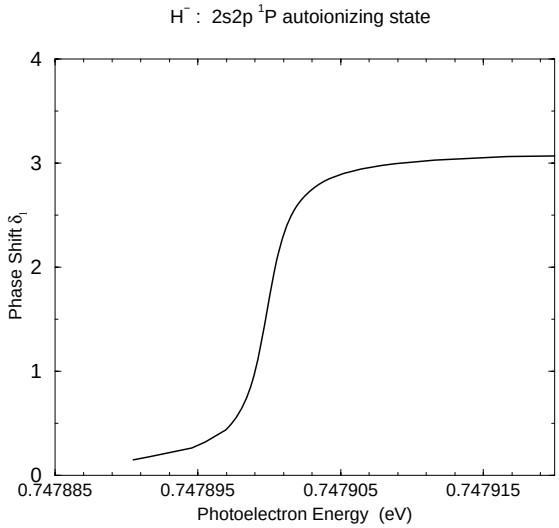

Figure 1.15: Scattering phase shift of the $|2s2p^1P\rangle$ autoionizing state of negative hydrogen

Therefore the atom initially excited in the $|2s2p\rangle$ state decays irreversibly to the $|1s\varepsilon p\rangle$ continuum through the interaction $1/r_{12}$. This decay, which is a radiationless process is called "autoionization". The decay rate Γ_a is related to the matrix element $\langle 2s2p|1/r_{12}|1s\varepsilon p\rangle$. Notice that, an additional effect of the $1/r_{12}$ interaction is the energy shift of the state $|2s2p\rangle$ [30], which however, depends on the basis.

The autoionizing structure, embedded in the continuum is manifested in various atomic quantities, such as the scattering phase shifts of the states around the structure [78], the probability density ρ_{1sp} for the $|1s\varepsilon p\rangle$ channel [10] (Fig.1.16), and the electric dipole transition cross section [30]. (Fig. 3.1). The scattering phase shift $\delta_l(k)$, changes rapidly by π for continuum energies below and above the autoionizing resonance. In photoionization studies the cross section of the process, multiphoton or not, often exhibits an asymmetric peak around the autoionizating structure. Accurate determination of the width Γ_a and the energy position E_a of the "isolated " autoionizing state[14] through the scattering phase shift can be done by fit-

[14]The term "isolated" means no other autoinizing state exists within an energy range of the order of the width Γ_a of the state.

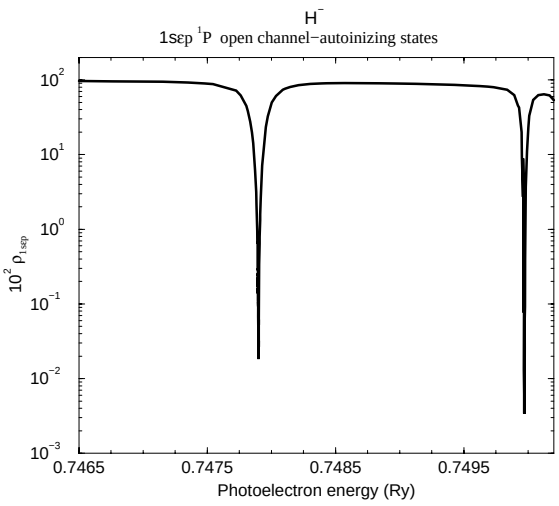

Figure 1.16: Probability density of the $|1s\varepsilon p^1P\rangle$ open channel of negative hydrogen.

ting the calculated [15] or measured data[16] with a function of the type [12], $\delta(E) = \sum_{i=0,2} a_i E^i + \tan^{-1}(\Gamma/2(E_a - E))$. After the diagonalization of the matrix, corresponding to the total Hamiltonian H, we have in hand the eigenenergies E_{nL} and the corresponding eigenstates Φ_{nL}. However, determination of the phase shifts $\delta_L(E_{nL})$ requires maching between the state representing the open channel and its asymptotic form $\sin(\phi(r) + \delta_L)$ (see equation 1.32). A technical complication arises with the fitting function, since the denominator diverges when $E = E_a$.

An alternative approach employed from Chang [10] fits the probability density ρ_{1sp} of the singly excited ionized channel. The advantage of fitting the probability density ρ_{1sp} instead of the phase shift is that the necessary data (which are the coefficients $C_{nl,n'l'}$) are available from the diagonalization of H. Also, because of the symmetric nature of the variation of ρ_{1sp}, it is fitted easily by a Lorentzian function.

In figure 1.15, we plot the scattering phase shift as a function of the

[15] In practice, with our method, we obtain the necessary resolution in energy by choosing large box radius, for a dense discretazion of the continuum and varying it (the box radius R) slightly.

[16] For narrow resonances, the experimental energy resolution is inadequate for the detection of the resonance. Therefore, widths are in general more readily available from theoretical calculation than experiment data.

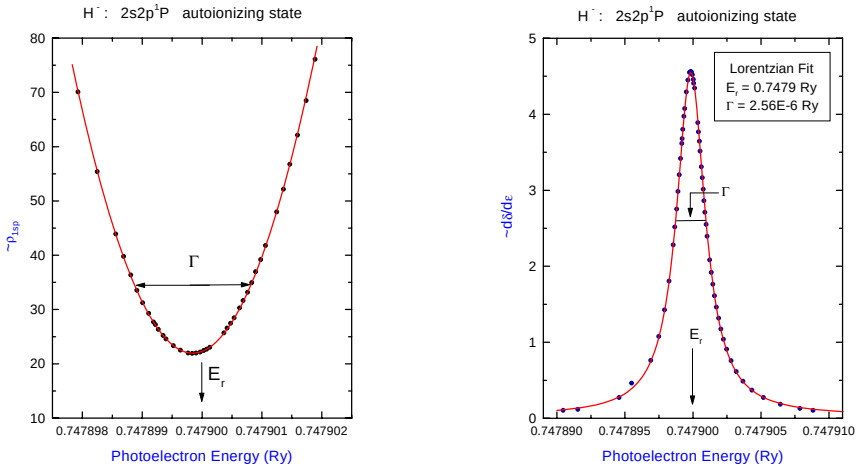

Figure 1.17: Fits of the probability density and the its inverse function with a Lorentzian type function.

photoelectron energy around the first resonance (denoted by $|2s2p\rangle$) of the $|2snp\rangle$ autoionizing series, belonging to the ^1P continuum of H^-. Higher in energy, there is another narrower and weaker autoionizing state. (Fig. 3.2). In figure 1.17 we plot a function analogous to $1/\rho_{1sp}$ and we fit the calculated data with a Lorentzian function :

$$y(E) = y_0 + \frac{A}{\pi}\frac{\Gamma_a/2}{(E-E_a)^2 + (\Gamma_a/2)^2}. \qquad (1.66)$$

The results of fitting gives for the width[17], $\Gamma_a = 1.28\,10^{-6} a.u$ and for the position $E_a = 0.7479 Ry$, which are in very good agreement with other theoretical and experimental results.

Electron correlation. In the CI procedure, the description of a two-electron atomic system (i.e. H^-,He and alkaline earths (K,Mg,..)), as mentioned earlier, begins with the construction of a set of basis functions ($\Psi^{\Lambda}_{nl,n'l'}$), eigenstates of the total angular momentum and spin. These basis functions are properly antisymmetrized products of one-electron functions ($\phi_{nlm}(\mathbf{r}_1), \phi_{n'l'm'}(\mathbf{r}_2)$), containing the dependence on the electron's coordinates, in a separated form. Although, a certain amount of electron correlation has been included in the two-electron function, because of its antisymmetrized nature, in general it is not accurate since treats the two electrons

[17] Note that $\hbar/\Gamma_a = \hbar/2.56\,10^{-6} Ry = \hbar/3.48\,10^{-5} eV \sim 10^{-10} sec$

in a separate manner. This formulation, assumes that each of the electrons moves separately, in one-electron orbitals with no other interaction between them, except the exchange interaction. The existence of the Coulomb interaction term $1/r_{12}$, in the Hamiltonian, however, forces the electrons to move to a distance somewhat larger than the zeroth order wavefunction ($\Psi^{\Lambda}_{nl,n'l'}$), would predict. Thus, in most cases the incorporation of the configuration interaction (CI) term is critical for a sufficient description of a two-electron wavefunction. In general, the contribution of this term to the total energy of the atom is much smaller than the contribution due to the zeroth-order wavefunction. Nevertheless, as experience shows, this interaction changes drastically the atomic structure and the properties of the interaction a two-electron atomic system with electromagnetic (EM) fields, in comparison with those of a one-electron atom. If the zeroth-order two-electron orbital wavefunctions are $|a\rangle, |b\rangle$ then the configuration interaction modifies these orbitals as follows:

$$|\psi_a\rangle = |a\rangle + \sum_{b \neq a} \frac{\langle a|1/r_{12}|b\rangle}{\omega_a - \omega_b} \tag{1.67}$$

For most atomic systems, not all of the terms of the sum are significant in magnitude and only a finite number of terms is sufficient for the convergence of the sum. Note that, even if the matrix element is quite small, the relevant term can contribute significantly in the sum if $\omega_a \sim \omega_b$, corresponding to nearly degenerate configurations.

The extreme example of a strongly correlated system, is the negative hydrogen (H^-), where its formation is imposible without the electron-electron (e-e) interaction. Although, from an academic point of view, including an infinite number of the proper configurations $(nl, n'l')$ the two-electron wavefunction is exact, in practice the convergence of the CI series is very slow. This is the main drawback of the CI method, due to the initial selection of separation of the electrons' coordinates. On the other hand, the most important advantage of the CI approach over other methods[18] is its simplicity and its straightforward application to a many-electron atomic system and time-dependent SE.

Because of the limited memory space disc and computing time, special attention should be given to the selection of the involved two-electron configurations $(nl, n'l')$ for the construction of the basis set. From angular

[18]Other common methods for treating two-electron atomic systems are the complex-coordinate rotational method, the pseudostate close-coupling method, the R-matrix theory, the hyperspherical-coordinate method the model potential etc.

momentum and parity conservation arguments, CI is non-vanishing for the configurations $|a\rangle, |b\rangle$, when :

1. $|a\rangle, |b\rangle$, belongs to the same total angular momentum,
2. For LS-coupling[19] (ignoring spin-orbit coupling) $|a\rangle, |b\rangle$, have the same total spin and total angular momentum.
3. $|a\rangle, |b\rangle$, have the same parity given by $(-1)^{l_a+l_b}$,

There are also some qualitative criteria, which one can follow for the optimum choice of the configurations. The quantity which gives the strength of CI between two configurations $|a\rangle, |b\rangle$, is the matrix element $\langle a|1/r_{12}|b\rangle$, which leads to an integration of the one-electron orbitals over the entire space.

The angular distibution of the one-electron wavefunctions (determined by the partial angular momentum l, l') is an important parameter for the value of the overlapping integrals. Consider, for instance, the configuration $|2p^2\rangle$ which leads to the symmetries ^1S,^1D,^3P. The correlation energy for the state ^1S is larger in comparison with the other symmetries because the p-electrons are "closest" in distance ($\langle r_{12}\rangle_{^1S} < \langle r_{12}\rangle_{^1S}, \langle r_{12}\rangle_{^1S}$). Also, the correlation energy of the configuration $|2p^2\rangle$ is larger than $|2s2p\rangle$ where the relevant overlapping functions do not "match".

The principal number n is another parameter for the estimation of the overlapping integral. Bound-bound (BB) configurations are expected to have much larger values than bound-continuum (BC) and continuum-continuum (CC) configurations. This happens because the relevant functions have their maxima at different regions of space. However, it is possible a CI to have significant value when the configurations involved have very small energy difference (nearly degenerate configurations).

Finally, the choice of the basis is not unrelated to the atomic system under consideration. For example, for Helium the ratio of the correlation energy[20] to the "exact" energy (E_{corr}/E_{exact}) of the ground state is about 0.014 while in H^- is about 0.08 [31]. Note here, that the central potential of atomic systems increases proportional to Z, while the configuration interaction matrix element $\langle a|1/r_{12}|b\rangle$ is independent of Z. As expected, this ratio decreases rapidly for the heavier elements, since the atomic charge Z increases. This suggests a very slow convergence for the accurate determi-

[19] If spin-orbit coupling is taken into account $\sim$ **LS** introduces an aditional CI between the configurations. This spin-orbit CI couples configurations, with different $\mathbf{J} = \mathbf{L}+\mathbf{S}, M_J$ as well as n, n'.

[20] The correlation energy, in the CI context, is defined as the difference between the energy of the zeroth-order two-electron wavefunction and the "exact" value, $E_{corr} \equiv E_{exact} - E_0$.

nation of the ground state of H^- in comparison other two-electron atomic systems; And this is the case. The ground state of negative hydrogen is a strongly correlated state (as mentioned, its existence is imposible without the $1/r_{12}$ e-e interaction) and its converged calculation demands even the inclusion of CC configurations, except the BB and BC configurations. A very careful analysis of the importance of the CC configurations in the formation of the $|1s^2.^1S^e\rangle$ and $|2p^2.^1P^e\rangle$ states of negative hydrogen[21] has been presented by Chang and Wang [84]. They have found among other things that the CC configurations contribute about 15% to the ground state energy of the H^-.

Within the method we use, photoionization studies, where the inclusion of the continuum states is inevitable for the correct treatment of the atom-field interaction, lead to the choice of large box radius, thus making the procedure much more demanding than simple calculations of bound state properties. For a radius box of about $R = 1000\, a.u.$, even with the inclusion of about 2.000 configurations, the calculated ground state energy differs by about 16% from that calculated by Pekeris[22] [63]. Improvement of the ground state energy is achieved by increasing either the total number of the configurations involved or the highest partial angular momentum l, l'. The convergence of the ground state energy for such large boxes, however, is extremely slow. Adoption of an appreciably smaller box $i.e. R \sim 20 a.u.$ gives easily a very accurate energy for the ground state of H^-.

Checking the results A calculation has converged, when upon varying (usually increasing) the basis-set no further change of the calculated quantity takes place. Such parameters are, within the CI method, the total number of configurations and the highest partial angular momentum. For the B-splines approach, more specifically, such parameters can be the box radius, the order and the number of B-splines or the knot distribution.

A very useful atomic quantity is the oscilator strength f of a dipole transition from an initial state $a(^{2S+1}L_a)$ to an other state $b(^{2S+1}L_b)$. For the LS-coupling approximation these f-values are defined as [9]:

$$f_l = \frac{2}{3}\Delta E \frac{|\langle a|\,(\mathbf{r}_1 + \mathbf{r}_2)\,|b\rangle|^2}{2L_a + 1}, \tag{1.68}$$

$$f_v = \frac{2}{3\Delta E} \frac{|\langle a|\,(\nabla_1 + \nabla_2)\,|b\rangle|^2}{2L_a + 1}, \tag{1.69}$$

[21] A similar study has been conducted by Charlotte Fischer for the H^-, He, Li^+ ground states.

[22] He used variatonal wavefunctions containing explicitly the interparticle coordinates (or Hylerraas coordinates) in the two-electron wavefunction, treating thus in a very direct way the correlation between the two electrons.

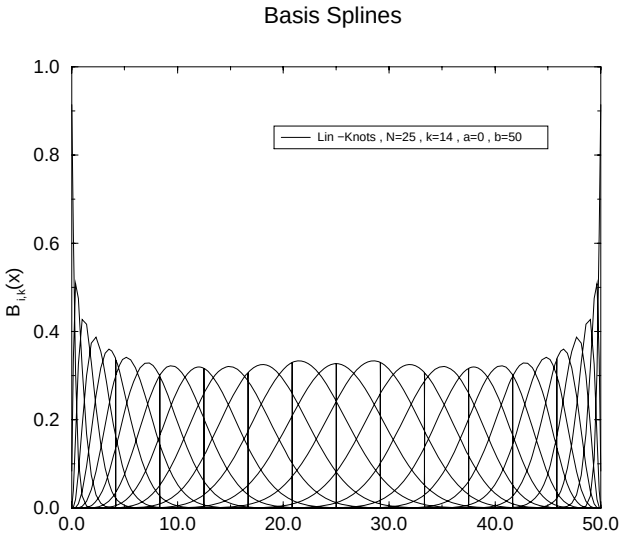

Figure 1.18: B-splines polynomials. Parameters are given in the figure.

with $\Delta E = E_b - E_a$ in a.u. . The f_l, f_v quantities are the length and velocity forms, respectively. If the wavefunctions are exact, these values will be equal[23].

1.8 Appendix: B-splines, summary

For the construction of a B-splines basis set, the specification of a knot sequence $t_i, t_{i+1} > t_i$ inside an interval $[a, b]$ is needed. Then the B-splines of order-k are defined through a recursive procedure:

$$B_{i,1}(x) = \begin{cases} 1, & t_i \leq x \leq t_{i+1} \\ 0, & \text{otherwise} \end{cases} \tag{1.70}$$

and

$$B_{i,k}(x) = \frac{x - t_i}{t_{i+k-1} - t_i} B_{i,k-1}(x) + \frac{t_{i+k} - x}{t_{i+k} - ti + 1} B_{i+1,k-1}(x)\,. \tag{1.71}$$

From the above definitions, we see that the i-Bspline of order-k is a polynomial of order $k-1$, non-vanishing only for points inside the interval $[t_i, t_{i+k}]$.

[23] There is an important exception to that rule when the wavefunctions are calculated by an l-dependent model potential. See relevant discussion in the section that deals with the model potential.

It is possible to define a knot sequence, allowing multiplicitly of the knot points. For our purposes the end points have k-multiplicitly which means ($t_1 = t_2 = ... = t_k = 0$) and ($t_n = t_{n+1} = ... = t_{n+k} = 0$).

In Figure 1.18 we plot the B-splines for $n = 25, k = 14, a = 0, b = 50$ and linear knot distribution.

Chapter 2

Atoms and E/M fields

2.1 Classical theory of radiation

Maxwell-Lorentz E/M field theory. In the presence of the charge density $\rho(\mathbf{r},t)$ and the corresponding current density $\mathbf{j}(\mathbf{r},t) = \rho(\mathbf{r},t)\mathbf{v}$, where $\mathbf{v}$ is the velocity of the charge density, the generated electromagnetic(E/M) field is described by two vector fields, namely the electric $\mathbf{E}(\mathbf{r},t)$ and the magnetic field $\mathbf{B}(\mathbf{r},t)$, interrelated through the M-L equations:

$$\nabla\mathbf{E} = 4\pi\rho \quad , \quad \nabla\times\mathbf{E} = -\frac{1}{c}\partial_t\mathbf{B}, \tag{2.1}$$

$$\nabla\mathbf{B} = 0 \quad , \quad \nabla\times\mathbf{B} = -\frac{1}{c}\partial_t\mathbf{E} + \frac{4\pi}{c}\mathbf{j}. \tag{2.2}$$

An additional basic equation can be derived from the M-L equations, the continuity equation for the charge-current density: $\nabla\mathbf{j} + \partial_t\rho = 0$. Given the E/M field $(\mathbf{E},\mathbf{B})$, the motion of a point-like electric charge, $\rho = e\delta(\mathbf{r}-\mathbf{r}_i)$ is determined via the Lorentz EM force, $\mathbf{F}_e = e\,(\mathbf{E} + \mathbf{v}\times\mathbf{B})$, acting on it. In the non-relativistic limit (low particle velocities) the equation of motion will be the third Newton law, $m\ddot{\mathbf{r}} = F_e$.

A very convenient alternative description for the E/M field is possible through the introduction of two potentials, the vector $\mathbf{A}(\mathbf{r},\mathbf{t})$ and the scalar $\Phi(\mathbf{r},t)$ potentials related with the electric and magnetic field components with:

$$\mathbf{E} = -\nabla\Phi - \frac{1}{c}\mathbf{A}, \qquad \mathbf{B} = \nabla\times\mathbf{A}. \tag{2.3}$$

The differential equations which the E/M potentias satisfy $\nabla^2\mathbf{A} - c^{-2}\partial_{tt}\mathbf{A} + \nabla\left(\nabla\mathbf{A} + c^{-1}\partial_t\Phi\right) = (4\pi/c)\mathbf{j}$, $\nabla^2\mathbf{\Phi} - c^{-1}\partial_t\nabla\mathbf{A} = 4\pi\rho$ are derived from the M-L equations and equations (2.3). It is important to note that given the

potentials $\mathbf{A}, \Phi$ we can determine the electric and the magnetic field using (2.3), but the opposite is not possible. It is obvious from these equations that also the potentials $(\mathbf{A} + \nabla\chi(\mathbf{r},t), \Phi + c^{-1}\partial_t\chi(\mathbf{r},t))$ can produce the same $(\mathbf{E},\mathbf{B})$, with $\chi(\mathbf{r},t)$ being an arbritary function. The specific choice of the arbitrary function χ is called gauge selection and utilizing this freedom it is possible, depending on the physical context we work in, to make the relevant equations more convenient to use. The invariance of the E/M field under the transformation:

$$\mathbf{A} \to \mathbf{A} + \nabla\chi(\mathbf{r},t), \qquad \Phi \to \Phi + \frac{1}{c}\partial_t\chi(\mathbf{r},t) \tag{2.4}$$

is called gauge invariance of the E/M field. The most important gauges in use are the so-called Lorentz and Coulomb(or radiation) gauge. Since the Coulomb gauge is more convenient for problems that involve the long-distance part of the E/M field (the radiation part), the quantum theory of radiation is developed mainly in this gauge.

Radiation gauge or transverse gauge. In this gauge, we require the vector potential $\mathbf{A}$ to be transverse with respect to the propagation direction of the E/M wave $\nabla \cdot \mathbf{A} = 0$. E/M potential then satisfy the following equations:

$$\nabla^2\mathbf{A} - \frac{1}{c^2}\frac{\partial^2\Phi}{\partial t} + \frac{1}{c}\partial_t\nabla\Phi = \frac{4\pi}{c^2}\mathbf{j} \qquad \nabla^2\mathbf{A} = -4\pi\rho \tag{2.5}$$

Notice that the second equation is the familiar Poisson equation.

2.2 Short laser pulses

For fields involving a large number of photons, in a more or less coherent state,the classical description is used as developed in the previous section. We can, therefore, write for a linearly polarized field generated by a laser, ignoring phase fluctuations:

$$E(t) = \frac{1}{2}\mathcal{E}(t)e^{i\omega_L t} + \frac{1}{2}\mathcal{E}^*(t)e^{-i\omega_L t}, \tag{2.6}$$

where the variaton of $\mathcal{E}(t)$ with respect to time is very small during times of the order $\sim 1/\omega$ ($|\dot{\mathcal{E}}(t)| \ll \omega|\mathcal{E}(t)|$). Representing the electric field this way, it follows that this field is not strictly monochromatic but consists of a band around the central frequency ω_L, extended over a range (Fourier bandwidth) of the order $\Delta\omega \sim \tau_L$, where τ_L is the duration of the pulse.

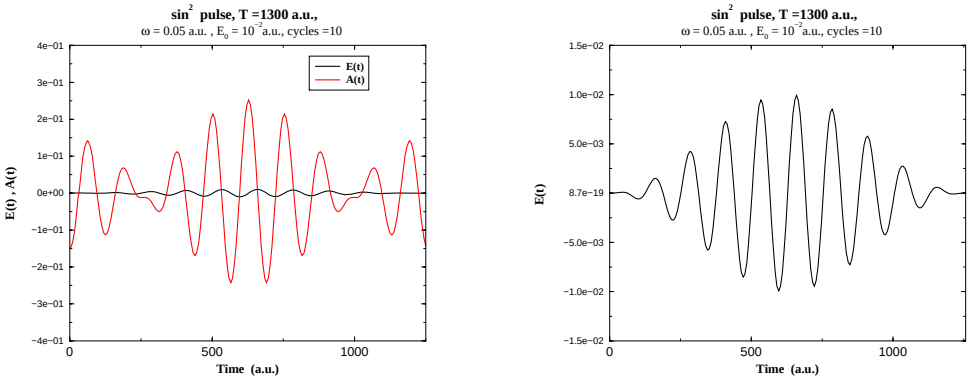

Figure 2.1: Electric and vector potential of a $\sin^2$ pulse.

The concept of the duration for a laser pulse is a critical parameter for E/M processes (multiphoton or not) which is necessary to take into account for the analysis of either theoretical or experimental data. Two examples of this kind (where the duration of the pulse plays a chief role in the explanation of the experimental results) are the resonance fluoresence for weak field (see pages 53-57 of reference [68]) and the above threshold ionization (ATI) of atomic systems in strong laser fields. Briefly, in fluorensence the decay of an excited state, of natural width Γ in a two level system (TLS) leads to coherent or incoherent radiation depending on the broadband ($\Gamma \ll \Delta\omega$) or narrowband ($\Delta\omega \ll \Gamma$) excitation. Here with the term "coherent" we mean that the emitted pulse has the same shape as the primary field. Many different envelopes can be adopted for the realization of the laser pulses, although for practical reasons, from the computational point of view two forms are in common use, namely, the Gaussian and the $\sin^2$ form.

$$\mathcal{E}(t) = e^{-(t/T)^2} \qquad -5T \leq t \leq 5T \qquad \text{gaussian} \tag{2.7}$$

$$\mathcal{E}(t) = \sin^2 \frac{\pi t}{T} \qquad 0 \leq t \leq T, \qquad \sin^2 \tag{2.8}$$

The $\sin^2$ pulse is used, mainly because of the strict finiteness of the pulse inside the interval $[0, T]$, while the gaussian pulse, has in principle an infinite extent. Note that, results from different pulses are comparable, when the E/M energy transferred to the atomic system is the same, From elemenatry analysis, it is verified that, when the duration of a square pulse is T, the duration of the $\sin^2$ pulse should be $2T$ and the duration of the gaussian pulse $0.6T$.

2.3 Schrödinger Equation of atoms in E/M fields

The Hamiltonian of charged particles, in the non-relativistic limit (low relative to c velocities, small interaction volume $\sim \alpha_0^3$) is given by the relation:

$$H_{a\tau} = \sum_i \frac{\mathbf{p}_i^2}{2m_i} + U_c, \tag{2.9}$$

where $\mathbf{p}_i$ is the momentum of the particle-i and U_c represents the static E/M interaction between nucleus -electrons and electron-electrons. For an atomic system subject to an external E/M field $(\mathbf{A}_e(\mathbf{r},t), \Phi_e(\mathbf{r},t))$, the new hamiltonian of the total system (atom + field) is obtained through the minimal substitution, $(H \rightarrow H + e\Phi$ and $\mathbf{p} \rightarrow \mathbf{p} - (e/c)\mathbf{A}_e)$):

$$\begin{aligned} H &= \sum_i \frac{\mathbf{p}_i - (e/c)\mathbf{A}_e(\mathbf{r_i},t)}{2m_i} + U_c + e\Phi(\mathbf{r}_i,t) + H_R \\ &= H_{a\tau} + \sum_i \left[-\frac{e}{mc}\mathbf{p}_i\mathbf{A}(\mathbf{r}_i,t) + \frac{e^2}{2mc^2}\mathbf{A}^2(\mathbf{r}_i,t) \right] + H_R \end{aligned} \tag{2.10}$$

The Coulomb gauge is chosen, with zero scalar potential ($\nabla\mathbf{A} = \Phi = 0$) for reasons explained in the previous chapter. We have also used implicitly the property that in this gauge $\mathbf{pA} = \mathbf{Ap}$. With H_R, we denote the Hamiltonian of the E/M field, but dealing with strong laser fields it is not necessary to quantize the laser field. In the dipole approximation, the terms H_R and A^2 involve only field observables having thus no effect to atomic parameters. This allows to us to ignore these terms. The case of one-active electron is now assumed, since in the present section the primary interest is on aspects of the interaction term between atom and field. We write, therefore the total Hamiltonian as $H = H_{a\tau} + H_I + H_R$, with $H_I = -(e/mc)\mathbf{pA}_e((\mathbf{r}),t))$ with the vector potential being represented by $\mathbf{A}_e = \hat{e}A_0 e^{i(kr-\omega t)} + \hat{e}^\star A_0 e^{i(kr+\omega t)}$.

Longwavelength or dipole approximation. For optical frequencies ($\sim 10^{15} sec^{-1} \sim eV$ the corresponding wavelength (λ) will be much larger than the atomic radius ($2\pi\alpha_0/\lambda = k\alpha_0 \ll 1$), with α_0 being the Bohr radius. The spatial extent of the E/M field for a region of the order of the atomic radius ($R_{a\tau} \sim nZ\alpha_0$) is practically constant. Expanding the term $e^{i\mathbf{kr}}$ we keep only the first term since ($\mathbf{kr} \ll 1$) which is equivalent to the substitution $\mathbf{A_e}(\mathbf{r},t) \rightarrow \mathbf{A_e}(0,t)$, with the center of mass for the atom located at the origin of the axes.

It is worthwhile to note here that within this approximation, we have for the magnetic field, $B_e = \nabla \times \mathbf{A_e}(0,t) = 0$ which implies that phenomena

concerning magnetic effects are neglected. This approximation is, nevertheless, well justified since for optical frequencies magnetic interactions are $\alpha^2 \sim 10^{-4}$ times smaller than the electric ones. Therefore, the following relations holds for the E/M field :

$$\mathbf{A}(t) = \hat{e}A_0(t)cos(\omega t), \tag{2.11}$$

$$\mathbf{E}(t) = -\frac{1}{c}\partial_t \mathbf{A}, \quad \mathbf{B} = 0. \tag{2.12}$$

We assume the general case of a non-monochromatic field in the sense that we have a time-dependent pulse (Fourier limited bandwidth).

Velocity gauge. At this point (after making the dipole approximation), we are able to reduce further the expression for the atom-field hamiltonian H. The quantities $(e^2/2mc)\mathbf{A}^2$ and $H_R = \int d^3\mathbf{r}\mathbf{E}^2/4\pi$ does not include any atomic operator, and in combination with the assumption that the external field is so strong that its state is not changed by the interaction with the atom, it is possible to ignore them since they represent a constant term of the total hamiltonian. More formally, making the unitary transformation, $\psi \rightarrow T\psi$, and $H \rightarrow THT^{\dagger}$ with $T = exp(-\frac{e^2}{2mc\hbar}\int_0^t dt' A^2 + \frac{i}{\hbar}H_R t)$ we have for the atom-field hamiltonian, $H = H_{a\tau} + H_I$ with the interaction term, known as velocity-gauge interaction form, being:

$$H_I = -\frac{e}{mc}\mathbf{p}\mathbf{A}(t) \tag{2.13}$$

Length gauge. Another expression, equivalent to the velocity-gauge interaction, within the dipole approximation, and with respect to the observable quantities, but with different computational properties, is the so-called length-gauge interaction term introduced by Pauli-Zieneu[1]. Having in mind equation (2.11), assume a gauge transformation $\chi(\mathbf{r}, t) = -rA(0, t)$ with the results (easily verified through equations) (2.4), $\mathbf{A} = 0$ and $\Phi = \mathbf{r}\mathbf{E}(t)$. For the length gauge the interaction term takes the form:

$$H_I = -\mathbf{r}\mathbf{E}(t). \tag{2.14}$$

2.4 Dirac Equation of atoms in E/M fields

Assuming elementary familiarity with the Dirac Equation (DE), as presented in the textbook of Sakurai [68], we shall derive the hamiltonian of an atom with one active electron (one-electron atom) of charge $q = -e$, subject to a

[1] Pauli-Zieneu,1931

static, central Coulomb potential (representing the average field 'seen' from the nucleus and the other electrons) and to an external E/M field. Again, considering strong fields we assume E/M fields in their classical form. As in the Schrödinger equation, we assume nucleus infinitely heavy, motionless and point-like, although the last approximation is no longer valid for heavy atoms. The incorporation of finite volume of the nucleus charge distribution can be introduced at a later step.

The natural procedure for deriving the Hamiltonian form of charged particle subject to classical E/M fields is to start from the covariant form of the DE. Adopting, for the time being, the four-dimensional space of special relativity (Mincofski space), where its with coordinates are defined as, $x^\mu = (x^0, x^1, x^2, x^3) \equiv (ct, \mathbf{r})$ we have for the DE:

$$[\gamma_\mu (p^\mu + A^\mu) - c]\,\psi(x) = 0, \tag{2.15}$$

where $A^\mu(x) = (\Phi(x)/c, \mathbf{A}(x))$ is the four-dimensional E/M potential including all the E/M fields and $p^\mu = i\partial/\partial x^\mu = (\partial/\partial(ct), \nabla)$, is the four-dimensional momentum of the electron. With $\gamma_\mu, \mu = 1,2,3,4$ we denote 4×4 matrices satisfying the conditions $\{\gamma_\mu, \gamma_\nu\} = \gamma_\mu\gamma_\nu + \gamma_\mu\gamma_\nu = 2g_{\mu\nu}$, with $g_{\mu,\nu}$ matrix having only four non-vanishing elements $g_{00} = -g_{11} = -g_{22} = -g_{33} = 1$. Multiplying equation (2.15) by $c\gamma_0$ we obtain the Hamitonian form of the DE :

$$i\frac{\partial}{\partial t}\psi(x) = \left\{c\alpha\,[\mathbf{p} + e\mathbf{A}(x)] - e\Phi(x) + \beta mc^2\right\}\psi(x) \tag{2.16}$$

where α, β are matrices defined by equation (1.8). The E/M field can be separated as $A = A_c + A_e = (\Phi_c + \Phi_e, \mathbf{A}_c + \mathbf{A}_e)$ where the first part A_c represents the nucleus-electron and electron-electron average potential and A_e the external E/M field in Coulomb gauge ($\nabla\mathbf{A}_e = \Phi_e = 0$). The A_c field ignores magnetic effects, and it is legitimate to choose $\mathbf{A}(x) = 0$. The static field satisfiying the Poisson equation $\nabla^2\Phi(x) = -\rho(\mathbf{r})/\epsilon_0$, with ρ the classical nucleus charge distribution, influenced by the electrons surrounding the nucleus. From the above we are led to the final form of the Hamiltonian:

$$\begin{aligned} i\frac{\partial}{\partial t}\psi(\mathbf{r},t) &= \left\{\left[c\alpha\mathbf{p} + \beta mc^2 + U_c(r)\right] - e\alpha\mathbf{A_e}(\mathbf{r},t)\right\}\psi(\mathbf{r},t) \quad (2.17)\\ &= [H_D + H_I(t)]\,\psi(\mathbf{r},t), \quad (2.18)\end{aligned}$$

with H_D the free-field Dirac Hamiltonian, $H_I = -e\alpha\mathbf{A_e}(\mathbf{r},t)$ the interaction between the electron and the external E/M field[2] and $U_c(r) = -e\Phi_c(r)$.

[2]Note here the similarity of the interaction term with that of the non-relativistic limit, $-e\alpha A \overset{c\alpha\to\mathbf{p}}{\to} -epA/c$

2.5 Time Dependent Dirac Equation, (TDDE)

The basic idea of the method is similar in spirit to that for the non-relativistic limit (TDSE). The TDDE is given by the equation $i\partial_t\Psi(\mathbf{r},t) = (H_D + H_I)\Psi(\mathbf{r},t)$, with H_D the free-field Dirac hamiltonian, and $H_I = -e\alpha\mathbf{A_e}(\mathbf{r},t)$ the interaction with the classical external field in Coulomb gauge. We expand $\Psi(\mathbf{r},t)$ in the basis of the eigenstates of the field-free Hamiltonian H_D,

$$\Psi(\mathbf{r},t) = \sum_{nkm_j} b_{nkm_j}(t)\psi_{nkm_j}(\mathbf{r}). \tag{2.19}$$

The quantum numbers take the values $n = \pm1, \pm2... \pm N$, $k = \pm1, \pm2...$ and $m_j = \pm1/2$. The negative sign for the quantum number n corresponds to negative energy state and the positive sign to positive energy states. Substituting equation (2.19) in the TDDE we obtain a system of coupled first order differential equations of the unknown coefficients $b_{nkm_j}(t)$:

$$\begin{aligned} i\frac{d}{dt}b_{nkm_j} &= \sum_{n',k'}\left[E_{nkm_j}\,\delta_{nn'}\delta_{kk'}\delta_{m_jm_j'} - V_{nkm_j,n'k'm_j'}(t)\right]b_{n'k'm_j'}, \\ & |b_{n=1,k=-1,m_j=\pm1/2}(t=0)|^2 = 1. \end{aligned}$$

The initial condition for the coeeficient is of the form,
$b_{nkm_j}(0) = \delta_{nn_0}\delta_{kk_0}\delta_{m_jm_{j_0}}$, where $\psi_{n_0k_0m_{j_0}}$ is the initial state of the atomis system for time $t = 0$. The matrix element $V_{nkm_j,n'k'm_j'}(t)$ represent transitions between Dirac states and their calculation for the general case has been developed in a previous section. Introducing, however, the dipole approximation ($\mathbf{kr} \ll 1$) for the external field and assuming linear polarization, the TD equations simplify further, since the possible paths for the different initial states with respect to the magnetic quantum number $m_j = \pm1/2$ decouple and become independent of each other. We can proceed, by considering the magnetic number m_j fixed during the process, and in addition the final results independent of the initial value of m_j, since either the eigenenergies or the interaction matrix elements are independent of the m_j. We are also able to exclude the negative energy states (restricting n to positive values only), which is a well justified approximation since their effects are significant for photon energies equal the rest mass of electron ($\sim mc^2$). We rewrite therefore the relevant equations as following:

$$\Psi(\mathbf{r},t) = \sum_{nk} b_{nk}(t)\psi_{nk}(\mathbf{r}) \tag{2.20}$$

and

$$i\frac{d}{dt}b_{nk} = \sum_{n'k'}\left[E_{nk}\,\delta_{nn'}\delta_{kk'} - V_{nk,n'k'}\right]b_{n'k'}, \quad (2.21)$$
$$|b_{n=1,k=-1}(t=0)|^2 = 1,$$

with $n = 1, 2...N$, $k = \pm 1, \pm 2, ...$ and m_j is considered to the fixed value $1/2$ or $-1/2$.

An additional simplification of the TTDE equations concerning the quantum number k comes from the selection rules for dipole transitions. For one photon transition within the dipole approximation and for linearly polarized light the change of the quantum number can be such that the relation $|\delta k| = 1, 2k$ holds true.

An alternative representation for the TTDE (2.24), making more evident its similarity with the corresponding TDSE equation is the following:

$$i\frac{d}{dt}b_{nk} = \sum_{n',k'}^{k>0}\left[E_{nk}\,\delta_{nn'}\delta_{kk'} - V_{nk,n'k'}\right]b_{n'k'}, \quad (2.22)$$
$$+ \sum_{n',k',m'_j}^{k<0}\left[E_{nk}\,\delta_{nn'}\delta_{kk'} - V_{nk,n'k'}\right]b_{n'k'}, \quad (2.23)$$
$$|b_{n=1,k=-1}(t=0)|^2 = 1.$$

In practice, the maximum value for the quantum number k is a criterion of the convergence of the solutions, depending, strongly, on the peak intensity of the field.

2.6 Appendix: pA versus -rE gauge

In the velocity gauge we have for the TDSE,

$$i\frac{\partial}{\partial t}\psi^V(\mathbf{r},t) = \left(H_{a\tau} + H_I^V\right)\psi^V(\mathbf{r},t), \quad (2.24)$$

with $H_I^V = -c^{-1}\mathbf{pA}$ being the interaction term and ψ^V the state of the system. Making the gauge transformation $\chi(\mathbf{r},t) = -\mathbf{rA}(t)$ we have for the transformed TDSE,

$$i\frac{\partial}{\partial t}\psi^L(\mathbf{r},t) = \left(H_{a\tau} + H_I^L\right)\psi^L(\mathbf{r},t), \quad (2.25)$$

through $H_I^L = -\mathbf{rE}$ the interaction term and the state ψ^L of the system in the length gauge. The two wavefunctions are connected with the relation,

$$\begin{aligned} \psi^L(\mathbf{r},t) &= e^{\frac{i}{\hbar}e\chi(\mathbf{r},t)}\psi^V(\mathbf{r},t) \\ &= e^{-\frac{i}{\hbar}e\mathbf{rA}(t)}\psi^V(\mathbf{r},t). \end{aligned} \tag{2.26}$$

In both cases, the 'pure' atomic operator $H_{a\tau}$ has the same form $H_{a\tau} = \mathbf{p}^2/2m + V_c(r)$. In the length gauge $H_{a\tau}$ represents the energy operator of the system, defined as the sum of the kinetic and potential energies of the particles constituting the system (in the present case we assume one particle). In the velocity gauge, however, that is no longer true. In other words, within the velocity gauge, the solution of the eigenvalue problem for the $H_{a\tau}$ does not give, the eigenstates or the eigenenergies of the unperturbed system. At the same time the hamiltonian that governs the time-evolution of the interacting system is the operator $H_{a\tau} + H_I^V$ in velocity gauge and $H_{a\tau} + H_I^L$ in the length gauge.

For the solution of the TDSE, we initially solve the unperturbed problem, $H_{a\tau}\psi_{nl}(\mathbf{r}) = \varepsilon_{nl}\psi_{nl}(\mathbf{r})$, as we have already discussed, and then we expand the time-dependent wavefunction $\Psi(\mathbf{r},t)$ in terms of the unperturbed eigenstates $\psi_{nl}(\mathbf{r})$ in order to substitute them to the TDSE. The relevant equations are the following:

Length gauge:

$$\Psi^L(\mathbf{r},t) = \sum_{nl} b_{nl}^L(t)\psi_{nl}(\mathbf{r}) \tag{2.27}$$

$$b_{nl}^L(t)\,, = \langle\psi_{nl}|\Psi^L(\mathbf{r},t)\rangle \tag{2.28}$$

$$i\frac{d}{dt}b_{nl}^L\,, = \sum_{nl}\left[\varepsilon_{nl}\delta_{nn'}\delta_{ll'} - \langle nl|H_I^L|n'l'\rangle\right] b_{nl}^L\,, \tag{2.29}$$

Velocity gauge:

$$\Psi^V(\mathbf{r},t) = \sum_{nl} b_{nl}^V(t)\psi_{nl}(\mathbf{r}) \tag{2.30}$$

$$b_{nl}^V(t)\,, = \langle\psi_{nl}||\Psi^V(\mathbf{r},t)\rangle \tag{2.31}$$

$$i\frac{d}{dt}b_{nl}^V\,, = \sum_{nl}\left[\varepsilon_{nl}\delta_{nn'}\delta_{ll'} - \langle nl|H_I^V|n'l'\rangle\right] b_{nl}^V\,. \tag{2.32}$$

At first sight, a question arises at this point. It is an axiom of quantum theory that the observable quantities (experimentally measured quantities),

are gauge independent and this is valid for the probabilities $|\langle\psi_{nl}|\Psi(\mathbf{r},t)\rangle|^2$. It follows, that using either equations (2.29) or equations (2.32), the final results must be identical (ignoring computational rounding or truncated basis set errors). From the previous equations this is not obvious, since we know that for the matrix elements of the interaction term, the relation $\langle a|H_I^V|b\rangle = (\omega_L/(\omega_a-\omega_b)\langle a|H_I^L|b\rangle$ holds, where a, b are arbitrary eigenstates of the $H_{a\,\tau}$ operator, while at the same time we keep ε_{nl} the same. We expect therefore that in general the amplitudes $b_{nl}^V(t)$ and $b_{nl}^L(t)$ will be different. And this is indeed the case, as we shall see. Combining the expressions for the amplitudes $b_{nl}^V(t)$ and $b_{nl}^L(t)$ we obtain:

$$\begin{aligned} b_{nl}^L &= \langle\psi_{nl}|e^{-ira(t)}|\Psi^V(\mathbf{r},t)\rangle \\ &= \langle\psi_{nl}|\Psi^V(\mathbf{r},t)\rangle + \langle\psi_{nl}|\sum_{m\neq 1}\frac{(-ie\mathbf{r}\mathbf{A}(t))^m}{m!}|\Psi^V(\mathbf{r},t)\rangle \\ &= b_{nl}^V + \langle\psi_{nl}|\sum_{m\neq 1}\frac{(-ierA(t))^m}{m!}|\Psi^V(\mathbf{r},t)\rangle\,. \end{aligned} \tag{2.33}$$

For the above relations, we have used the expansion $e^{-i\mathbf{kr}} = 1-(i\mathbf{kr}+...)$. From the last relation, it is obvious that the coefficients b_{nl}^V and b_{nl}^L are different for every finite time t and therefore the same is true for their absolute squares, $|b_{nl}^V|^2$ and $|b_{nl}^L|^2$. If this is the case, why are the calculated observables such as ionization yields, photoelectron energy spectra (PES) and photoelectron angular distributions (PADs) (given by absolute squares of b_{nl}^L and b_{nl}^V the same no matter which gauge we use for our calculations?

The key idea is the initial condition for the external E/M field, its finite duration and the fact that the observables are calculated after the end of the pulse ($t\to\infty$). We use pulses such that the relation, $\lim_{t\to\pm\infty}\mathbf{A}(t) = \pi\mathbf{E}(0) = 0$ is valid which guarantees that the initial conditions for both gauges are the same and the E/M field vanishes[3] for $t\to\infty$. At the same time, we need the coefficients for times after the end of the pulse (in practice for times much longer than the full width half maximum (FWHM) of the pulse) and noticing that $\mathbf{r}\mathbf{A}(t\to\infty)\to 0$ it follows that $\langle\psi_{nl}|\sum_{m\neq 1}\frac{(-ierA(t))^m}{m!}|\Psi^V(\mathbf{r},t)\rangle\to 0$. Therefore, for the amplitudes b_{nl}^L and b_{nl}^V the following relation [4], holds

$$\lim_{t\to\infty} b_{nl}^L(t) = \lim_{t\to\infty} b_{nl}^V(t) \tag{2.34}$$

[3] This is not true for square pulses with sudden switching-on.

[4] The same can be viewed more quickly, noticing that, $\lim_{t\to\pm\infty}\Psi^L(\mathbf{r},t) = \lim_{t\to\pm\infty} e^{-i\frac{e\mathbf{r}\mathbf{A}(t)}{\hbar}}\Psi^V(\mathbf{r},t) = 1\cdot\lim_{t\to\pm\infty}\Psi^V(\mathbf{r},t)$

In practice, the vector potential needs to satisfy the boundary conditions, $\mathbf{A}(t_1) = \mathbf{A}(t_2) = 0$, with t_1 and t_2 any finite time, with respect to time for the results to be independent on the gauge used.

Note that, although the final amplitudes are the same, their time evolution is completely different with important practical consequences for the computation. It is well known that time-dependent calculations converge faster in the velocity gauge than in the length gauge [46, 90, 18].

Chapter 3

One, two and three-photon LOPT of H^-

3.1 Introduction

It has been known [4, 50, 60] for quite some time now that multiphoton ionization of atoms with radiation elliptically polarized can lead to photoelectron angular distributions (PAD) lacking the usual four-fold symmetry found under linearly or circularly polarized radiation. This effect is present in the fundamental description of the process in perturbation theory and has been identified to be connected to the non-zero value of the phase shift of the final continuum state. Formally the phase shift leads to a complex multiphoton transition amplitude which in turn combined with the ellipticity parameter produces terms which, depending on the values of the other parameters (such as radial matrix elements), can lead in general to a more or less asymmetric PAD. From the structure of the resulting expressions it is evident that if the phase shifts of all partial waves were zero (corresponding to plane waves) the asymmetry would disappear. The continuum state resulting from electron detachment of a negative ion might be thought of as coming as close to a plane wave as one can expect in a real system with a bound initial state. This aspect has been investigated experimentally by Blondel and collaborators who have produced extensive results on PAD's including elliptical polarization which has not shown any significant asymmetry. Is it because of a near plane wave character of the final state?
ATI adds a further aspect to this question. A multiphoton transition amplitude involving absorptions within the continuum, as ATI does, is by necessity complex because of the presence of poles within the continuum. This led

Lambropoulos and Tang [50] sometime ago, to the assertion that the asymmetry should be present in ATI even if all phase shifts were zero, which has to be understood as the limit to plane waves. As we shall see later on, that assertion was overenthousiastic and the actual situation is subtler. It was nevertheless that question in fact that motivated Blondel and collaborators to search for that asymmetry in negative ions including ATI in one case. It is against this background that we undertook the present work in negative Hydrogen.
Our chief objective was to explore in a quantitative setting the question of the asymmetry including ATI. Negative Hydrogen being a two-electron system poses serious demands on the calculations of multiphoton transitions as illustrated by previous work [65, 64, 56, 12, 82, 72, 25] on aspects of this system. Our approach has evolved as a side product of our work on the non-perturbative solution of the time-dependent Schrödinger equation for two-electron atoms in strong laser fields [90, 89, 91, 17], with the atomic structure handled in terms of L^2 discretized bases constructed as linear combinations of B-splines [73, 43]. The calculation of ATI through a discretized basis also requires the appropriate handling as has been discussed elsewhere[16], where a new versatile method applicable to any discretized basis has been shown to provide accurate results within perturbation theory, which is the case of interest here. Through a combination of the above techniques, we have been in the position to obtain results on 2 and 3-photon ionization including ATI over an extensive energy range which by a happy coincidence also covers the range of experimental data reported most recently by Zhao et al [92]. We have at the same time examined PAD's for polarization of varying degree of ellipticity and ,as discussed in the following sections, the asymmetry is in general present depending of course on the degree of ellipticity and the wavelength of the radiation, as expected to be the case. One of the chief advantages of and motivation for studies in negative hydrogen is its fundamental significance as a negative ion and at the same time a very special two-electron system combined with the possibility of performing accurate ab-initio calculations. Atomic units are used throughout this work.

3.2 Photoelectron Angular Distributions

The transition probability per unit time within lowest non-vanishing order of perturbation theory for non resonant N photon ionization can be written as :

$$W_{fg}^{(N)} = \hat{\sigma}_N I^N \,, \tag{3.1}$$

where $\hat{\sigma}_N$ is the total angle-integrated generalized cross section given by:

$$\hat{\sigma}_N = \frac{(2\pi\alpha)^N k}{4\pi^2}\omega_L^N \int d\Omega_{\mathbf{k}} \, |M_{fg}^{(N)}|^2 \ , \tag{3.2}$$

with α being the fine structure constant, $\mathbf{k}$ the wave vector of the outgoing photoelectron related to its energy by $E_k = k^2/2$, the integration is over all angles of propagation of the photoelectron and the symbols f, g denote the final and initial state, respectively.
The dependence of the angular distribution of the photoelectrons on the atomic structure and the polarization $\hat{\mathbf{e}}$ of the field is now contained in the quantity $M_{fg}^{(N)}$ defined by:

$$M_{fg}^{(N)} = \sum\!\!\!\!\!\!\int_{\nu_{N-1}} \cdots \sum\!\!\!\!\!\!\int_{\nu_1} \frac{\langle f|\mathbf{D}\hat{\mathbf{e}}|\nu_{N-1}\rangle \cdots \langle \nu_1|\mathbf{D}\hat{\mathbf{e}}|g\rangle}{[\omega_g + (N-1)\omega_L - \omega_{\nu_{N-1}}] \cdots [\omega_g + \omega_L - \omega_{\nu_1}]} \, , \tag{3.3}$$

where $\mathbf{D}$ is the atomic dipole moment operator that can be expressed either in the length ($\mathbf{D} = -\mathbf{r}$) or in the velocity gauge ($\mathbf{D} = -\nabla/\omega_L$). The summations are carried out over all possible intermediate states including the discrete and continuous parts of the atomic spectrum. The generalization of equation (3.3) to ATI of order $N + R$, where N photons are needed to ionize the atom plus R extra photons which are absorbed in the continuum, involves the presence of poles in the integral. In that case, equation (3.3) requires the removal of the poles from the real axis through quantities ϵ_i and taking their limits to zero[34].
Although spin-orbit coupling plays no role in this work, we have chosen, for the sake of completeness of the formalism to exhibit the spin variable m_s in the final state of the photoelectron and the core. Alternatively, we could have written all equations without reference to spin. In general, in order to calculate the photoelectron angular distribution for a process that leaves the residual core in a state characterized by l_c, m_c and m_{s_c} quantum numbers, the continuum states are expanded as:

$$|f_{l_c,m_c,m_{s_c}}; \hat{\mathbf{k}}, m_s > = \sum_{J_f,l,m} i^l e^{-i\delta_l} Y_{lm}^{\star}(\hat{\mathbf{k}}) \, (SLJ_f M_{J_F}|SM_S LM_L)$$

$$\times (s_c s S M_S | s_c m_{s_c} s m_s)(l_c l L M_L | l_c m_c l m)|SLJ_f M_{J_f} > \ , \tag{3.4}$$

where J_f are the allowed angular momenta and l, m, m_s the associated partial waves for the outgoing photoelectron. The explicit presence of the core states, as we already discussed, is here important only when one wants to calculate photoelectron angular distributions. The angles in the spherical

harmonic specify the direction of propagation $\mathbf{k}$ of the photoelectron. These angles are in reference to a Cartesian system of coordinates whose z-axis is taken along $\hat{e}$ for linearly polarized light and along the photon propagation vector for elliptically or circularly polarized light. In the present case, the polarization vector is written as $\hat{\mathbf{e}} = (1+\eta^2)^{-1/2}(\hat{x} + i\eta\hat{y})$ where the ellipticity parameter η varies from 1 to -1. Substituting the above state representation into equation (3.3) and carrying out the angular momentum algebra we obtain [82]:

$$M^{(N)}(l_c, m_c, m_{s_c}; \hat{\mathbf{k}}, m_s; \eta) = \sum_{J_f, l, m} i^l e^{-i\delta_l} (-1)^{L-S+l-l_c-M_{J_f}-M_S-M_L}$$

$$\times Y^{\star}_{lm}(\hat{\mathbf{k}})\, D^{(N)}_{J_f}(\eta)\, [(2J_f+1)(2L+1)(2S+1)]^{1/2}$$

$$\times \begin{pmatrix} S & L & J_f \\ M_S & M_L & -M_f \end{pmatrix} \begin{pmatrix} s_c & s & S \\ m_{s_c} & m & -M_L \end{pmatrix} \begin{pmatrix} l_c & l & L \\ m_c & m & -M_L \end{pmatrix} . \quad (3.5)$$

Here $D^{(N)}_{J_f}$ is given from equation (3.3) with the difference that the final state is of the form $|SLJ_fM_{J_f}>$.

$$D^{(N)}_{J_f} \equiv \sum\!\!\!\!\!\!\int_{\nu_{N-1}} \cdots \sum\!\!\!\!\!\!\int_{\nu_1} \frac{\langle SLJ_fM_{J_f}|\mathbf{D}\hat{\mathbf{e}}|\nu_{N-1}\rangle \cdots \langle \nu_1|\mathbf{D}\hat{\mathbf{e}}|g\rangle}{[\omega_g + (N-1)\omega_L - \omega_{\nu_{N-1}}] \cdots [\omega_g + \omega_L - \omega_{\nu_1}]} . \quad (3.6)$$

The differential cross section for N-photon ionization is given by:

$$\frac{d\hat{\sigma_N}(l_c; \hat{\mathbf{k}}; \eta)}{d\Omega} = 2\pi(2\,\pi\,\alpha)^N \sum_{m_c, m_{s_c}, m_s} |M^{(N)}(l_c, m_c, m_{s_c}; \hat{\mathbf{k}}, m_s; \eta)|^2 , \quad (3.7)$$

from which integrating over all angles we obtain the N-photon generalized cross section as:

$$\hat{\sigma_N} = 2\pi(2\,\pi\,\alpha)^N \sum_{J_f} |D^{(N)}_{J_f}(\eta)|^2 . \quad (3.8)$$

The exact dependence on the photoelectron angles and the ellipticity η of the quantity $M^{(N)}_{fg}$, for $N = 2, 3$, are given by equations (3.11,3.15). Given the initial and final ion state, equation (3.5) contains all the necessary information to calculate angular distributions since $|M^{(N)}|^2$ is proportional to $d\hat{\sigma_N}/d\Omega$. The unknown quantities are the $D^{(N)}_{J_f}$ for each ionization channel.

3.3 Two- and Three-Photon Transition rates

Here we present the explicit dependence on the ellipticity of the light of the two- and three-photon total transition rates. The following formulas apply to ionization or detachment from an atomic system having angular momentum $L = 0$ in its ground state. For a two-photon transition the amplitude given by equation (3.5) is :

$$M^{(2)}(\eta) = \frac{\sqrt{\pi}}{3\,(1+\eta^2)} \Big\{ (1-\eta^2)\,(2A_S - A_D) + 3A_D \Big[(1-\eta^2) cos^2\theta_k - (1+\eta^2)\, sin^2\theta_k\, cos2\phi_k - i\,2\,\eta\, sin^2\theta_k\, sin2\phi_k \Big] \Big\} \,, \quad (3.9)$$

where the quantities A_S, A_D are complex in general and given by :

$$A_i \equiv \sum\!\!\!\!\!\!\int_{\nu} \frac{R^{\nu,P}_{1,S} R^{\mathbf{k},i}_{\nu,P}}{\omega_g - \omega_{\nu P} - \omega_L} \,, \qquad i = S, D, \quad (3.10)$$

The R's are reduced matrix elements [20] and the subscript i refers to the final value of the angular momentum for each channel. Here the intermediate states, denoted by ν, should be understood as belonging to the discrete and continuum spectrum of symmetry P. The relation between ellipticity η and the polarization vector of the field has already been defined in the main text. The angular variables (θ_k, ϕ_k) determine the direction of the photoelectron in the final state. Integrating the quantity $|M^{(2)}(\eta)|^2$ over these angles, we obtain the total cross section through equations (3.1) and (3.2) :

$$\frac{\Gamma^{(2)}(\eta)}{2\pi(2\pi\alpha\, I)^2} = \frac{16\pi^2}{45} \left[5 \left(\frac{1-\eta^2}{1+\eta^2} \right)^2 |A_S|^2 + 4\, \frac{1+4\eta^2+\eta^4}{(1+\eta^2)^2} |A_D|^2 \right] \,. \quad (3.11)$$

For the three-photon transition, the amplitude is:

$$\begin{aligned} M^{(3)}(\eta) \quad &= -i \frac{2\sqrt{\pi}}{(1+\eta^2)^{3/2}} sin\theta_k \times \quad (3.12) \\ &\Big\{ (1-\eta^2) \left[Q_P + \frac{3\,Q_F}{5} (5\, cos^2\theta_k - 1) \right] (cos\phi_k + i\,\eta\, sin\phi_k) \\ - \quad &Q_F\, sin^2\theta_k \left[(1+3\eta^2)\, cos3\phi_k + i\,\eta\,(3+\eta^2)\, \sin 3\phi_k \right] \Big\} \,, \end{aligned}$$

with Q_P, Q_F :

$$Q_P = \frac{5\,A_{SP} + 4\,A_{DP}}{15}, \qquad Q_F = \frac{A_{DF}}{4} \,, \quad (3.13)$$

and A_{SP}, A_{DP}, A_{DF} defined through integrals of reduced matrix elements over discrete and continuum states :

$$A_{L_1,L_2} \equiv \sum_{\nu_1}^{f} \sum_{\nu_2}^{f} \frac{R_{1,S}^{\nu_1,P}\, R_{\nu_1,P}^{\nu_2,L_1}\, R_{\nu_2,L_1}^{\mathbf{k},L_2}}{(\omega_g - \omega_{\nu_1 P} - \omega_L)(\omega_g - \omega_{\nu_2 L_1} - 2\,\omega_L)} \;, \tag{3.14}$$

where $L_1 = S, D$ and $L_2 = P, F$. From the quantity $|M^{(3)}(\eta)|^2$, performing the integral over the angles, we obtain for the total three-photon transition rate :

$$\frac{\Gamma^{(3)}(\eta)}{2\pi(2\pi\alpha\, I)^3} = \frac{16\pi^2}{525}\left[175\left(\frac{1-\eta^2}{1+\eta^2}\right)^2 |Q_P|^2 + 192\,\frac{1+8\eta^2+\eta^4}{(1+\eta^2)^2}\,|Q_F|^2\right] . \tag{3.15}$$

3.4 Atomic basis

The computational procedure used here has been presented in detail in a series of articles [84, 13, 9]. Briefly, we use one-electron hydrogenic orbitals:

$$\phi_{nlmm_s}(\mathbf{r}) = \frac{P_{nl}(r)}{r} Y_{lm}(\theta,\phi)\sigma(m_s) \;. \tag{3.16}$$

The radial functions $P_{nl}(r)$ satisfy the equation:

$$\left[-\frac{1}{2}\frac{d^2}{dr^2} - \frac{1}{r} + \frac{1}{2}\frac{l(l+1)}{r^2}\right] P_{nl}(r) = E_{nl}\, P_{nl}(r) \;, \tag{3.17}$$

with E_{nl} being the eigenvalue. The P_{nl} functions with negative or positive eigenvalues are expanded on a set of B-splines of order k and total number n defined in the finite interval $[0, R]$. Two-electron orbital states with total angular momentum L are constructed in the LS coupling of two-electron configuration space $\Psi^{SL}_{n_1 l_1, n_2 l_2}(\mathbf{r_1}, \mathbf{r_2}) = A|l_1 s_1 l_2 s_2 LM SM_S\rangle R_{n_1 l_1, n_2 l_2}(r_1, r_2)$, where A represents the antisymmetrization operator. The two-electron energy eigenfunctions are written in the form [11]:

$$\Phi^{SL}_{n(E)}(\mathbf{r}_1, \mathbf{r}_2) = \sum_{(n_1 l_1, n_2 l_2)} C^{SL}_{n(E)}(n_1 l_1, n_2 l_2)\, \Psi^{SL}_{n_1 l_1, n_2 l_2}(\mathbf{r_1}, \mathbf{r_2}) \,, \tag{3.18}$$

where $C^{SL}_{n(E)}(n_1 l_1, n_2 l_2)$ is the eigenvector of the atomic Hamiltonian matrix for the nth energy eigenvalue. Here $|C^{SL}_{n(E)}(n_1 l_1, n_2 l_2)|^2$ is the probability density for the configuration $(n_1 l_1, n_2 n_2)$ in the nth energy eigenstate. For

$E > 0$, $\Phi^{SL}_{n(E)}$ represents discretized continuum states. In the present case, the order of B-splines is $k = 9$ with $n = 150$ and $R = 150a.u.$.The knot sequence that we use is sine-like used first by Tang and Chang[84] for calculations of multiphoton processes. In that reference, one can find the details of the method we have used to calculate the phase shifts for each channel L=0,1,2,3 needed for the PAD's. In order to calculate the summations over intermediate states in the ATI case, we use the recently developed extrapolation method whose details can be found in [16]. Because of the discretization of the continuum, the detachment rates and phase shifts are calculated for discrete energies. Consequently, these rates and phase shifts in general do not coincide for different channels. For the energy region that we examine, the smoothness and density of data points are sufficient to use a cybic spline interpolation in order to obtain data for intermediate energies. The value of the ground state differs by about 14% from that calculated by Pekeris [63]. To obtain a better ground state energy, we would have to include a large number of states within each series of configurations associated with each excited 'inner' electron. Calculations of ATI by a discretized basis requires a sufficiently dense spacing of continuum states which must also extend high in energy. In order to have continuum wavefunctions, as well as the correlated ground state simultaneously, our primary criterion was the agreement between velocity and length gauge for the calculated dipole matrix elements. With much more effort, the ground state energy could be improved,but would not have a significant effect on the quantities of interest in this work.

3.5 One-Photon Detachment

In figure (3.1) we plot the one-photon detachment cross section from the ground state as a function of the photoelectron energy, given by the relation:

$$\Gamma^{(1)} = 2\pi(2\pi\alpha)|D(\eta=0)|\,I, \tag{3.19}$$

$$D(\eta=0) \equiv \langle 1s^2\ {}^1S|\varepsilon\mathbf{r}|2s\varepsilon p\ {}^1P\rangle. \tag{3.20}$$

In this figure, is evident the abrupt rising of the cross section for photoelectron energies near to zero in accordance with the Wigner threshold law,

$$\sigma_l \sim \epsilon^{l+1/2}. \tag{3.21}$$

This particular behavior for negative ions originates from the absence of a long range Coulomb potential for the outgoing photoelectron. The detachment rate, takes its maximum for photoelectron energy at about $0.28eV$

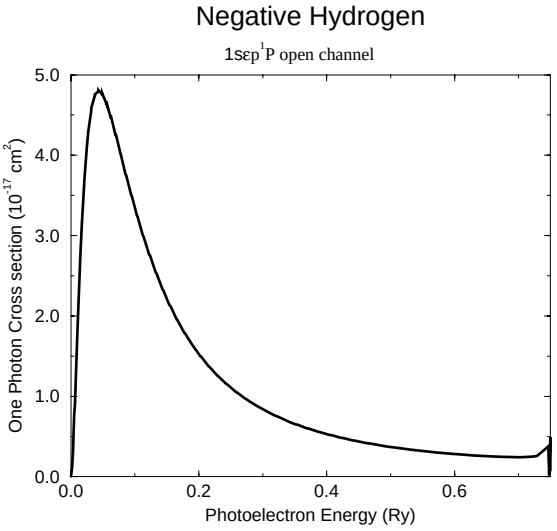

Figure 3.1: Photodetachment rate in a.u. for one-photon ionization.

which is very close to the ionization potential of H^-. For higher energies, below the second ionization threshold, the detachment rate decreases gradually. Just below the second ionization threshold the doubly excited states of H^- embedded in ^1P continuum give rise to resonances of the cross section. In figure 3.2 are presented two of those resonances. We have obtained this resolution in energy, varying slightly the radius of the box R.

These resonances are the first two members of an infinite series of autoionizing states converging (exponentially in energy) to the second ionization threshold [33]. Within the CI terminology we denote the first resonance as $|2s2p\,^1P\rangle$ since this specific two-electronic configuration orbital dominates over the others. Many theoretical calculations and experiments have been done for the determination of the autoionizing parameters of the first two autoionizing states [12, 10, 41, 19, 54, 85, 55] Fewer are the works for the second autoionizing state. Only recently calculations have presented [85, 55] The first resonance situated $10.92eV$ above the ground state of the system has been studied experimentally by MacArthur [57] and the Aarhus group [2]. The last group (at the present days seems to be the only active on H^- experiments [2, 1, 80]) has succeeded to detect also the second resonance which is narrower and much weaker than the first (by a factor 20). If relativistic and radiative effects are taken into account, then gives rise to

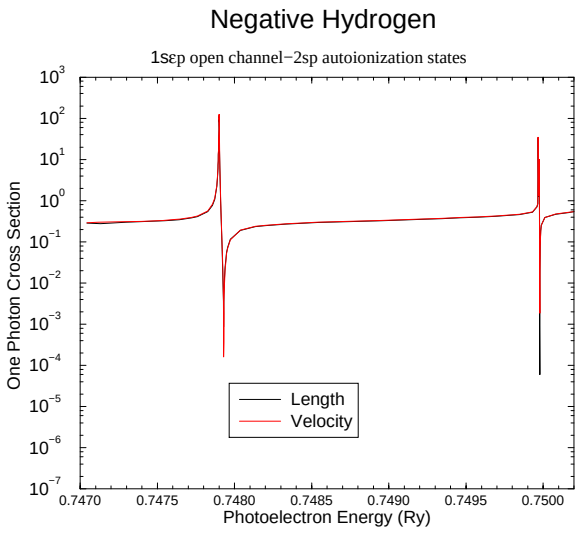

Figure 3.2: Photodetachment rate in a.u. for one-photon ionization.

the energy splitting of the hydrogenic levels with the same principal quantum number. This splitting has the consequence to limit the number of the formed autodetaching states from infinite to three [55].

The shape of the resonances is explained invoking the Fano formalism for cross section behavior around autoionizing states[30]. Briefly, the asymmetric peaks follows the Fano profile formula:

$$\sigma(\omega) = \sigma_b \frac{(q+\varepsilon)^2}{1+\varepsilon^2}\,, \qquad \varepsilon = \frac{(E-E_a)}{\Gamma/2}\,. \tag{3.22}$$

According to Fano theory, the three resonance parameters, namely the resonance energy $E_a - E$, the autoionizing width Γ and the shape parameter q are sufficient to describe in a quantitatively the deviation of the cross section from its background (σ_0). The cross section takes its maximum value $\sigma_{max} = \sigma_b(1+q^2)$ at energy $E_{max} = E_a + q\Gamma/2$ and its minimum value $\sigma = 0$ at energy $E_{min} = E_a - q\Gamma/2$. The q-value measures the strength of the interference between transitions from the initial bound state to the respective bound and continuum components of the final wave function. Experimentalists use the Fano formula for fitting their data, in order to calculate the parameters of the autoionizing state. It should be noted here, that the asymmetry in the cross section of the photoionization process is derived from the expression (3.20) through the form of the eigenfunctions. Asymmetry for

Table 3.1: Resonances energies, widths and q-values are presented for the two autoionizining states of the ^1P symmetry.

	$-E_a(a.u.)$	$10^6 \times \Gamma_a(a.u.)$	q
Present	0.126 05	1.28	-17.12
Lindroth et al[1]	0.126 050 9	1.36	-17
Venuti and Decleva[2]	0.126 049 581	1.3369	-16.475
Lindroth[3]	0.126 05	1.25	-17.1
Chang [4]	0.126 049	1.47	
Cortes and Martin[5]	0.126 049	1.19	-15.865
Andersen et al (Exp.)[6]	0.126 275 5	$0.7 < \Gamma_a < 2.2$	$-30 < q < -10$
Present	0.125 011 5	(?)	-11.7
Lindroth et al[1]	0.125 036 5	0.073	-11
Venuti and Decleva[2]	0.125 035 391	0.072313	-11.726
Lindroth[3]	0.125 04	< 0.08	-12.7
Cortes and Martin[5]	0.125 035	0.0625	-11.632
Andersen et al[6] (Exp)	0.126 276		

[a][55]
[b][85]
[c][54]
[d][10]
[e][19]
[e][1]

this case is inherent in the involved two-electron wavefunctions, the initial bound state and the final wavefunction with energies around the resonance energy E_a.

There is an upper limit about the amplitude of the external E/M field so that Fano theory to be applicable, connected with the relative strength of the configuration interaction $1/r_{12} \sim \Gamma$ to that of the electric dipole coupling of the atomic states. The situation for strong E/M fields is entirely different since the transition is not describable in terms of a simple rate [51, 49].

3.6 Two-Photon Detachment

We consider absorption of two photons from the ground state of negative Hydrogen in the photoelectron energy region ($0 - 0.15$ a.u.). From the dipole

selection rules, the number of independent channels are two, with final total angular momenta $L = 0, 2$ (i.e. ^1S and ^1D). The resulting H atom for these energies remains in its ground state and so we also have $J_f = 0, 2$. In Fig.3.3, we show, for linearly polarized light, the partial photodetachment rates $\Gamma(S)$ and $\Gamma(D)$ where Γ is the intensity-independent rate in a.u. defined by:

$$\Gamma^{(2)}(i) = 2\pi(2\pi\alpha)^2 |D_i^{(2)}(\eta = 0)|^2 \, I^2 \qquad i = S, D \tag{3.23}$$

Our calculations are in good agreement with those of Hugo Van der Hart

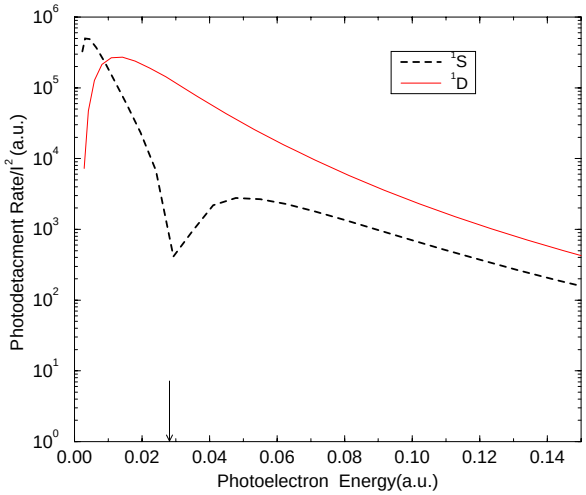

Figure 3.3: Photodetachment partial rates in a.u. for two photon ionization. Energy region covers ionization with and without ATI, which begins at photoelectron energy 0.0277 a.u. (indicated by the arrow). Note that 1a.u. of energy is $27.112ev$, while 1a.u. of rate is $2.41 \times 10^{-17}s^{-1}$.

[25] in the case without ATI. The same holds true for the calculations that Proulx and Shakeshaft [65, 64] have performed for two photon ionization for a wide photon energy region. Calculations of cross sections for two-photon above threshold detachment of negative Hydrogen have also performed by Sanchez et al [72] for a different photon energy region. Very recently, in experimental work [92] in negative Hydrogen with ATI at photoelectron energy about $0.058a.u.$ the branching ratio of the S and D partial waves has been measured. For this particular energy, the reported data show branching by

$90\% \pm 10\%$ into the D wave,an observation that is in excellent agreement with our calculations,which predict 89%. Furthermore, the agreement between our theoretical values with the experimantal ones suggests that for laser intensities at least up to $3 \times 10^{10} W/cm^2$ the interaction between the negative Hydrogen and the laser field can be described well by perturbation theory.

Turning now to our results, we see that the dominant contribution comes from the D symmetry. We also note the threshold behavior where the dominant channel is the channel with the lowest angular momentum, due to the Wigner law. Also we note that a rise in the detachment rate for the partial wave, that corresponds to the lowest angular momentum , occurs when the photoelectron reaches an energy of about $0.028\, a.u.$. The agreement between length and velocity gauge remains satisfactory throughout the energy region under consideration. The difference is within the thickness of the line of the graphs. Using equation (3.5), after the interpolation in energies and phase shifts for the channels S and D (Fig.1.5), we produce angular distributions for different photon energies and various values of the ellipticity parameter η (Fig.3.4). These graphs reveal a gradually increasing asymmetry on angle θ, as the absolute value of the ellipticity parameter increases. The value $\eta = 0$ corresponds to linear polarization where it is well established that the angular distributions have four-fold symmetry. The asymmetry can in principle always be present for elliptical polarization, independently of whether we have excess photon absorption or not A brief argument as to why that happens is the following. The structure of the angular dependence of the outgoing photoelectron in the case of elliptical polarization for a fixed θ and for arbitrary number of absorbed photons will be of the type [60]:

$$M_{fg}^{(N+R)} = |\sum_m a_m e^{im\phi}|^2 \,, \tag{3.24}$$

where all the non-vanishing terms have either even or odd m. The amplitudes a_m are integrals over the intermediate states involving the reduced radial elements. From the above formula, we are led to fourfold symmetry when the amplitudes are real. The amplitudes in a multiphoton process are complex for two reasons [50]. First, because in the continuum, in the absence of spin which for this argument is unimportant, the wave functions of photoelectrons can be written as [48]:

$$f_{\mathbf{k}}(\mathbf{r}) = 4\pi \sum_{l=0}^{\infty} \sum_{m_l=-l}^{l} i^l e^{-i\delta_l(k)} G_{kl}(k,r) Y_{lm_l}(\theta,\phi) Y^*_{lm_l}(\theta_k,\phi_k) \,, \tag{3.25}$$

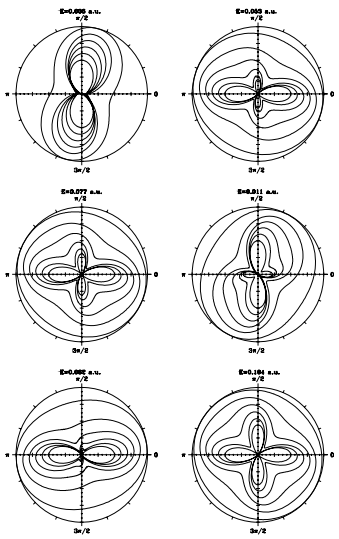

Figure 3.4: Two-photon detachment angular distributions as functions of ϕ of photoelectrons for kinetic energies $E_p = 0.006, 0.053, 0.077,$ $0.011, 0.062, 0.104$ a.u. and for various values of the ellipticity parameter (starting from the inner graphs) $\eta = 0.0, 0.18, 0.36,\ 0.54, 0.70, 0.90$. For visual facility, the azimuthal angular dependence distribution is on the polarization plane($\theta_k = \pi/2$) and the polar plots have been expanded with increasing ellipticity. This does not imply increasing rate with ellipticity.

where $\delta_l(k)$ are the phase shifts due to the potential of the atom and $G_{kl}(k, r)$ are real radial functions. Therefore the complex amplitude here is due to the existence of phase shifts. The second reason has to do with the case in which we have an excess photon absorption(ATI). The presence of the poles at certain energies in the integrals α_m introduces an imaginary part at these energies. Thus even when we have no ATI, in the elliptical case, the asymmetry in angular distributions can appear because of the phase shifts. In the present case, the existence of the asymmetry when we do not have ATI suggests that the state of the outgoing photoelectron is not a plane wave. Now regarding the ATI case, it can be proven (see appendix) that in the perturbation theory regime and the plane wave approximation, under the assumption that there are no other bound states except the ground one, the fourfold symmetry is conserved. A different argument by M.Crance [21], assuming plane waves for the photoelectron, leads to the same conclu-

sion. Finally we present the total detachment rate (Fig.3.5) as a function of the ellipticity η of the light for selected photoelectron energies. From this graph it is apparent that when the dominant partial wave corresponds to the lower angular momentum (here the S wave) there is a large decrease for the transition rate with increasing ellipticity of the light; i.e. going from linear toward circular. That is what is expected in general, since the number of possible paths that end up to the final state, for a multiphoton process, is the maximum one when the light is linearly polarized. But when the dominant partial wave corresponds to higher angular momentum (here D wave) it is possible to observe a different behavior for the transition rate,namely its increase with increasing ellipticity of the light. But there is an upper limit for this increase $\Gamma(\eta = 1)/\Gamma(\eta = 0) \rightarrow 1.5$ when $A_S/A_D \rightarrow 0$, as is known [47],which is easily obtained if one considers the two limiting cases $\eta = 0$ (linear light) and $\eta = 1$ (circular light) in the corresponding formulae (3.15,3.15).

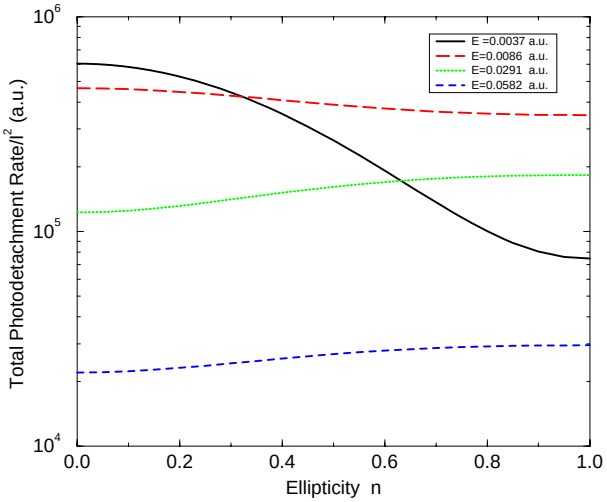

Figure 3.5: Total two-photon detachment rate as a function of the ellipticity η of the light for four photoelectron energies. Photoelectron energies correspond to ATI and no-ATI cases.

3.7 Three-Photon Detachment

Here we calculate partial photodetachment rates (3.26) and angular distributions for elliptically polarized light, for the case of three photon ionization in the energy region where it is possible to have one and two excess photon absorptions.

$$\Gamma^{(3)}(i) = 2\pi(2\pi\alpha)^3 |D_i^{(3)}(\eta = 0)|^2 I^3 \qquad i = P, F\,, \tag{3.26}$$

Now the angular momentum of the final states can be $L = 1, 3$ and again we consider the case where the resulting H atom remains in its ground state. The order of the process now is higher than for the two photon case and we need to enlarge the atomic basis in order to preserve the reliability of the calculations. The reason for this is that the extrapolation method [16] we use demands a sufficiently high density of states in the energy region where the poles occur. The suitable density of states depends also on the photon energy, independently of the order of the process. Consequently we enlarge the box radius to $250 a.u.$ and at the same time we improve the quality of the B-splines set taking $k = 11$, $N = 202$ and a knot sequence that is dense in the energy region close to the nucleus and decreases nearly linearly far away from the nucleus. The value of the ground state that we obtain differs from that of Pekeris as much as in the two photon case. In Fig.3.6, we show partial photodetachment rates for the symmetries L=1,3. Again the dominant contribution to the detachment rate near the threshold, comes from the partial wave with the lower angular momentum as expected from Wigner's law.

At this point, it is perhaps useful to discuss a feature of N-photon detachment,namely the rise of the rate at every photoelectron energy where a threshold is crossed. This is a general effect that should happen for all negative ions in the ATI case, at energies which can be determined given the electron affinity, the order of the process and the number of the excess photons. The number of such rises is exactly N, the order of the overall process. The reason for this is again the Wigner threshold law and occurs every time the number of excess photons in ATI increases. The rise is present for each channel, but the Wigner law leads to a sharper rise for the channel with the lowest angular momentum. If the electron affinity is E_{af}, the order of the process N, and the number of the excess photons R, then the photoelectron energies E_r at which one should expect rises for the detachment rates (if there is no other reason for this, such as autoionizing states) are given by

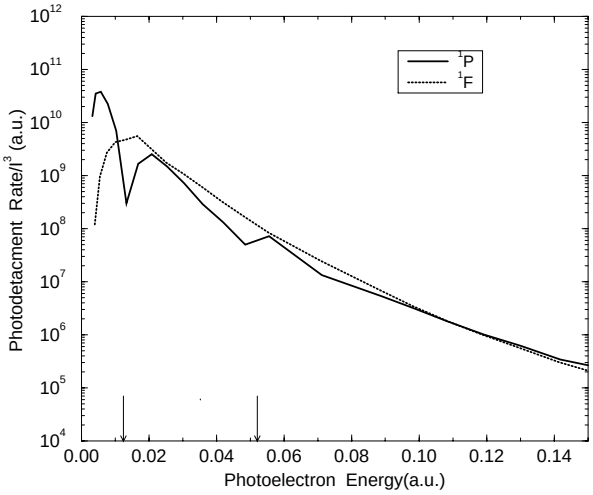

Figure 3.6: Photodetachment partial rates in a.u. for three photon ionization. Energy region covers ionization with and without ATI, which begins at 0.0139 a.u. (arrow) while the ATI involving two photons begins at 0.0554 a.u. (second arrow).

the formula:

$$E_r^{(R)} = E_{af}\frac{R}{N-R}\,, \qquad R = 0, 1, 2...N-1\,. \tag{3.27}$$

Therefore, for the two- and three-photon detachment rates and for the energy region that we consider, since there is no structured continuum, the rises occur at the expected energies and they are completely predictable as we can see from the corresponding figures (Fig.3.3 and 3.6).

$$E_r^{(0)} = 0, \qquad E_r^{(1)} = E_{af}\,, \qquad N = 2\,, \tag{3.28}$$

$$E_r^{(0)} = 0, \qquad E_r^{(1)} = E_{af}/2\,, \qquad E_r^{(2)} = 2\,E_{af}\,, \qquad N = 3\,. \tag{3.29}$$

Now, regarding how large these rises are for a given photoelectron energy,it depends on the number of the excess photons needed to reach this energy. Increasing this number, we should expect a tendency for the rises to be less sharp, since the order of the process is increased. The above analysis is compatible with the observation of Proulx and Shakeshaft [64] in their

investigation of the two- and three-photon detachment rates of negative hydrogen. In the case of three-photon detachment, they found a rise of the detachment rate due completely to a rise in the partial wave corresponding to the lowest angular momentum $L = 1$ at a photoelectron energy where the two-photon detachment threshold is located, but not in the two-photon case. That is correct if one examines the total two- or three-photon rates, as Proulx and Shakeshaft did. Since the $L = 2$ wave in the two-photon case overwhelms the $L = 0$ (see Fig. 3.3), the rise is masked in the total two-photon rate. On the contrary the $L = 1$ and $L = 3$ contributions at the position of the rise are comparable in the three-photon case (see Fig. 3.6), which makes the rise discernible even when the total rate is examined. We have chosen to emphasize the partial wave features, since these threshold effects are intimately connected with the angular momentum. Also, we

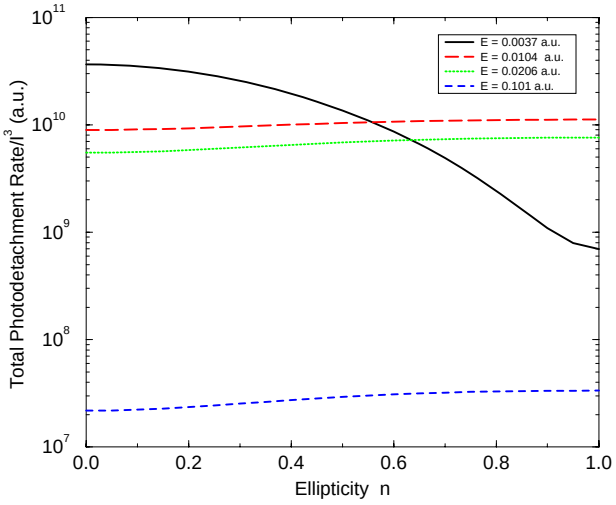

Figure 3.7: Total three-photon detachment rate as a function of the ellipticity η of the light for four photoelectron energies. Photoelectron energies correspond to ATI and no-ATI cases.

present total detachment rates (Fig.3.7) as a function of the ellipticity of the light. Behavior, similar to that of the two-photon case, is observed for the three-photon transition rate for selected photoelectron energies. Angular distributions for different energies and various ellipticities are shown in

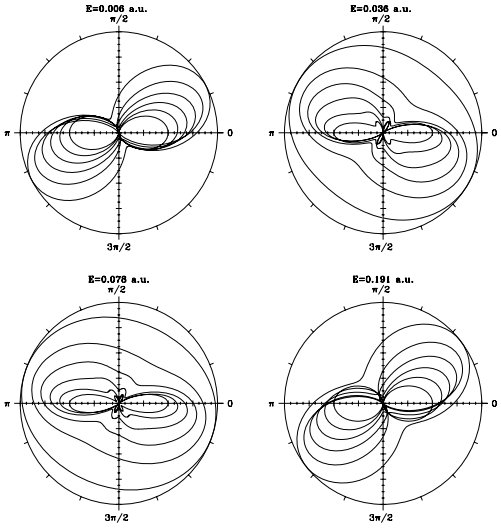

Figure 3.8: Three-photon detachment angular distributions as functions of ϕ of photoelectrons for kinetic energies $E_p = 0.006, 0.036, 0.078, 0.191$ a.u. and for various values of the ellipticity parameter as in the two-photon case. For visual facility, the azimuthal angular dependence distribution is on the polarization plane($\theta_k = \pi/2$) and the polar plots have been expanded with increasing ellipticity. This does not imply increasing rate with ellipticity.

Fig.3.8. Here again the asymmetry is observable and increases gradually with increasing ellipticity of the light. Note also the energies of the photoelectrons corresponding to ATI with one ($E_p = 0.01018, 0.0532$a.u.) and two excess ($E_p = 0.0617$a.u.) photons.

3.8 Asymmetry parameters

Multiphoton detachment or ionization in the majority of the experiments is performed using linearly polarized light. Beyond the one-photon ionization (detachment) the quantitative analysis of the PADs uses Yang's formulae [87]. For an N-photon detachment from a spherically symmetric atomic system by linearly polarized light, the PAD reads:

$$\frac{d\hat{\sigma}_N}{d\Omega} = \frac{\hat{\sigma}_N}{4\pi}\left[1 + \sum_{p=1}^{N} \beta_{2p} P_{2p}(\cos\theta)\right] , \qquad (3.30)$$

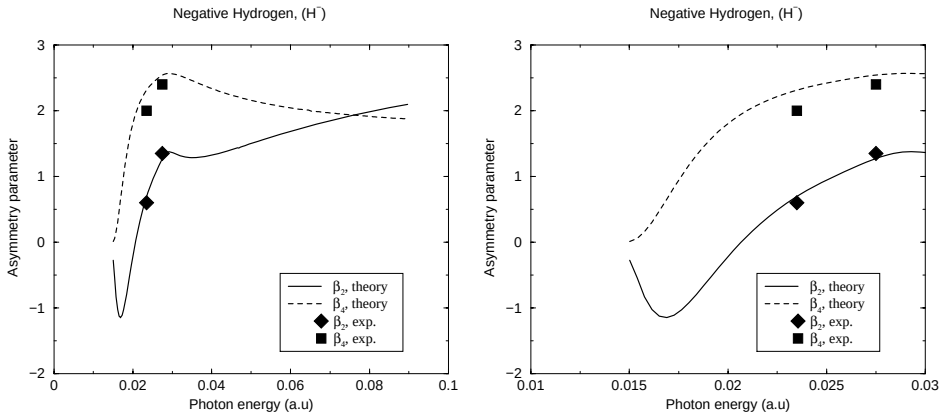

Figure 3.9: Calculated asymmetry parameters of 2-photon ionization. Experimental data are also presented.

where θ is the angle of the detection with respect to the photon polarization, $P_{2p}(x)$ is the Legendre polynomial of $2p$-order and $\hat{\sigma}_N$ is the cross section of the process. The parameters β_{2p} are known in the bibliography as "asymmetry parameters". The name has its origin in the fact that the parameters β_{2p} give rise to deviation of PADs from spherical symmetry, which corresponds to when $\beta_{2p} = 0, p = 1, 2...N$ as equation (3.30) predicts. In general, asymmetry parameters are complicated functions of the possible excitation amplitudes, the frequency of the light and the phase shift of the outgoing electron. An example of such calculations was presented by Zernik [88] who discussed the two-photon ionization of the atomic Hydrogen. To be more specific, for the two- and three-photon ionization (detachment) equation (3.30) is written as:

Two-Photon :

$$\beta_2 = \frac{2}{7} \cdot \frac{5 + 7\sqrt{5Q_2}\cos\delta_{SD}}{1 + Q_2} \tag{3.31}$$

$$\beta_4 = \frac{18}{7} \cdot \frac{1}{1 + Q_2} \tag{3.32}$$

with Q being $Q_2 = \Gamma^{(2)}(S)/\Gamma^{(2)}(D)$ and $\Gamma^{(2)}(S), \Gamma^{(2)}(D)$ the partial two-photon transition rates given by equation (3.23) and relation (3.11) for $\eta = 0$. The quantity δ_{SD} denotes the phase shift difference between the partial waves S, D, namely, $\delta_{SD} \equiv \delta_S - \delta_D$.

Three-Photon :

$$\beta_2 = \frac{1}{3} \cdot \frac{1 + 1.5Q_3 - 4.5\sqrt{3Q_3/7}\,\cos\delta_{PF}}{1 + Q_3} \tag{3.33}$$

$$\beta_4 = \frac{63}{22} \cdot \frac{1 - (22/3\sqrt{21})\sqrt{Q_3}\,\cos\delta_{PF}}{1 + Q_3} \tag{3.34}$$

$$\beta_6 = \frac{4}{33} \cdot \frac{1}{1 + Q_3} \tag{3.35}$$

where, $Q_3 = \Gamma^{(3)}(P)/\Gamma^{(3)}(F)$ and $\Gamma^{(3)}(P), \Gamma^{(3)}(F)$ are the partial three-photon transition rates given by equation 3.15 and relation (3.26) for $\eta = 0$. As in the two-photon case, we have $\delta_{PF} \equiv \delta_P - \delta_F$. In figures 3.9,

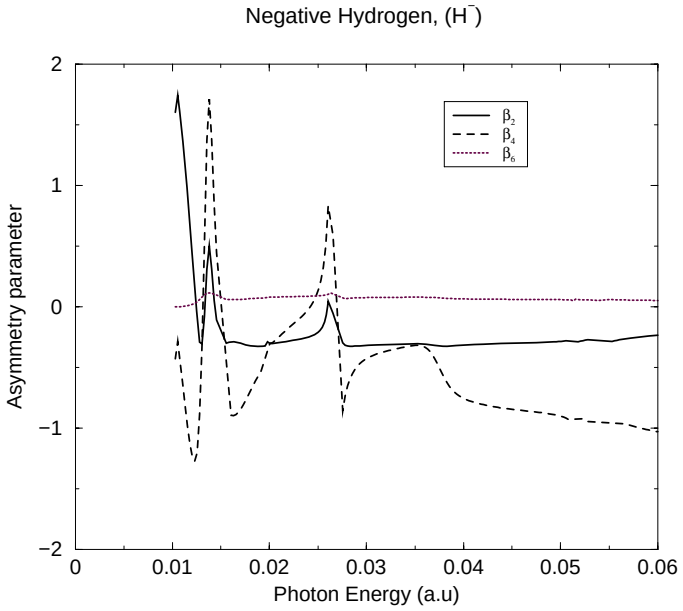

Figure 3.10: Asymmetry parameters for 3-photon ionization of negative hydrogen.

we present results of calculations for the asymmetry parameters of two-photon detachment. Until recently no experimental work on H^- had been reported, with data on PAD's. In a recent experiment, Præstergaad et al have reported asymmetry parameters of the two-photon detachment for two photon energies $\omega = 0.63eV$ and $\omega = 0.75eV$ [80]. The reported data

are presented for comparison in the relevant figures. In response to that experiment, Sánchez et al, in a refinement of a previous work [70], have calculated these asymmetry parameters as a function of the photon energy [71]. Their results are also in good agreement with the reported experimental values. There is an excellent agreement between their calculations and ours, especially for photon energies below the first ionization threshold. For this photon energy region, the parameters β_2, β_4 are very sensitive to the quantity Q_2, which gives the ratio between the S and D wave. From figure 3.9 we see that the asymmetry parameters tends to the value $\beta_2 \to 1.9$. At the same time we notice that for the phase shift we have $\delta_{SD} \to 0$ for high photoelectron energy (see Fig. 1.5). Therefore from the equation (3.32) for the β_4, we obtain $Q_2 \to 0.3$ and for β_2 we get $\beta_2 \to 3$. In addition, in figure 3.10 we present asymmetry parameters of the three-photon detachment as function of the photon energy. There is an evident strong variation of the β_2, β_4 with the quantity Q_3, which gives the ratio between the P, F wave. Noticing from figures 3.6 and 1.5 that asymptotically, $Q_3 \to 1$ and $\delta_{PF} \to 0$, we obtain from equation (3.35), that $\beta_2 \to -0.3$, $\beta_4 \to -0.8$, $\beta_6 \to 0.06$.

3.9 Conclusion

As far as the photoelectron angular distributions are concerned,we have shown that elliptical polarization will in principle lead to the breakdown of the fourfold symmetry as is the case with neutral atoms. Of course the degree of asymmetry will depend on the ellipticity parameter as well as the wavelength and absence of the asymmetry at some wavelength does not imply its non existence. Although our results have been obtained for a case of an S_0 initial state leading to an S_0 residual core, the effect should, if anything, be even more pronounced in more general cases. We have in addition shown that, in the case of a single bound state, the absence of non-zero phase shifts in the continuum states (plane waves) preserves the fourfold asymmetry even in the presence of ATI. This modifies the validity of an assertion made by Lambropoulos and Tang in an earlier paper [50]. Finally we have provided results for phase shifts and rates into the channels of final states which are in excellent agreement with recent experimental data [92], as well as for the results for 3-photon detachment which may be of use in extensions of the relevant ATI experiments. This work at the same time served as an example of the versatility of the techniques we have employed which can be readily extended to provide answers even in the non-perturbative regime, when related experimental data become available; as has been shown in the

case of two electron atoms [90, 89, 91].

3.10 Appendix : ATI of negative ions in the plane-wave approximation.

In this appendix, we prove that for systems without bound states other than the ground state, in the plane wave approximation and in the perturbation theory regime, angular distributions preserve the fourfold symmetry in the elliptical polarization case. In order to discuss a case from which the generalization to N-photon is straightforward, we consider two excess photons. We also consider photon energy such that one-photon detachment is allowed, which does not mean that this procedure is not applicable for more general situations. The crucial point is that there are no sums over discrete states, since they are absent, but only integrals containing Dirac delta functions.

In this case, generalization of equation (3.3) reads as:

$$M_{fg}^{(1+2)} = \lim_{(\epsilon_1,\epsilon_2)\to 0} \sum\!\!\!\!\!\!\int_{\nu_1\nu_2} \frac{\langle f|\mathbf{D}\hat{\mathbf{e}}|\nu_2\rangle\langle\nu_2|\mathbf{D}\hat{\mathbf{e}}|\nu_1\rangle\langle\nu_1|\mathbf{D}\hat{\mathbf{e}}|g\rangle}{(\omega_g + 2\omega_L - \omega_{\nu_2} + i\epsilon_2)(\omega_g + \omega_L - \omega_{\nu_1} + i\epsilon_1)} \,. \quad (3.36)$$

Now the poles are at the positions $k_1^2/2 = \omega_1 = \omega_g + \omega_L$,$k_2^2/2 = \omega_2 = \omega_g + 2\omega_L$ When one-photon ionization is allowed using the well known identity,

$$\lim_{\varepsilon\to 0} \frac{1}{x + i\varepsilon} = P(\frac{1}{x}) - i\pi\delta(x)\,, \quad (3.37)$$

the relation (3.36) is written as:

$$\begin{aligned} M_{fg}^{(1+2)} &= P \sum\!\!\!\!\!\!\int_{\nu_1\nu_2} \frac{\langle \mathbf{k}_f|\mathbf{D}\hat{\mathbf{e}}|\nu_2\rangle\langle\nu_2|\mathbf{D}\hat{\mathbf{e}}|\nu_1\rangle\langle\nu_1|\mathbf{D}\hat{\mathbf{e}}|g\rangle}{(\omega_1 - \omega_{\nu_1})(\omega_2 - \omega_{\nu_2})} \\ &- \pi^2\langle \mathbf{k}_f|\mathbf{D}\hat{\mathbf{e}}|\mathbf{k_2}\rangle\langle\mathbf{k_2}|\mathbf{D}\hat{\mathbf{e}}|\mathbf{k_1}\rangle\langle\mathbf{k_1}|\mathbf{D}\hat{\mathbf{e}}|g\rangle \quad (3.38) \\ &- i\pi\langle \mathbf{k}_f|\mathbf{D}\hat{\mathbf{e}}|\mathbf{k_2}\rangle P \sum\!\!\!\!\!\!\int_{\nu_1} \frac{\langle\mathbf{k_2}|\mathbf{D}\hat{\mathbf{e}}|\nu_1\rangle\langle\nu_1|\mathbf{D}\hat{\mathbf{e}}|g\rangle}{\omega_1 - \omega_{\nu_1}} \\ &- i\pi\langle \mathbf{k_1}|\mathbf{D}\hat{\mathbf{e}}|g\rangle P \sum\!\!\!\!\!\!\int_{\nu_2} \frac{\langle \mathbf{k}_f|\mathbf{D}\hat{\mathbf{e}}|\nu_2\rangle\langle\nu_2|\mathbf{D}\hat{\mathbf{e}}|\mathbf{k_1}\rangle}{\omega_2 - \omega_{\nu_2}} \,. \end{aligned}$$

In the plane wave approximation, the continuum wavefunctions are written as:

$$f_{\mathbf{k}}(\mathbf{r} = \langle\mathbf{r}|\mathbf{k}\rangle = \frac{1}{(2\pi)^{3/2}} e^{i\mathbf{kr}} \,. \quad (3.39)$$

Using the velocity gauge, it can be shown easily that the dipole matrix element between two continuum states leads to the Dirac delta-function, namely,

$$\langle \mathbf{k}|\mathbf{D}\hat{\mathbf{e}}|\mathbf{q}\rangle = \mathbf{k}\hat{\mathbf{e}}\,\delta(\mathbf{k}-\mathbf{q})\,. \tag{3.40}$$

Thus from the above relation we have:

$$\langle \mathbf{k}_f|\mathbf{D}\hat{\mathbf{e}}|\mathbf{k}_2\rangle = \mathbf{k_f}\hat{\mathbf{e}}\delta(\mathbf{k}_f-\mathbf{k}_2) = 0\,, \tag{3.41}$$

since $k_f^2/2 = \omega_g + 3\omega_L$ and $k_f - k_2 = 2\omega_L/(k_f+k_1) \neq 0$. Finally we have:

$$\begin{aligned}\langle \mathbf{k}_f|\mathbf{D}\hat{\mathbf{e}}|\mathbf{k_2}\rangle &= 0,\\ \langle \mathbf{k}_f|\mathbf{D}\hat{\mathbf{e}}|\mathbf{k_2}\rangle\langle \mathbf{k_2}|\mathbf{D}\hat{\mathbf{e}}|\mathbf{k_1}\rangle &= (\mathbf{k}_f)^2\,\delta(\mathbf{k}_f-\mathbf{k}_2)\,\delta(\mathbf{k}_2-\mathbf{k}_1)\end{aligned}$$

The sum-integral,

$$P\sum\!\!\!\!\!\!\int_{\nu_2} \frac{\langle \mathbf{k}_f|\mathbf{D}\hat{\mathbf{e}}|\nu_2\rangle\langle\nu_2|\mathbf{D}\hat{\mathbf{e}}|\mathbf{k_1}\rangle}{\omega_2-\omega_{\nu_2}}\,,$$

can be separated into a sum over bound states and an integral that contains only the continuum. The integral vanishes because of equation (3.41) and only the sum over the intermediate bound states remains. This sum makes the amplitudes of equation (3.24) complex and therefore reduces the four-fold symmetry of angular distributions to two-fold symmetry. Under the assumption that the negative ion has no intermediate bound states, the final expression is :

$$M_{fg}^{(1+2)} = P\int d^3\mathbf{k}_2 d^3\mathbf{k}_1 \frac{\langle \mathbf{k}_f|\mathbf{D}\hat{\mathbf{e}}|\mathbf{k}_2\rangle\langle \mathbf{k}_2|\mathbf{D}\hat{\mathbf{e}}|\mathbf{k}_1\rangle\langle \mathbf{k}_1|\mathbf{D}\hat{\mathbf{e}}|g\rangle}{(\omega_1-\omega_{k_1})(\omega_2-\omega_{k_2})}\,.$$

Since the matrix elements are delta functions, it is easy to calculate the integral and therefore we have:

$$M_{fg}^{(1+2)} = \frac{(\hat{\mathbf{e}}\mathbf{k}_f)^2}{2!\,\omega_L^2}\langle \mathbf{k}_f|\hat{\mathbf{e}}\mathbf{D}|g\rangle$$

Noticing that $k_f^2/2 = \omega_g + 3\omega_L$ and using the relations:

$$\begin{aligned}\langle \mathbf{k}_f|\hat{\mathbf{e}}\mathbf{D}|g\rangle &= \hat{\mathbf{e}}\mathbf{k}_f\Phi_g(\mathbf{k}_f)\,,\\ \hat{\mathbf{e}}\mathbf{k}_f &= k_f sin\theta\frac{cos\phi + i\eta sin\phi}{\sqrt{1+\eta^2}}\,,\end{aligned}$$

we obtain for the angular distributions the formula:

$$|M_{fg}^{(1+2)}|^2 = \frac{(\omega_g+3\omega_L)^3}{(2^3 2!)^2(1+\eta^2)^3\,\omega_L^4}|\Phi_g(\mathbf{k}_f)|^2(sin\theta_f)^6(cos^2\phi_f+\eta^2 sin^2\phi_f)^3\,,$$

where $\Phi_g(\mathbf{k})$ is the Fourier transform of the ground state. From the above formula, the four-fold symmetry of the PAD for elliptic polarization is evident. Under the same assumptions, it is possible to generalize the above formula to N-photon ionization, with the result:

$$|M_{fg}^{(N)}|^2 = \frac{(\omega_g + N\omega_L)^N \, |\Phi_g(\mathbf{k}_f)|^2}{\left[2^N(N-1)!\right]^2 (1+\eta^2)^N \omega_L^{2(N-1)}} (\sin\theta_f)^{2N} \left(cos^2\phi_f + \eta^2 sin^2\phi_f\right)^N .$$

Chapter 4

One-photon Core Excitation of H^-

4.1 Introduction

Assume a two-electron atom subject to an E/M field, with photon energy so that one-photon ionization is allowed, while the core remains in its ground state. . If the initial two-electron state is $|g\rangle = |1s^2\ ^1S\rangle$ then one-photon ionization, within the dipole approximation, leaves the system in $|c\rangle = |1s\varepsilon p^1P\rangle$ two-electron state, with $\varepsilon = k^2/2$ the kinetic energy of the outgoing electron. For 'weak' fields, the photoelectron energy spectrum (PES) after the end of the pulse has a Lorentzian peak in photoelctron energy $\varepsilon = \omega + E_g$, where E_g is the ground-state energy. For stronger laser fields, above-threshold ionization (ATI) make its appearance and the well-established ATI-peaks structure of the PES is developed [**?**]. This picture is valid, whenever the final continuum state has a smooth dependence on energy, otherwise the existence of autoionizing states (AIS) complicates the spectrum to a degree depending mainly on the intensity of the light [30, 51]. For smooth continua, strong modification of the PES is possible, if the photon energy approaches the energy separation between two bound states of the core [36]. Assumming photon energy resonant with a core transition energy, the modification of the PES is dependent mainly on the intensity of the pulse, and in a secondary way, on the duration and the shape of the pulse. For instance, in the case of the negative hydrogen, for single-electron ionization, the remaining core is the hydrogen, and the core transition could be the 1s-2p transition, with energy $\omega_R = 0.375$ a.u. 10.2eV. The absorption of a second photon, when the atomic system is in the state $|1s\varepsilon^1P\rangle$ can leave the system in the

states $|1s(\varepsilon+\omega)s^1S\rangle$, $|1s(\varepsilon+\omega)d^1D\rangle$, $|(n_1/\varepsilon_1)p\varepsilon_2 d^1D\rangle$, $|c_1\rangle = |2p\varepsilon' p^1S\rangle$ and $|c_2\rangle = |2p\varepsilon' p^1D\rangle$. Provided that, the photon energy is far from any core resonance the dominant channels are the first three states which gives rise to the ATI structure of the PES. However, when the photon energy is close to any core resonance the dominant channels are the last two, which represents, in a simplified terminology, the excitation of the 'inner' electron, thus leaving the outgoing electron with kinetic energy modified by the detuning $\Delta = \omega - \omega_R$, namely, $\varepsilon' = \varepsilon + \Delta$. Note that, in exact resonance the outgoing electron occupies the same kinetic energy. Assuming, small detuning for the field, it is legitimate to ignore the first two channels, concentrating on the channels representing core excitation.

Although, the transitions $|1s(\varepsilon+\omega)p^1P\rangle \rightarrow |2p\varepsilon' p^1S\rangle$ and $|1s(\varepsilon+\omega)p^1P\rangle \rightarrow |2p\varepsilon' p^1D\rangle$ are transitions between continuum states (CC transitions), their nature and strength is determined mainly by the bound-bound one-electron dipole transition (BB transition) of the core, $|H(1s)\rangle \rightarrow |H(2p)\rangle$. For a more quantitative discussion let denote the strengths of the transitions $|g\rangle \rightarrow |c\rangle, |c\rangle \rightarrow |c_1\rangle, |c\rangle \rightarrow |c_2\rangle$ by $\Gamma_g, \Omega_1, \Omega_2$ respectively. Depending on the relative magnitude of that strengths in combination with the intensity and the duration of the pulse, a drastic change of the single lorentzian peak is possible. Suppose, that $\Gamma_g, T^{-1} \gg \Omega_1$, with T the duration of the pulse (Ω_2 has the same order of magnitude with Ω_1) then no signifigant change happens even at exact resonance ($\omega = \omega_R$). For the intensities we use ($I_0 \leq 10^{14} W/cm^2$), the Rabi frequencies are much larger than the decay rate of the ground state[1] Γ_g, $\Omega_1, \Omega_2 \gg \Gamma_g$. This is an interesting result since, the resonant transition $1s-2p$ is saturated, thus giving rise to a non-linear depedence on the intensity even for weak-fields. In other words, for $\omega \sim 0.375$ a.u. the ionization rate of the ground state is not a simple function of the first power of intensity, even for weak fields, an assumption valid within LOPT. Then, a step beyond the LOPT is necessary for the correct treatment of the process. The net effect of that saturation (with increasing the intensity) is the splitting of the Lorentzian peak of the PES in a doublet, with features depending on the parameters of the problem, either atomic or of the pulse. This phenomenon is closely related with the AC-stark splitting of two bound states coupled with an E/M field [29].

Until now, we considered continua which are have smooth energy dependence. Coupling, between continua with structure, complicates the spectrum considerably. The existence of an AIS, introduces another one parameter in the underlying physics, namely the autoionizing width of the AIS, Γ_a.

[1] Note that $\Gamma_g \sim I$, while $\Omega \sim I^{1/2}$.

In principle, one can imagine situations where complexity is increased due either to the atom under question or the pulse characteristics.

The doublet of the PES, was first predicted by Grobe and Eberly [36]. In a one-dimensional model negative ion, produced by the soft-core potential $V(x) = -1/\sqrt{1+x^2}$, they solve numerically the TDSE using a $\sin^2$ pulse. In a subsequent paper, Grobe and Haan [37], present results of a model neutral atoms with the ground state decaying to a structured continuum ($|c\rangle$), modelled by a transition around an AIS. In response to those predictions, Walker et al [86], made the first observation of that ac-Stark splitting of the PES in experiment on Ca. In a series of papers Hanson, Zhang and Lambropoulos [38, 39, 40] present quantitative results in Ca, with excellent agreement with the experiment performed by Walker. The photon energy used in that experiment, is near resonance with an ionic core state and also with an atomic resonance, which complicate the problem. They produce the two-electron states with a CI approach, extending thus the existing theoretical predictions for more realistic situations. They do produce a more complicated PES due to the involved structured continua as well as to the additional (except the ionic resonance) atomic resonance.

The subject of the present work is to investigate the PES in H^-, when the photon energy is near or on resonance with the $1s \leftrightarrow 2p$ hydrogenic transition. In general, the effect in the PES under this strongly driven transition depends on the specific atomic parameters, the pulse parameters and the interplay between them. Quantitative results, are obtained by numerical integration of the TDSE in the subspace of states, selected by first-order energy conservation of the transitions. The method is known as essential state approximation (ESA), assumes the rotating wave approximation (RWA) for the transitions, thus excluding it from a strictly non-perturbative approach of the atom-E/M field interactions [49]. On the other hand, within the limited basis set the E/M coupling is treated exactly, thus allowing AC-stark shifts and decay rates to the continuum (obtained perturbatively) of the states to be included in the model.

4.2 Formulation

We consider the negative hydrogen in its ground state $(1s)^2\,{}^1S_0$ in the presence of a monochromatic field of frequency ω and N photons in the initial state. The states involved are the following :

$$\begin{aligned} |g\rangle &= |H^-(1s)^2\ {}^1S; N\rangle \equiv |(1s)^2\ {}^1S; N\rangle \\ |c\rangle &= |H(1s) + e^-_{\epsilon_c}; N-1\rangle \equiv |1s\epsilon p\ {}^1P; N-1\rangle \end{aligned}$$

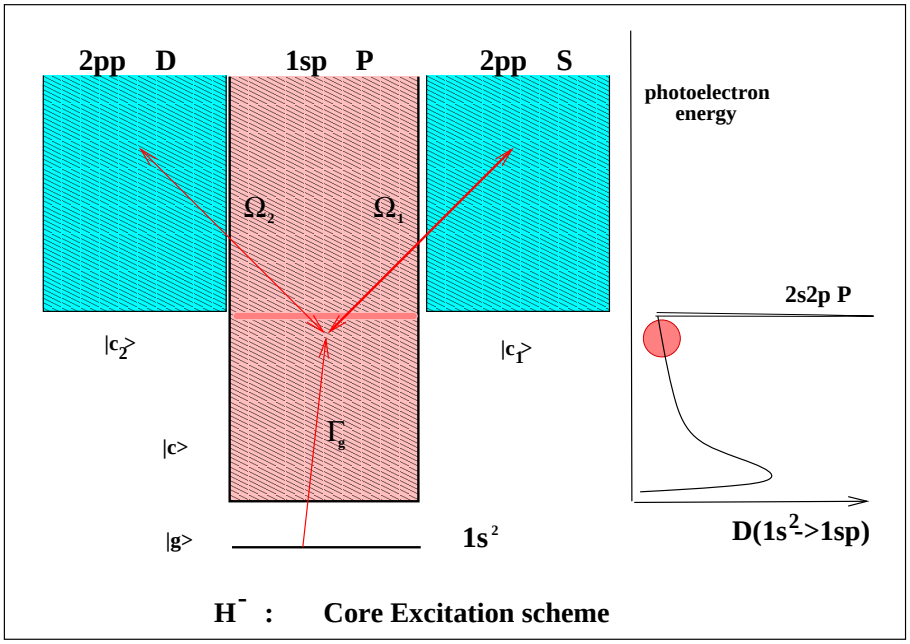

Figure 4.1: Negative Hydrogen core excitation scheme.

$$\begin{aligned} |c_1\rangle &= |H(2p) + e^-_{\epsilon_c}; N-2\rangle \equiv |2p\epsilon p\ ^1S; N-2\rangle \\ |c_2\rangle &= |H(2p) + e^-_{\epsilon_c}; N-2\rangle \equiv |2p\epsilon p\ ^1D; N-2\rangle \end{aligned} \tag{4.1}$$

Representation of the states (atom + field) in this way implies the quantized form of the E/M field. The energies of the above states are given by the relations:

$$\begin{aligned} E_g &= E(H^-(1s)^2\ ^1S) + N\hbar\omega \\ E_c &= E(H(1s)) + \epsilon_c + (N-1)\hbar\omega \\ E_{\overline{c}} &= E_{c_1} = E_{c_2} = E(H(2p)) + \epsilon_c + (N-2)\hbar\omega \end{aligned} \tag{4.2}$$

The photon energy of the field is sufficient to ionize the negative hydrogen from its ground state exciting one of the electrons in the (^1P) continuum with kinetic energy ϵ_c. For photon energies near resonance with that of the hydrogen atomic transition $1s-2p$ ($\hbar\omega = 10.2$eV) the core state (Hydrogen ground state$(H(1s))$, absorbs one more photon and brings into play the excited $(H(2p))$ core state. It is important to note here that the second electron remains with the same kinetic energy as in the first continuum

(denoted by $|c\rangle$). The two continua correspond to different core states. After the second photon absorption, the atomic state can be found either with total angular momentum $L = 0$ (^1S) or $L = 2$ (^1D). These states (atom + field) are denoted by $|c_1\rangle$ and $|c_2\rangle$ respectively. Notice also that these states are degenerate, thus having the same energy (denoted by $E_{\bar{c}}$). The Hamiltonian of the system is $H = H_A + H_R + D = H_0 + D$ where H_A and H_R are the field-free atomic hamiltonian and the free E/M field respectively. Operator D is the interaction between the atom and the field in the dipole approximation. In this approximation and in the rotating wave approximation (RWA) H_A and D are written as:

$$H_0 = E_g|g\rangle\langle g| + \int d\epsilon_c E_c\ |c\rangle\langle c| + \sum_{i=1,2}\int d\epsilon_{c_i} E_{c_i}\ |c_i\rangle\langle c_i| \tag{4.3}$$

$$\begin{aligned} D &= \int d\epsilon_c \left[D_{gc}\,|g\rangle\langle c| + D_{cg}\,|c\rangle\langle g|\right] \\ &+ \sum_{i=1,2}\int d\epsilon_{c_i}\left[D_{cc_i}\,|c\rangle\langle c_i| + D_{c_ic}\,|c_i\rangle\langle c|\right] \end{aligned} \tag{4.4}$$

In the above subspace the most general form of the state of the system in time t will be of the form :

$$|\psi(t)\rangle = U_{gg}(t)|g\rangle + \int d\epsilon_c U_{cg}(t)|c\rangle + \sum_{i=1,2}\int d\epsilon_{c_i} U_{c_ig}(t)|c_i\rangle \tag{4.5}$$

Finally, we should note that the populations in the continuua satisfy the orthonormality condition,

$$|U_{gg}(t)|^2 + \int d\epsilon_c |U_{cg}(t)|^2 + \sum_{i=1,2}\int d\epsilon_c |U_{c_ig}(t)|^2 = 1 \tag{4.6}$$

Our intention is to determine the time evolution of the state $\psi(t)$ through the amplitudes $U_{ag}(t), a \equiv g, c, c_1, c_2$, which will allow us to find the population of the ground state (yield) and the population in each of the continua involved as a function of the photoelectron energy (PES). The dynamics of the system are governed by the TDSE which reads:

$$i\partial_t|\psi(t)\rangle = [H_0 + D(t)]\,|\psi(t)\rangle\,, \qquad |\psi(t=0)\rangle \equiv |g\rangle. \tag{4.7}$$

Inserting equation (4.5) into equation (4.7) we obtain a system of first order integro-differential equations for the amplitudes of the state vector $U_a(t), a \equiv g, c, c_1, c_2$, The coupling of the ground state with the continuum $|c\rangle$ D_{cg} and the coupling of the continuum $|c\rangle$ with the continua $|c_1\rangle$ (D_{cc_1}) and

$|c_2\rangle$ (D_{cc_2}) complicates the problem considerably since the time evolution of each amplitude depends on the time evolution of an infinite number of states (the continuum states). In first approximation under certain conditions, the problem is solved analytically when the couplings D are assumed to be of constant magnitude, as in the case of a square pulse.

In general, the classical limit of a multimode quantized field linearly polarized, is of the type (ignoring phase fluctuations):

$$E(t) = \frac{1}{2}E_0(t)e^{i\omega t} + \frac{1}{2}E_0^{\star}(t)e^{-i\omega t} \tag{4.8}$$

Accordingly, the classical limit of the dipole operator D is written as $D = -\mathbf{r}\mathbf{E}(t)$. The purpose of the present chapter is two-fold. We are interested in solving the problem with constant amplitude radiation field for the real negative hydrogen. Whether this is possible is proven to depend on the intensity and the photon energy of the pulse. Especially the most interesting effect of that interaction is when the photon energy equals the hydrogen core transition. Then in the PES instead of a single peak a doublet appears, as AC-stark splitting due to the strong core transition. Furthermore, the solution of the problem using time-dependent amplitudes of the laser pulses is examined and a direct comparison of the calculated quantities (mainly PES) with that of the square pulse is made. In order to reach the first target (square pulse) we have to remove the integrals from the time-dependent equations for the amplitudes $U(t)$. In other words, we have to eliminate the continua from the equations. This is done, more conveniently, in the energy-space instead the time-domain, using the resolvent operator formalism as developed in [34, 48]. However, this approach is applicable directly in time-independent hamiltonians. Quantization of the E/M field leads to such hamiltonians as in our case. This is the reason we have choosen the quantized form of the E/M field for square pulses. Square pulse, means single mode quantized laser field, where conservation of the energy selects in a natural way the atomic states that are essential for the dynamics of the system. Note that, this selection is equivalent with the rotating wave approximation (RWA) when we use the classical form of the E/M field. The amplitude equations, after the elimination of the continuum, are used for the analytical solution of the problem. However, this final form is usefull for the examination of the problem for a general pulse shape as well. Transforming back to the time-domain we obtain a simplified system of equations for the amplitudes $U(t)$. Then direct numerical propagation is possible, allowing us to extract information for more practical situations.

Atomic Basis The two-electron states of H^- are calculated through

the CI method in combination with the B-spline technique, as presented at the last section (Two-electron atoms) of the first chapter. After obtaining the two-electron eigenstates states and the corresponding eigenergies the necessary dipole matrix elements $|1s^2\ ^1S\rangle \rightarrow |1s\varepsilon p^1P\rangle$ are calculated. The dipole matrix elements have an energy dependence (either photon or photo-electron energy) as presented in figure 3.1. The B-splines basis set and the two-electron configuration states used for the calculations, are the same as discussed in the chapter dealing with -one,two and three-photon transitions in H^-.

4.3 Square pulse

The resolvent operator is defined by, $(z - H_0 - D)G(z) = \mathbf{1}$, with z being a complex number. If the evolution operator of the system is $U(t)$, $\psi(t) = U(t)\psi(t=0) = U(t)|g\rangle$. Then the matrix elements of $U(t)$ are obtained as the inverse Laplace transform of $G(z)$.

$$U_{ag}(t) = -\frac{1}{2\pi i}\lim_{\eta\rightarrow 0^+}\int_{-\infty}^{+\infty} dx G_a(x+i\eta) \tag{4.9}$$

We need, the matrix elements[2] $G_g, G_c, G_{c_1}, G_{c_2}$. Writing $(z - H_0 - D)\cdot\mathbf{1}\cdot G(z)|g\rangle = |g\rangle$ and multiplying the right side with the states $\langle g|, \langle c|, \langle c_1|, \langle c_2|$ we obtain for the amplitudes $G_g, G_c, G_{c_1}, G_{c_1}$ in the Laplace-space the following system of algebraic equations:

$$\begin{aligned}
(z-E_g)G_g - \int d\epsilon_{c'} D_{gc'} G_{c'} &= \mathbf{1} \\
-D_{cg}G_g + (z-E_c)G_c - \sum_{i=1,2}\int d\epsilon_{c_i'} D_{cc_i'} G_{c_i'} &= 0 \\
-\int d\epsilon_{c'} D_{c_1c'} G_{c'} + (z-E_{c_1})G_{c_1} &= 0 \\
-\int d\epsilon_{c'} D_{c_2c'} G_{c'} + (z-E_{c_2})G_{c_2} &= 0
\end{aligned} \tag{4.10}$$

We introduce now the following approximations:

$$\begin{aligned}
\int d\epsilon_{c_i'} D_{cc_i'} G_{c_i'} &= D_{c_ic}G_c = \Omega_i^\star(t)G_c(z) \\
\int d\epsilon_{c'} D_{c_ic'} G_{c'} &= D_{cc_i}G_{c_i} = \Omega_i(t)G_{c_i}(z)\,, \qquad i=1,2
\end{aligned} \tag{4.11}$$

[2]For simplifiying the notation we write, $\langle a|G(z)|g\rangle = G_a(z) = G_{ag}(z)$.

where Ω_1, Ω_2 are the Rabi frequency of the two-electron CC transitions $|c\rangle \leftrightarrow |c_1\rangle, |c_2\rangle$ defined by (4.25). Detailed discussion of that approximation is presented in a subsection (CC matrix elements) of the present section.

Substituting (4.11) in (4.10) and solving for $G_g, G_c, G_{c_1}, G_{c_2}$ we get:

$$\begin{aligned}
G_g(z) &= \frac{1}{z - E_g - I_g(z)} \\
G_c(z) &= \frac{(z - E_{\bar{c}})D_{cg}}{(z - E_c)(z - E_c + \Delta_c) - (|\Omega_1|^2 + |\Omega_2|^2)} G_g(z) \\
G_{c_1}(z) &= \frac{D_{c_1 c} D_{cg}}{(z - E_c)(z - E_c + \Delta_c) - (|\Omega_1|^2 + |\Omega_2|^2)} G_g(z) \\
G_{c_2}(z) &= \frac{D_{c_2 c} D_{cg}}{(z - E_c)(z - E_c + \Delta_c) - (|\Omega_1|^2 + |\Omega_2|^2)} G_g(z)
\end{aligned}$$

With $\Delta_c = E_c - E_{\bar{c}}, I_{g(z)}$ are given by:

$$I_g(z) = \int d\epsilon_c \frac{|D_{cg}|^2 (z - E_{\bar{c}})}{(z - E_c)(z - E_c + \Delta_c) - (|\Omega_1|^2 + |\Omega_2|^2)} \tag{4.12}$$

The continuum is now represented by the integral $I_g(z)$, which under certain conditions leads to well-known decay rate and energy shift of a few degree of freedom system (here the atomic ground state) coupled to an infinite degree of freedom system (the atomic continuum states). These conditions depend on the atomic system under consideration in combination with the pulse parameters. For photon energies near the $1s - 2p$ hydrogenic transition and for pulse intensities $I \leq 3 \times 10^{13}$ (see discussion at the end of this section) we can safely approximate $I_g(z)$ as:

$$I_g = S_g - i\frac{\Gamma_g}{2}, \tag{4.13}$$

$$S_g = P\int d\epsilon_c \frac{|D_{gc}|^2}{E_g - E_c}, \tag{4.14}$$

$$\Gamma_g = 2\pi |D_{gc}(E_c = E_g^{'} + \hbar\omega)|^2 . \tag{4.15}$$

S_g represents the shift of the ground state energy E_g' due to its interaction with the continuum and Γ_g the decay rate of the ground state to the continuum $|c\rangle$. Substituting S_g, Γ_g and taking now the inverse Laplace-transform (equation 4.9) for the amplitudes $G_c(z), G_{c_1}(z), G_{c_2}(z)$ we can calculate the amplitudes $U_{gg}(t), U_{cg}(t), U_{c_1,g}(t), U_{c_2 g}(t)$. The photoelectron energy spectrum (PES) is defined as the population of the continuum in the long-time

limit (in practice at the end of the pulse) given by:

$$\begin{aligned} S(\epsilon_c) &= \lim_{t\to\infty}\left[|U_{cg}(\epsilon_c,t)|^2+|U_{c_1,g}(\epsilon_c,t)|^2+|U_{c_2,g}(\epsilon_c,t)|^2\right] \\ &= \frac{\Gamma}{8\pi}(\frac{\Omega_0}{\Omega_c})^2\left[\frac{1+\left(\frac{\Omega_0}{\Omega_c-\Delta_c}\right)^2}{\mu_+^2(\epsilon_c)+(\frac{\Gamma}{2})^2}+\frac{1+\left(\frac{\Omega_0}{\Omega_c+\Delta_c}\right)^2}{\mu_-^2(\epsilon_c)+(\frac{\Gamma}{2})^2}\right] \end{aligned} \tag{4.16}$$

with,

$$\begin{aligned} \Omega_c^2 &= \Delta_c^2+\Omega_0^2=\Delta_c^2+4|D_{c\bar{c}}|^2, \\ |D_{c\bar{c}}|^2 &= |D_{cc_2}|^2+|D_{cc_1}|^2, \\ \mu_\pm &= (E_c-E_{\bar{c}})/2-\bar{E}_g\pm\Omega_c/2 \\ \Delta_c &= E_c-E_{\bar{c}} \\ \bar{E}_g &= E_g+S_g(t), \end{aligned}$$

From elementary analysis of equation (4.17), two peaks are expected, depending on the photon frequency and the laser intensity, at the positions determined from the equations $\mu_\pm(\epsilon_c) = -\Delta_c/2-\Delta^{'}\pm\Omega_c/2+\epsilon_c = 0$. Therefore the position and the height of these peaks are :

$$h_\pm = \frac{1}{2\pi\Gamma_g}(\frac{\Omega_0}{\Omega_c})^2\left[1+\left(\frac{\Omega_0}{\Omega_c\mp\Delta_c}\right)^2\right] \tag{4.17}$$

$$\epsilon_c^\pm = \Delta_c/2+\Delta^{'}\mp\Omega_c/2 \tag{4.18}$$

where $\Delta' = S_g+\omega+E_g'-E[H(1s)]$. It is evident that we have an assymetric doublet where the relative position along the energy axis depends on the sign of Δ_c and the distance from each other is a function only of Ω_c which is a measure of the strength of the core transition controlled by from the pulse parameters via photon frequency and intensity.

CC Matrix Elements In this paragraph we calculate the matrix elements D_{cc_1}, D_{cc_2}, which represent transitions between two-electron states,

$$\begin{aligned} D_{cc_1}(t) &= \langle 1s\varepsilon p\,{}^1P|\,D(t)\,|2p\varepsilon p\,{}^1S\rangle \\ D_{cc_2}(t) &= \langle 1s\varepsilon p\,{}^1P|\,D(t)\,|2p\varepsilon p\,{}^1S\rangle. \end{aligned} \tag{4.19}$$

Assuming the electric field linearly polarized, along the z-axis, the dipole operator D is written as:

$$D = -(\mathbf{r}_1+\mathbf{r_2})\mathbf{E}(t) = -E\,(z_1+z_2)\,, \tag{4.20}$$

The dipole matrix elements in equation (4.19) differ only in the total angular momentum (consequently in the angular part of the corresponding integral) and therefore it is possible to find a relation between them. Beacause of the similarity in the calculation of the above matrix elements we consider first the calculation of the $D_{cc_1} \equiv \langle c|D|c_1\rangle$ matrix element.

The two-electron states $\Phi(E,^1P) = |1s\varepsilon p\ ^1P\rangle$, $\Phi(E+\omega,^1S) = |2p\varepsilon p\ ^1S\rangle$, $\Phi(E+\omega,^1D) = |2p\varepsilon p\ ^1D\rangle$, are eigenstates of the hamiltonian $H = H_0(\mathbf{r}_1)+H_0(\mathbf{r}_2)+1/|\mathbf{r}_1-\mathbf{r}_2|$ (eq. 1.60), expanded (in principle) as an infinite sum of two-electron configuration orbitals (eq. 1.62), $\Psi(E,^1P)$, $\Psi(E+\omega,^1S)$, $\Psi(E+\omega,^1D)$ (eq. 1.63),

$$\begin{aligned}\Phi(E,^1P) &= \int d\epsilon C(1s\varepsilon p^1P)\Psi(1s\varepsilon p^1P) \\ &+ \sum_{n_1l_1,n_2l_2} C(n_1l_1;n_2l_2^1P)\Psi(n_1l_1;n_2l_2^1P)\end{aligned}$$

For energies E where the correlation interaction is insignificant the state $\Phi(E,^1P)$ is approximated sufficient well by the dominant two-electron configuration at the same energy. The two-electron continuum ^1P of H^-, has its first AIS $|2s2p^1P\rangle$ in position $E = 10.277$eV (with the hydrogen ground state energy as the zero of the energy axis) and width $\Gamma_a \sim 10^{-5}$ a.u. . On the other hand the transition $|1s^2\ ^1S\rangle \rightarrow |2p\varepsilon p\ ^1P\rangle$ brings the system to an energy $E = E_g + \omega \sim 9.46$eV. At this energy the CI of the ^1P continuum is neglilible, thus allowing us to make the approximation,

$$\Phi(E,^1P) \sim \Psi(1s(\varepsilon = E_g+\omega)p^1P). \tag{4.21}$$

Provided that, we deal with transitions sufficiently far from any continuum structure of the ^1P, such as the $2s2p^1P\rangle$AIS, the above approximation is quite valid. This condition is dependent on the intensity of the E/M field and its duration. The range of that paramaters will be discussed in more detail in a paragraph at the end of this section. For the same reasons, the other two states $\Phi(E+\omega,^1S)$, $\Phi(E+\omega,^1D)$, are approximated by the corresponding two-electron configuration states $\Psi(2p\varepsilon = E+\omega,^1S)$, $\Psi(2p\varepsilon = E+\omega,^1D)$. Therefore the two-electron states $|c\rangle, |c_1\rangle, |c_2\rangle$ are written as a sum of Slater determinants of one-electron orbitals of the type (1.62), namely:

$$|1s^2\ ^1S\rangle = \psi_{00}\,, \tag{4.22}$$

$$|1s\varepsilon p\ ^1S\rangle = \frac{1}{\sqrt{3}}\left[\psi_{11} - \psi_{10} + \psi_{1-1}\right]\,, \tag{4.23}$$

$$|1s\varepsilon p\ ^1D\rangle = \frac{1}{\sqrt{6}}\left[\psi_{11} + 2\psi_{10} + \psi_{1-1}\right]\,, \tag{4.24}$$

where $\psi_{m_{l_1},m_{l_2}}$ are the Slater determinants of the states $|(n_1/\varepsilon_1)l_1, s_1, m_{l_1}, m_{s_1}; (n_2/\varepsilon_2)l_2, s_2, m_{l_2}, m_{s_2}\rangle$. The one-orbital states are the hydrogenic bound and continuum states, $\phi_{1s}(\mathbf{r}), \phi_{2p}(\mathbf{r}), \phi_{\varepsilon p}(\mathbf{r}), \phi_{\varepsilon' p}(\mathbf{r})$ given by:

$$\begin{aligned}\phi_{1s}(\mathbf{r}) &= R_{1s}(r)\, Y_{00}(\theta,\phi)\,,\\ \phi_{2p}(\mathbf{r}) &= R_{2p}(r)\, Y_{10}(\theta,\phi).\end{aligned}$$

The asymptotic form of the continuum one-electron states is:

$$\begin{aligned}\phi_{\varepsilon p}(\mathbf{r}) &= R_{\varepsilon p}(r)\, Y_{10}(\theta,\phi) = \frac{\sin(kr-\pi/2-\delta_1^S(\varepsilon))}{r}\, Y_{10}(\theta,\phi)\,,\\ \phi_{\varepsilon' p}(\mathbf{r}) &= R_{\varepsilon' p}(r)\, Y_{10}(\theta,\phi) = \frac{\sin(kr-\pi/2-\delta_1^S(\varepsilon'))}{r}\, Y_{10}(\theta,\phi)\,,\end{aligned}$$

with $\varepsilon = k^2/2$ and $\delta_1^i(\varepsilon)$ the kinetic energy and the phase shift of the outgoing electron. The upperscript $i = S, D$ of the phase shifts implies the different potential 'experienced' by the outgoing electron due to the different angular configuration of the two-electron state.

Since it is now clear what the two-electron states represent we proceed to the calculation of the dipole matrix elements, which is straightforward though tedius, starting with the D_{cc_1}.

$$\begin{aligned}D_{cc_1} &= \langle c|-z_1E(t)|c_1\rangle + \langle c|-z_2E(t)|c_1\rangle = \ldots\ldots =\\ &= -\frac{4}{\sqrt{12}}\left[\langle\phi_{1s}|z|\phi_{2p}\rangle\langle\phi_{\varepsilon p}|\phi_{\varepsilon' p}\rangle + \langle\phi_{1s}|\phi_{2p}\rangle\langle\phi_{\varepsilon p}|z|\phi_{\varepsilon' p}\rangle\right]\, E(t)\\ &= -\frac{4}{\sqrt{12}}\langle\phi_{1s}|z|\phi_{2p}\rangle\langle\phi_{\varepsilon p}|\phi_{\varepsilon' p}\rangle\, E(t)\,,\end{aligned}$$

since it is obvious that, $\langle\phi_{1s}|\phi_{2p}\rangle = 0$. Somewhat more tricky, is the evaluation of the $\langle\phi_{\varepsilon p}|\phi_{\varepsilon' p}\rangle$ product.

$$\begin{aligned}\langle\phi_{\varepsilon p}|\phi_{\varepsilon' p}\rangle &= \int d^3\mathbf{r}\phi_{\varepsilon p}(\mathbf{r})\phi_{\varepsilon' p}(\mathbf{r}) = \int dr r^2 R_\varepsilon(r)R_\varepsilon(r)\\ &= \delta(\varepsilon-\varepsilon')\cos(\delta_1^S(\varepsilon)-\delta_1^D(\varepsilon)).\end{aligned}$$

For the H^- the phase shifts corresponding to the involved photoelectron kinetic energies ($\sim$ 0.37a.u.) are neglilible for both channels S or D (see figure 1.5). Finally we obtain $\langle\phi_{\varepsilon p}|\phi_{\varepsilon' p}\rangle = \delta(\varepsilon-\varepsilon')$, thus giving for the matrix element $D_{cc_1}(t) = -\frac{4}{\sqrt{12}}\langle\phi_{1s}|z|\phi_{2p}\rangle\delta(\varepsilon-\varepsilon')E(t)$. We have $\langle\phi_{1s}|z|\phi_{2p}\rangle = -d/\sqrt{3}$, where $d = 1.29$ a.u. is the radial dipole matrix element of the

hydrogenic $1s-2p$ transition. Noting now that the calculation of the other matrix element D_{cc_2} is similar with that of D_{cc_1}, we obtain finally, for the two-electron dipole matrix elements:

$$\begin{aligned} D_{cc_1}(t) &= -\frac{2}{\sqrt{3}}\, dE(t)\delta(\varepsilon-\varepsilon') = \Omega_1(t)\delta(\varepsilon-\varepsilon') \\ D_{cc_2}(t) &= \frac{2\sqrt{2}}{\sqrt{3}}\, dE(t)\delta(\varepsilon-\varepsilon') = \Omega_2(t)\delta(\varepsilon-\varepsilon') \end{aligned} \tag{4.25}$$

The strength of the transition into the continua $|c_1\rangle$ and $|c_2\rangle$ is $\Omega_2/\Omega_1 = 1\sqrt{(2)}$. Using equations (4.25) the approximations (4.11) are quite obvious.

Intensity dependence of Γ_g, S_g, Ω_c For the given transition $\omega_R = 0.375$ a.u. we have $\Gamma_g = 2\pi|D(\epsilon = \omega_R + E_g)|^2$, $S_g = -(E^2(t)/4)\alpha_g(\omega_R)$, for the decay rate and the shift of the ground state. The quantity $\alpha_g(\omega)$ is the dynamic dipole polarizability, defined by the relation (5.13). In first approximation, $\alpha(\omega_R) \sim -10$ as someone can be see from figure 5.4). On the other handHaving obtained the one-photon two-electron dipole matrix element (see figure **??**), and using equations (4.25) we find,

$$\begin{aligned} \Gamma_g &\sim 0.00123 I_0\,, \qquad S_g \sim 0.46 I_0\,, \\ \Omega_1 &= 0.86\sqrt{I}\,, \qquad \Omega_1 = 1.21\sqrt{I}\,, \end{aligned} \tag{4.26}$$

which are useful, for estimations of the relevant magnitude of the quantities. It is evident now, that for the intensities we use ($I_0 \leq 10^{14} W/cm^2$) the Rabi frequency of the core-couplings is much larger than the decay rate of the ground state Γ_g, $\Omega_c \gg \Gamma_g$. From the same relations, we can see that the ac-Stark shift is much less compared than the ground state energy E_g and the photon energy.

Approximations and pulse parameters range. The validity of both approximations, (4.15) and (4.11) depends on the pulse characteristics, such as the photon energy, intensity and duration. Given that we deal with the core excitation of H^-, we have for the photon energy $\omega = 0.375$ù. . The interaction of the ground state with the continuum $|1s\varepsilon p^1P\rangle$ is represented now, effectively, by the integral $I_g(z)$ (eq.4.12). In the absence of the core-resonant transition $\Omega_1 = \Omega_2 = 0$, this integral reduces to the well-known intgral form $\int d\epsilon_c |D_{gc}|^2/(z - E_c)$, where making the pole approximation gives the normal shift and decay rate of the ground state, because of its interaction with the continuum. The core-resonant coupling with the other two continua $|2p\varepsilon p^1S\rangle, |2p\varepsilon p^1D\rangle$, modifies accordingly the shift and the decay rate. The relevant algebra and formulas have been presented in detail

by Hanson et al [40]. As indicated in that work, provided that the coupling strengths are, in first approximation, constant over a range of the order of the Rabi frequencies Ω_1, Ω_2, then the shift and the decay rate of the ground state are given by relations (4.15). This means, that the results are not expected to be reliable if the peaks of the PES approach thresholds or AIS. Since the photon energy is $\omega = 0.375$ü. we normally have (weak fields) a Lorentzian peak at the position $\epsilon = 0.3473$. Increasing the intensity, the doublet starts to appear with peak separation equal to the Rabi frequency Ω_c. Around this region the dipole matrix elements have a smooth dependence on energy (very small negative derivative, see figure (??), while the first structure occurs very close to the $n = 2$ first excitation threshold of hydrogen, at the position $\epsilon \sim 0.375$ a.u. We must ensure that the intensities we use give Rabi frequencies restricted by the inequality, $\Omega_c < 2E_g$. Using equations (4.26) we obtain for the peak intensity of the pulse:

$$I_0 < 10^{14} W/cm^2 \,. \tag{4.27}$$

On the other hand, for finite duration pulses the Fourier bandwidth should be less than $E_g = 0.0277$ a.u., namely $\Delta\omega \ll E_g$. Noting that $\Delta\omega \sim T^{-1}$, with T being roughly the duration of the pulse, we obtain

$$T \gg 1 fs \,. \tag{4.28}$$

Using pulses, which satisfy the above conditions, approximation (4.11) is well justified, since for the involved energy region the two-electron continuum states have negliglible correlation interaction.

4.4 General pulse shape

Until now we had made the assumption of constant amplitude E/M field. We are going to study the same problem by using more realistic laser pulses, such as having a gaussian or $\sin^2$ shape. The resolvent operator method is still valid, if someone imagine application of that method in consecutive time-intervals, where the hamiltonian can be considered as constant. However, we will follow another way for treating the problem for finite-duration pulses. From equations (4.12) through the inverse Laplace transform we get the time-dependent equations for $G_g(t), G_c(t), G_{c_1}(t), G_{c_2}(t)$:

$$\begin{aligned} i\frac{dU_{gg}}{dt} &= \left[E_g + S_g(t) - i\frac{\Gamma_g(t)}{2}\right] U_{gg} \\ i\frac{dU_{cg}}{dt} &= E_c U_{cg} + D_{cc_1} \cdot U_{c_1 g} + D_{cc_2} \cdot U_{c_2 g} + D_{cg} \cdot U_{gg} \end{aligned}$$

$$
\begin{aligned}
i\frac{dU_{c_1 g}}{dt} &= E_{\bar{c}} U_{c_1 g} + D_{c_1 c} \cdot U_{cg} \\
i\frac{dG_{c_2}}{dt} &= E_{\bar{c}} U_{c_2 g} + D_{c_2 c} \cdot U_{cg}
\end{aligned}
$$

The quantities in the above equations are dependent on photoelectron energy ϵ_c and the time t namely, $\Gamma = \Gamma(t), S_g = S_g(t)$, $D_{cg} = D_{cg}(\epsilon_c, t)$, $U_{cg} = U_{cg}(\epsilon_c, t)$ $U_{c_1 g} = U_{c_1 g}(\epsilon_c, t)$ $U_{c_2 g} = U_{c_2 g}(\epsilon_c, t)$.

The resolvent operator, here is used first for the treatment of the constant laser pulse and secondly for the elimination of the continuum, in a consistent way. The time-dependent differential equations are free from integrals over the continuum states, since only the decay rate Γ_g and the energy shift S_g are included. The pulses we use have the form as given by equation (4.8) with the amplitude time-dependent either of gaussian or $\sin^2$ form (eq.2.8). In order to compare our results with different pulse shapes we choose in the duration of the pulses, so that the total E/M energy given to the atomic system as the same. If the duration of the square pulse is T, the duration of the $\sin^2$ pulse is $2T$ and the duration of the gaussian pulse is $0.6T$. As we shall see below, for those pulses the results does not differ significantly.

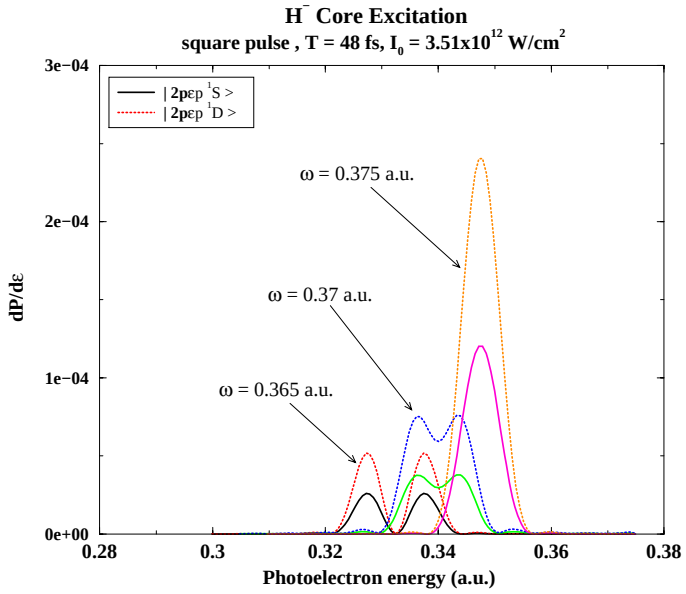

Figure 4.2: Partial PES of the excited core states as a function of the photon energy. The pulse used is of constant amplitude.

4.5 PES of H^- near Core Resonance

In figure 4.3 we plot the PES for various photon energies for the three pulses used. Starting with $\omega = 0.365$ a.u. we note an asymmetric peak of the PES. It is more obvious for $\omega = 0.37$ a.u. . The lower peak is due mainly to the excited core states $|2p\varepsilon p^1S\rangle, |2p\varepsilon p^1D\rangle$, and the higher peak is due to the ground core state $|1s^2\ ^1S\rangle$ (see figure 4.4). The structure of the PES is quite similar for all three-different in shape pulses, although the phenomena are more pronounced for the square pulse, due to the constant value of its amplitude. An example of such of phenomenon is the assymetric peak, mentioned before. Exactly on resonance the doublet makes its appearance, although not strongly. For the specific duration, the intensity of the light is not sufficient for the strong manifestation of the doublet. Finally, note the symmetry of the PES structure between the symmetric (regarding the resonant energy ω_R) photon energies $\omega = (0.365-0.385)a.u.$ and $\omega = (0.37-0.38)a.u.$.

In figures 4.4 and 4.2, we present partial PES where the population of the system in the ground and excited core state can be determined. For off resonance, photon energies the ground core states is highly populated in the expected photoelectron energy $\epsilon = \omega + E_g$. However, there is an appreciable population of the excited states in photoelectron energy $\epsilon = \omega + E_g - (\omega_R - \omega) = 2\omega + E_g - \omega_R$. In reality this peak is the lower-energy member of a doublet peak, occuring in the population of the excited states, the other peak being located at the energy $\epsilon = \omega + E_g$, thus overhelmed by the population of the ground state. The peaks are sharper in the case of the square pulse, though the structure is evident for the other shapes as well. As the photon energy approaches the core resonant energy the symmetric doublet begins to dissapear (figure 4.2), while on resonance we have one peak for the core-excited states. At the same time the population in the ground-core state decreases (to the benefit of those of the core-excited state) where on resonance they are of comparable magnitude (figure 4.4). Note that the core-excited state, belonging to the ^1D two-electron continuum has larger population than of that belonging to the ^1S two-electron continuum, as expected.

In figures 4.5 we plot the PES as a function of the peak intensity of the pulse, for the gaussian and the $\sin^2$ pulses. The development of the doublet from the single Lorentzian to the doublet of peaks is presented. The doublet peak structure begins to make its appearance for intensities at about $\sim 3 \times 10^{12} W/cm^2$, while for intensities up to $\sim 9 \times 10^{12} W/cm^2$ a strong symmetric doublet exists. No significant difference, due to the shape

of the pulses, exists in the PES.

Next, we present PES as a function of the duration of the pulses. Results for the square and the $\sin^2$ pulses are plotted (figures 4.6). The sharpness of the peaks with increasing the duration T is evident due to the corresponding sharpness of the Fourier bandwith ($\Delta\omega \sim T^{-1}$). However, a difference exists between the two pulses. The asymmetry of the peaks in the PES changes.

Finally, in figure 4.7, PES for pulses that differ only in shape is presented. Since the transferred E/M energy is the same for all pulses, the spectrum is very similar for all cases.

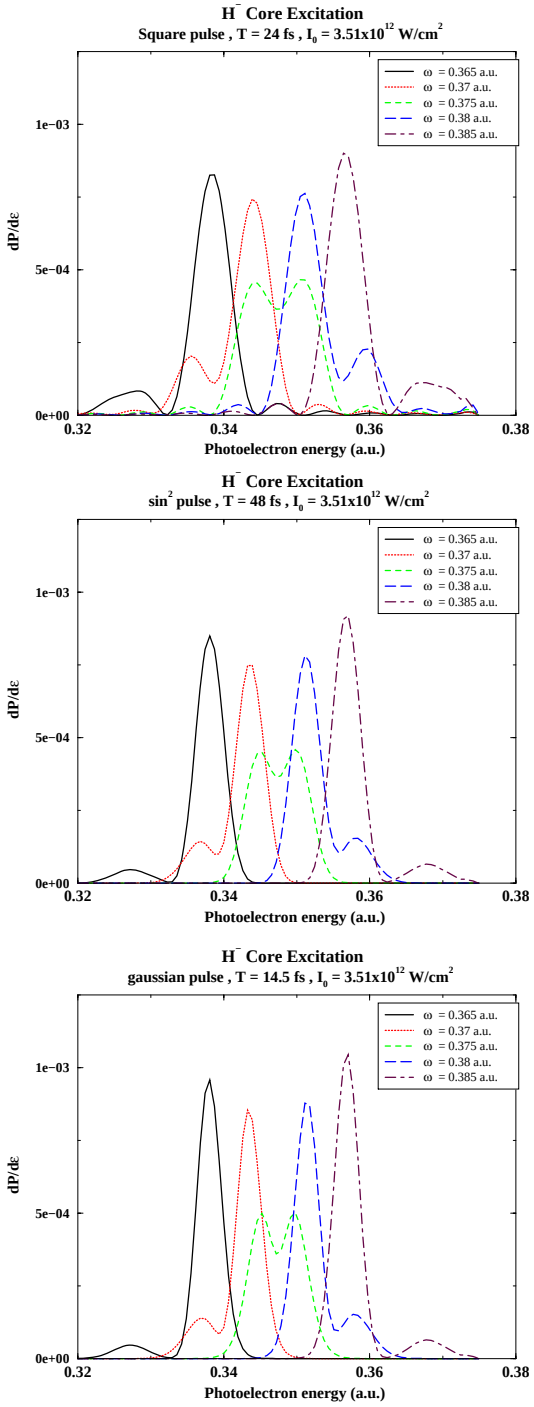

Figure 4.3: PES for various photon energies and for the three used pulses, square, sin^2 and gaussian

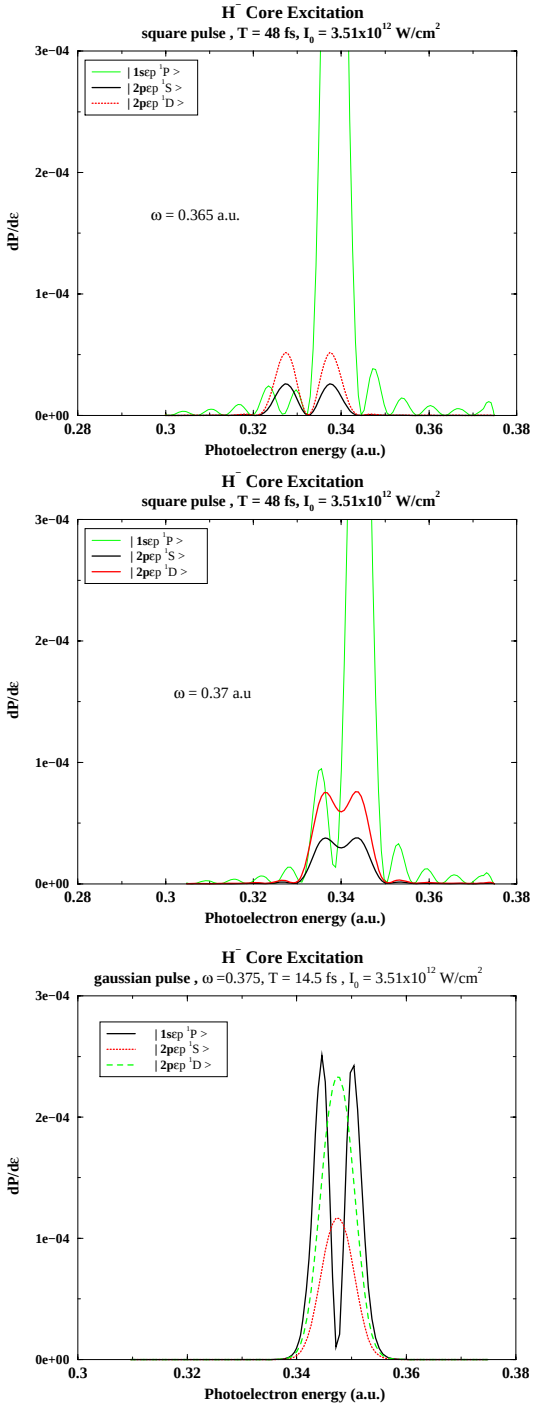

Figure 4.4: Partial PES, indicating the population in the ground and the excited states. Note the doublet in the PES of the excited states. This doublet dissapears on resonance.

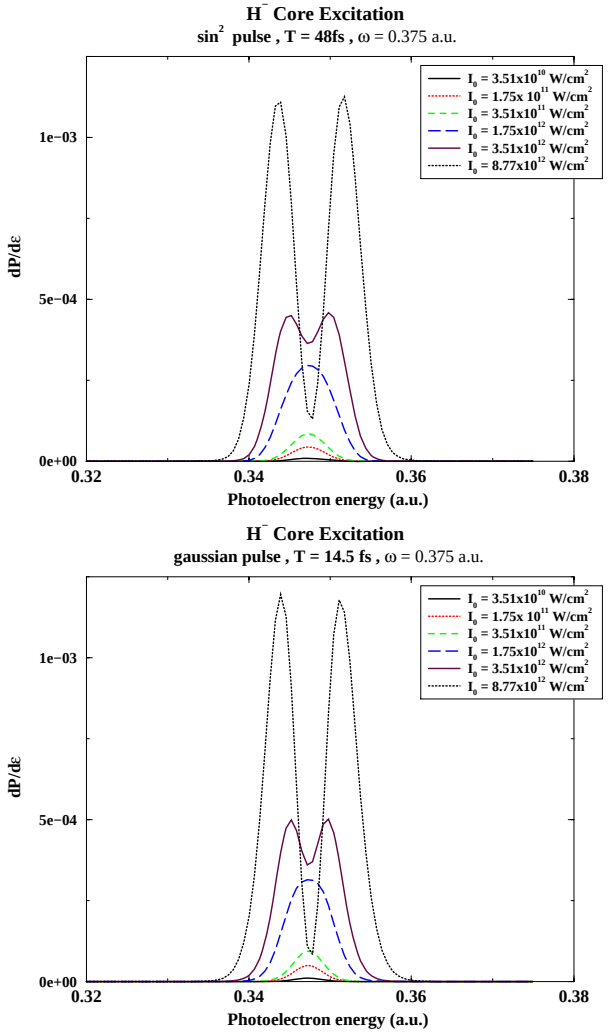

Figure 4.5: The development of the double structure of the PES as a function of the peak intensity of the pulse. The data are plotted for the sin^2 and gaussian pulse.

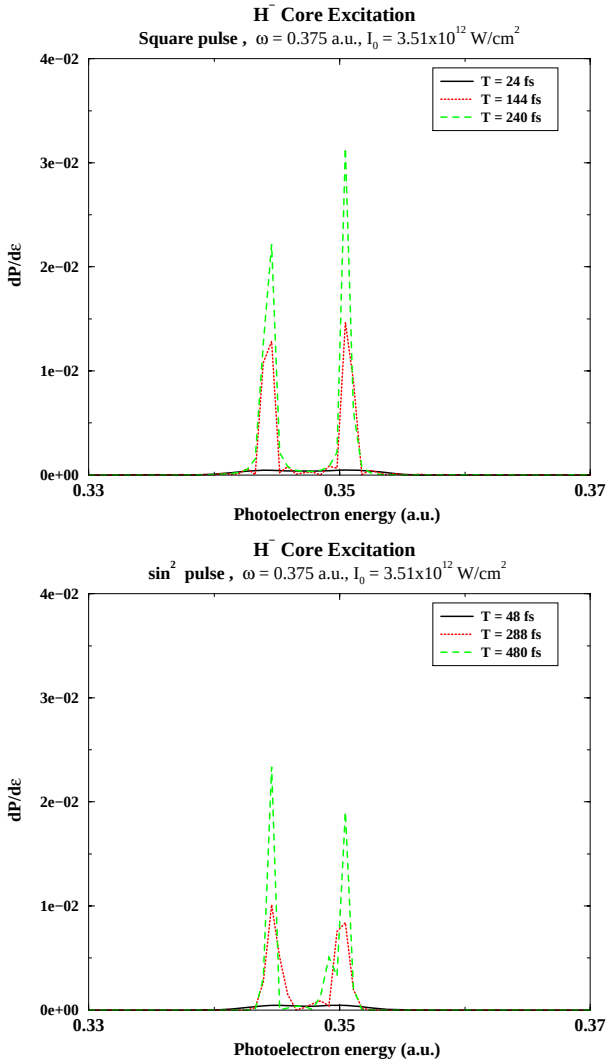

Figure 4.6: PES as a function of the duration of the pulses.

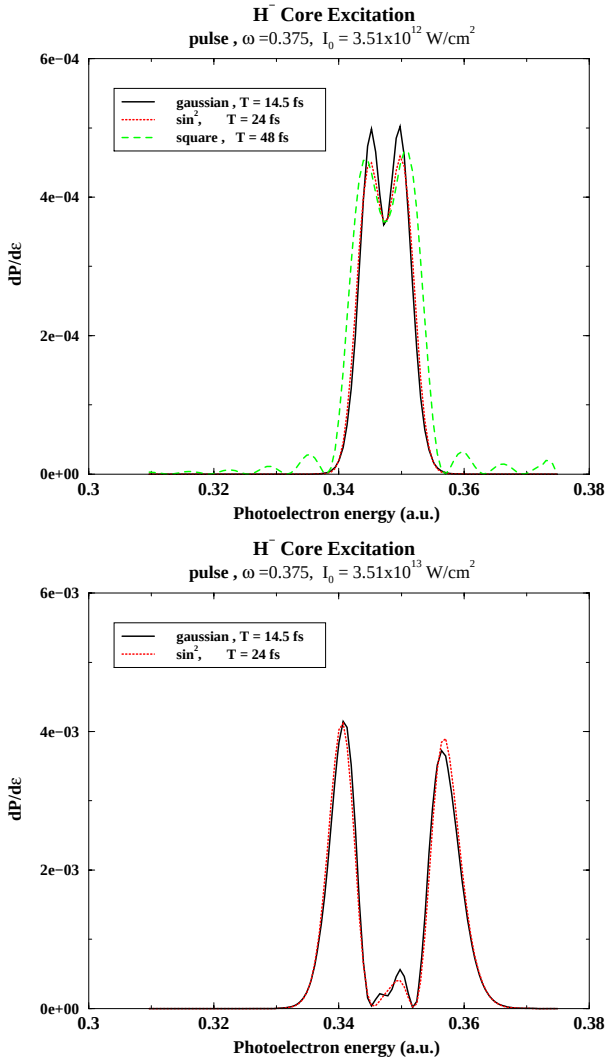

Figure 4.7: PES for different pulses, for two different peak intensities.

Chapter 5

TDSE of H^- in a strong laser field

5.1 Introduction

As a two-electron system the negative hydrogen ion (H^-) is rather unique in that its very existence as a bound system relies on strong electron correlation. It has thus served as a prototype in many studies of traditional single-photon absorption and continues attracting interest in that context [7, 5, 54, 85]. Naturally, it has also received attention in the context of ionization (detachment) under strong laser fields, as its behavior sheds light on subtle aspects not easily accessible in other two-electron systems such as Helium or the alkaline earths [56, 15, 66, 64, 26, 72, 75, 71]. Its low binding energy (~ 0.754eV), vis a vis the photon energy of available lasers, poses special difficulties in the experimental exploration of multiphoton processes and ATI (above threshold ionization) which has required particular inventiveness on the part of those who have conducted such studies [81, 92, 2, 1, 80], most notably Bryant and collaborators [81, 92] and references therein. Note that the frequency tuning in that series of experiments has been achieved through the Doppler shift of radiation from a CO_2 laser relative to a fast H^- beam. Interestingly, the most recent of their results [92] have made possible the measurement of the ratio of the S to the D partial wave in two-photon detachment at photon energy in the range of 1.165eV, in good agreement with theory [61, 83, 45].

Until now the interpretation of the relevant experimental data has proven successful within LOPT (Lowest-order perturbation theory) and sometime even on the basis of single-electron model. Yet the question of its behavior

under conditions requiring the non-perturbative solution of the TD (time-dependent) Schrödinger equation remains practically open. A beginning in that direction is represented by the very recent results of Scrinzi and Piraux [75], using an extension of their technique reported in an earlier paper [74], which, however, has not included photoelectron energy spectra and ATI. It is our purpose in this paper to report results obtained through a TD non-perturbative theory based on a fully correlated two-electron model providing complete information on the behavior of the system including ATI. To the best of our knowledge, this represents the first glimpse of ATI in H^- beyond the single-electron model and in a photon frequency range that has been examined experimentally, albeit at intensities corresponding to the perturbative regime. Some of our results, such as ionization yields as a function of laser power, offer the possibility of comparison with analogous results obtained by means of different techniques [56, 64, 26, 61], in addition to those of Scrinzi and Piraux, providing thus an assessment of the present state of understanding of this basic problem in strong field interactions beyond the single active electron approximation.

5.2 Time Dependent Schrödinger Equation

The time-dependent Schrodinger equation (TDSE) for a two-electron system in an external laser field is written as (in atomic units),

$$i\partial_t\psi(\mathbf{r_1},\mathbf{r_2},t) = [H_0 + V(t)]\ \psi(\mathbf{r_1},\mathbf{r_2},t) \tag{5.1}$$

with H_0 the free-field atomic hamiltonian and V the time-dependent interaction between the system and the laser field. In the velocity gauge, the interaction operator is

$$V(t) = -\frac{1}{c}(\mathbf{p_1} + \mathbf{p_2})\,\mathbf{A}(t), \tag{5.2}$$

with $\mathbf{p}_1, \mathbf{p}_2$ being the momenta of the two electrons and $\mathbf{A}$ the vector potential which is connected with the electric field through the relation $\mathbf{E} = -c^{-1}\partial_t\mathbf{A}$. In our calculations, we assume laser fields linearly polarized along the z-axis for which,

$$\mathbf{A}(t) = \mathbf{e}_z\, A_0\, f(t)\, \sin\omega t, \tag{5.3}$$

where $f(t) = \sin^2(\pi t/T)$ is the pulse envelope of duration T. The basic idea and the formal details of the construction of the two-electron states (with

total angular momentum L) can be found in [9, 11]. In brief, we use one-electron hydrogenic orbitals, $\phi_{nlmm_s}(\mathbf{r}) = r^{-1}P_{nl}(r)Y_{lm}(\theta,\phi)\sigma(m_s)$, with the radial functions $P_{nl}(r)$ satisfying the well known radial eigenvalue equation. The P_{nl} functions with negative or positive eigenvalues are expanded on a set of B-splines of order k and total number N defined in the finite interval $[0, R]$. The two-electron energy eigenfunctions of the system are then written in the form [11],

$$\Phi^{SL}_{n(E)}(\mathbf{r}_1,\mathbf{r}_2) = \sum_{n_1l_1,n_2l_2} C^{SL}_{n(E)}(n_1l_1,n_2l_2)\Psi^{SL}_{n_1l_1,n_2l_2}(\mathbf{r_1},\mathbf{r_2}), \tag{5.4}$$

where $\Psi^{SL}_{n_1l_1,n_2l_2}$ are the two-electron orbitals, of total angular momentum L, constructed in the LS coupling of two-electron configuration space. Here $|C^{SL}_{n(E)}(n_1l_1,n_2l_2)|^2$ is the probability density for the configuration (n_1l_1,n_2l_2) in the nth energy eigenstate belonging to the symmetry SL. For $E > 0$, $\Phi^{SL}_{n(E)}$ represent the discrete continuum states. The two-electrons eigenfunctions $\Phi^{SL}_{n(E)} \equiv \Phi_{nLM}$ satisfy the eigenvalue equation and the boundary conditions,

$$H_0\Phi_{nLM}(\mathbf{r}_1,\mathbf{r}_2), \;=\; E_{nL}\Phi_{nLM}(\mathbf{r}_1,\mathbf{r}_2) \tag{5.5}$$

$$\Phi_{nLM}(0,0) = \Phi_{nLM}(\mathbf{R},\mathbf{r}_2) \;=\; \Phi_{nLM}(\mathbf{r}_1,\mathbf{R}) = 0. \tag{5.6}$$

Yet the nature of this system requires particular care as outlined below. In order to construct the one-electron radial eigenfunctions P_{nl}, a box of radius $R = 1000a.u.$ with 992 B-splines of order $k = 9$ has been used. The two-electron basis functions $\Psi^{SL}_{n_1l_1,n_2l_2}(\mathbf{r_1},\mathbf{r_2})$ are constructed in terms of about 2000 configurations (n_1l_1,n_2l_2) for the symmetry $L = 0$ and about 1500 for each of the other symmetries up to L = 8.

Although, the matrix elements involved in our time-dependent calculations are in the velocity gauge, we have also calculated them in the length gauge in order to check the completeness of our two-electron basis. The basis we have chosen describes very well the continuum eigenstates but not very accurately the energy of the ground state. The value it yields for the ground state differs from that calculated by Pekeris [63] by about 16%. In principle, it is possible to improve, the strongly correlated ground state energy further by including many more configurations, which in practice means a larger computational effort, which would not alter our basic results in any significant way. It should be noted that we do obtain a much more accurate value, namely $E_g = -0.0277$ a.u., for the ground state energy if we use a much smaller box radius, namely $R = 20$ a.u. . This illustrates an inevitable conflict of requirements for an accurate ground state energy as opposed to

a box sufficiently large to accommodate excitation high into the continuum, a conflict that is inherent in strong field non-perturbative theory. Assuming the negative ion to be initially in its ground state with the field being linearly polarized along the z-axis, we need consider only the $M = 0$ singlet states ($S = 0$). Expanding, the time-dependent wavefunction, in the basis functions $\Phi^{SL}_{n(E)}$ as,

$$\psi(\mathbf{r_1}, \mathbf{r_2}, t) = \sum_{n,L} b_{nL}(t)\, \Phi^{SL}_{n(E)}(\mathbf{r_1}, \mathbf{r_2}), \tag{5.7}$$

and substituting in the TDSE we obtain a system of coupled first order differential equations for the unknown coefficients $b_{nL}(t)$:

$$i\frac{d}{dt}b_{n,L} = \sum_{n',L'} (E_{nL}\, \delta_{nn'}\delta_{LL'} - V_{nL,n'L'}(t))b_{n'L'}\,. \tag{5.8}$$

with the initial condition, $|b_{n=1,L=0}(t = 0)|^2 = 1$. Truncation of this system of equations (or equivalently the necessary number of states $\Phi^{SL}_{n(E)}$), depends on the specific structure of the atom or ion, the pulse characteristics (peak intensity, photon frequency, pulse duration) and finally the particular observable to be calculated, namely, ionization probability (Yield), photoelectron energy spectrum (PES), angular distributions (PAD) of photoelectrons or harmonic intensities.

The total number of coupled equations was about 250, corresponding to the total number of two-electron states, of which the higher 30 or so corresponded to double-electron excitation. This selection, does not include the double-ionization continuum, since its inclusion did not change the results. This is reasonable, because of the high-order process, in combination with the shortness of the pulse, which is needed to get significant population to those states. Therefore increasing the total number of states to about 400, the results had remained unchanged. We have also investigated the time-dependence of the population of the states involved during the time-evolution of the process. Roughly, the ratio of the population of the doubly-excited states to the population of the lower-energy states (single-ionization without core-excitation) was about 10^{-6}. In practice, neither the doubly-excited states nor the doubly-ionized states could have any significant influence on the yields. However, they might have some slight influence on the PES but this is insignificant for the pulse lengths we have used.

In the B-splines technique the density of states is determined by the radius of the "box", R. We have tested the convergence of the results, with respect to the density of states by increasing the radius of the "box". Between $R = 1000, 1250, 1500$ a.u. no appreciable change has been found.

5.3 Yield and PES of H^-

In the present study for the pulses we use, photon frequency ($\omega \sim (0.5 - 2)$eV), duration $\sim (10 - 40)$fs and peak intensity ($I_0 \leq 10^{13} W/cm^2$) the selected states do not need to include the double continuum. Propagating in time equation (5.8) until the end of the pulse, we are able to calculate, the ionization probability (P), the PES (S) and the PAD (A) through the relations,

$$P(t \to \infty) = \sum_{L,n(E\geq 0)} |b_{L,n(E)}(t)|^2, \tag{5.9}$$

$$S(E_c, t \to \infty) = \sum_{L,n(E=E_c)} |b_{L,n(E)}(t)|^2, \tag{5.10}$$

$$A(\theta, E, t \to \infty) \sim |\sum_{L=0}^{\infty} (-i)^L e^{i\delta_L} \sqrt{2L+1}\, P_L(\theta) b_{L,n(E)}(t)|^2, \tag{5.11}$$

respectively. Here δ_L is the scattering phase shift of the continuum eigenfunction and $P_L(\theta)$ is the Legendre polynomial of order L.

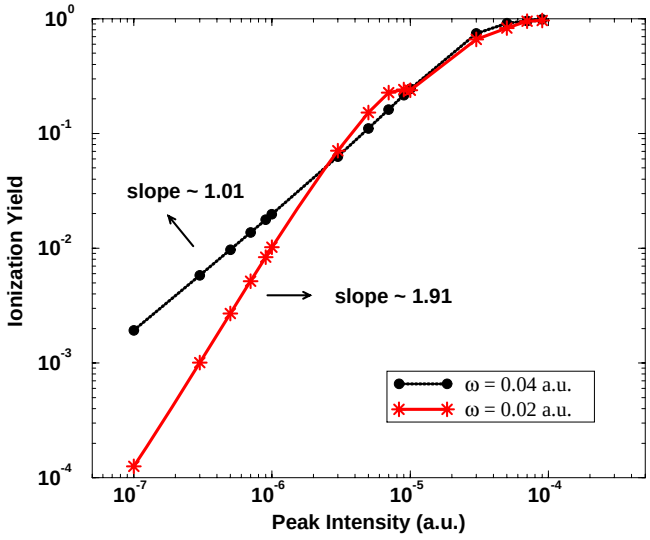

Figure 5.1: Ionization yields for photon energies $\omega = 0.02$ a.u. (0.54 eV) and $\omega = 0.04$ a.u. (1.17 eV). Pulse duration 10 optical cycles and R = 1000 a.u..

Ionization yields and photoelectron energy spectra have been calculated for three photon frequencies and for various pulse durations.

In Fig.5.1, ionization yields, as a function of the peak intensity (I_0) of the pulses, are presented for photon energies $\omega = 1.1$ eV (0.04 a.u.) and $\omega = 0.54$ eV (0.02 a.u.). The behavior of the yields in the low intensity limit, follows the LOPT as it should. Thus for $\omega = 1.1$ eV the yield is proportional to the peak intensity (yield $\sim I_0$) in accordance with LOPT for the rate (W_1) of one-photon detachment ($W_1 = \hat{\sigma}_1 I$, with $\hat{\sigma_1}$ being the usual one-photon cross section). In an analogous fashion, the yield for $\omega = 0.54$ eV has the expected intensity dependence ($\sim I_0^{1.9}$), since for this photon frequency the lowest-order photodetachment channel (and the dominant one), within LOPT corresponds to two-photon absorption. The slight deviations of the yields, from the LOPT power dependence with increasing intensity ($\hat{\sigma}_1 I_0$ for $\omega = 1.1$ eV and $\hat{\sigma}_2 I_0^2$ for $\omega = 0.54$ eV , where $\hat{\sigma_2}$ is the generalized two-photon cross section), are connected with the breakdown of LOPT due to ac-stark shifts, higher-order interaction terms and the finiteness of the pulse durations. Note that, for the smaller photon energy $\omega = 0.54$ eV, the deviation from the LOPT prediction is larger from that corresponding to $\omega = 1.1$ eV, which means that the non-perturbative behavior appears sooner as the intensity of the field increases and/or the photon frequency decreases. This is compatible with the dependence of the ponderomotive potential (U_p) on the field parameters ($\sim I_0/\omega^2$). The abrupt decrease of the slope of the yield for $\omega = 0.54$ eV, at the intensity $\sim 2 \times 10^{12} W/cm^2$, is due to this effect (the shifting of the ionization continuum by the ponderomotive potential), as the two-photon channel closes. Finally, the gradual decrease of the slope for each of the photon frequencies implies that saturation of the process has set in.

Turning now to the PES (Fig.5.2) we note the presence of ATI peaks (and their dependence on the peak intensity) as expected from formal theory. For $\omega = 1.1$ eV (Fig. 5.2) and peak intensity ($\sim 1.9 \times 10^{11} W/cm^2$), we find the normal decrease of the consecutive ATI peaks, with increasing photoelectron energy, in agreement with LOPT predictions, which suggests that non-perturbative phenomena are not significant at this intensity. For the higher intensities ($I_0 \sim 9.6 \times 10^{11} W/cm^2$ and $I_0 \sim 1.9 \times 10^{12} W/cm^2$), on the other hand, strong field non-perturbative behavior sets in and is manifested through the rise of the height of the first ATI peak, which approaches the height of the detachment peak. (For the higher intensity the two peaks are equal in height). We have also performed our calculations, for $\omega = 0.82$ eV with pulse duration and shape such that direct comparison to be possible with the very recent calculations by Scrinzi and Piraux

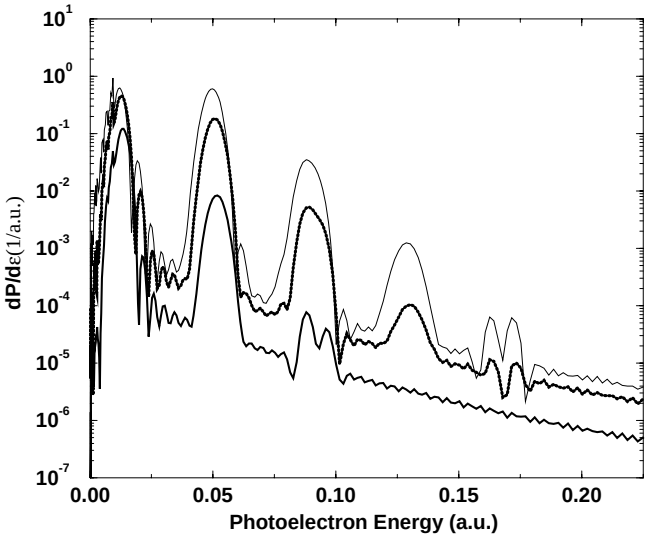

Figure 5.2: Intensity dependence of ATI spectrum for $\omega = 0.04$ a.u.(1.1 eV) Pulse duration 10 optical cycles and R = 1000 a.u. . The relevant intensities (starting from the lower graph) are $10^{-6}, 5 \times 10^{-6}$ and 10^{-5} a.u. .

[75]. In addition, we have spanned in our calculations a broader range of intensities extending from the perturbative regime ($\sim 10^{10} W/cm^2$) up to ($\sim 10^{13} W/cm^2$). In Fig.5.3 we present our results together with those of Scrinzi and Piraux, transformed in log-log plot. For peak intensities in the range of $(7 - 16) \times 10^{11} W/cm^2$, their results are in good agreement with ours. There is, however, an appreciable discrepancy, which increases with the duration of the pulse, for higher intensities. Their calculations, in comparison to ours, predict lower ionization yield for all cases, a discrepancy that increases with increasing the peak intensity. Note that the power dependence of our yield in the low intensity limit is proportional to the field intensity (yield $\sim I$) with high accuracy. Although, the one-photon channel closes for intensities at about $\sim 10^{12} W/cm^2$ no appreciable bend appears to the yield curves. The gradual change of slope is mainly due to saturation which seems to mask whatever effect the channel closing might have.

This behavior also reflects a disagreement with the results of Scrinzi and Piraux, without at this stage having a definitive reason to argue in favor of one or the other, or for that matter the results based on R-matrix Flo-

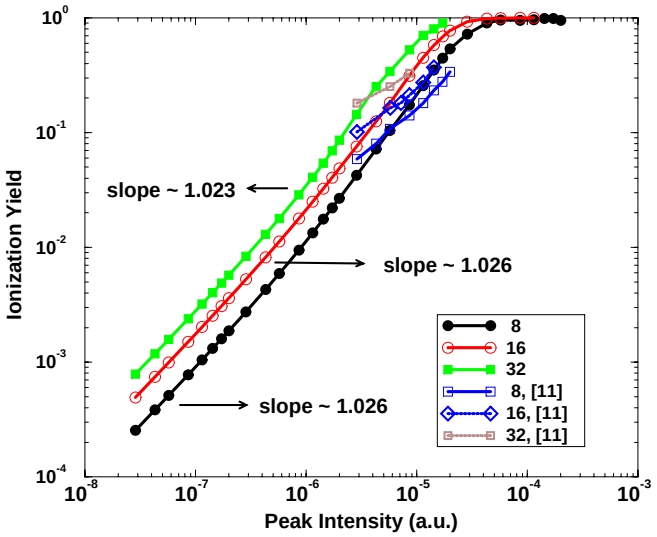

Figure 5.3: Ionization yields for photon energy $\omega = 0.03$ a.u. (0.82 eV) for various pulse durations. The numbers indicated inside the legend frame show the duration of the pulses in optical cycles. R = 1000 a.u. . Related results, taken from [75], are also plotted for comparison.

quet [66, 26] with which direct comparison is a bit problematic due to the time-independent nature of that method. One encouraging aspect of our results is the correcteness of the slopes in Fig. 5.1 and Fig. 5.3. We return now to PES for various peak intensities in one graph (Fig. 5.4), illustrating the dynamical rise of the height of the ATI peaks and their energy shifting, with increasing the intensity. The substructure on the side of the ATI peaks particularly evident at one intensity must correspond to the interference between photoelectron signal amplitude of equal energy generated symmetrically before and after the peak of the pulse. This effect was first predicted in a model calculation some time ago [3] and it has since been noticed in quantitative calculation in atomic hydrogen [17] as well at helium [90]. Its magnitude depends on an intricate interplay between intensity and pulse duration and it would require quite high photoelectron energy resolution to be detectable. In any case, its appearance in the PES of H^- provides a rather clear cut documentation, since in atoms there is always the possibility of additional complications due to structures originating from excited atomic

states which are totally absent here.

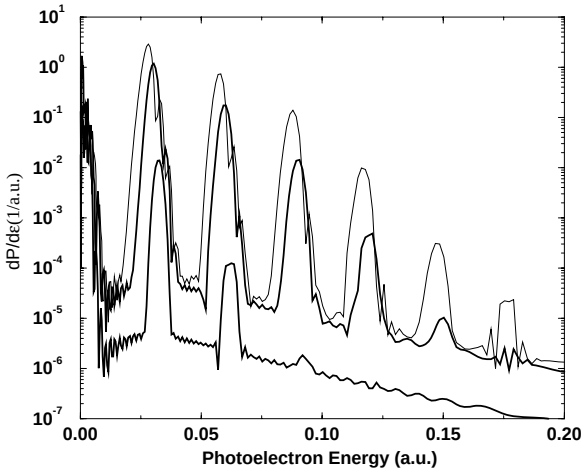

Figure 5.4: Intensity dependence of ATI spectrum for $\omega = 0.03$ a.u.(0.82 eV). Pulse duration 16 optical cycles and R = 1000 a.u. The relevant intensities (starting from the lower graph) are 0.427×10^{-6}, 0.57×10^{-5} and 1.14×10^{-5} a.u. .

An unusual feature appears in the spectra for the photon energy $\omega = 1.1$ eV, in the form of a splitting in the last peak for each intensity (Fig. 5.2). With increasing intensity it gradually disappears, while the energy separation of the two subpeaks is practically independent of the peak intensity. After detailed testing, we attribute it to the steep rise of the $s \rightarrow p$ transition matrix element as a function of energy (due to Wigner's threshold law [85]), in combination with the rise and fall of the pulse which is tracked by the ponderomotive potential. Specifically, for $\omega = 1.1$ eV the photon energy reaches the low energy wing of the $s \rightarrow p$ wave transition matrix element. As the pulse rises in time, the ponderomotive potential pushes the peak of the transition away which results to a drop of the detachment rate. If the pulse rises sufficiently fast, its intensity eventually more than makes up for the decreasing matrix element and the signal increases again up to the point where the pulse reaches its peak. A minimum is reached in between. The photoelectron energy shape is of course retraced as the pulse falls. The magnitude and hence the visibility of the effect depends on how steeply the matrix element changes with energy, in relation to how sharply the pulse rises (falls) in time. It appears at the higher order photoelectron

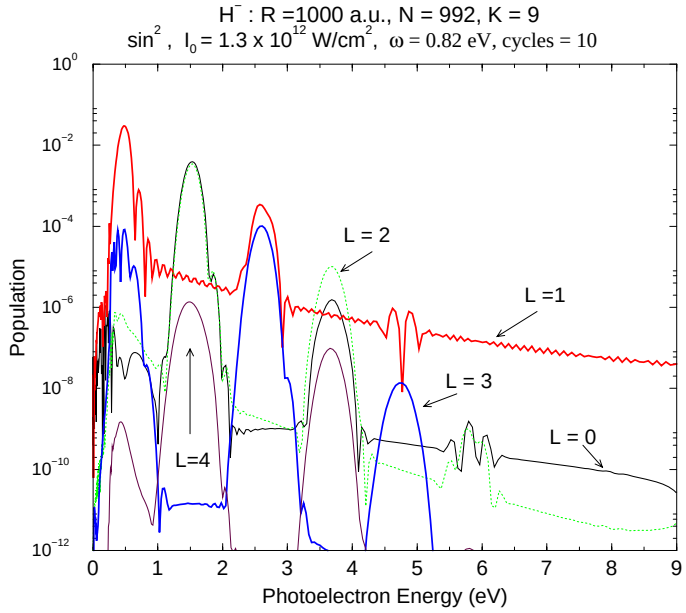

Figure 5.5: Population of the partial waves.

peaks because there the signal rises (falls) faster due to the higher order of non-linearity. Consistently with this picture, its magnitude decreases with increasing the peak intensity (at constant pulse duration) or increasing the pulse duration (at constant peak intensity); at least for the pulse-shape we have considered. It is more pronounced (in the overall signal) at peaks of odd order because its origin is connected with the $s \rightarrow p$-wave transition, but is present in the signal of all partial waves to a lesser degree, as it should. Finally, it should be totally absent for photon energies corresponding to a smoothly varying energy range of the matrix element; and it is. It must be stressed that the effect is very different from the one predicted in [3] some years ago.

5.4 Strong atom-field interaction features

Yield, PES and ionization rates. Perturbation theory gives the ionization rate of a N-photon process as a product of the cross section $\hat{\sigma}_N$ and the Nth power of the intensity of the field (see equation 3.1), $W^{(N)} = \hat{\sigma}_N I^N$. However, this relation is valid when no significant amount of ionization or

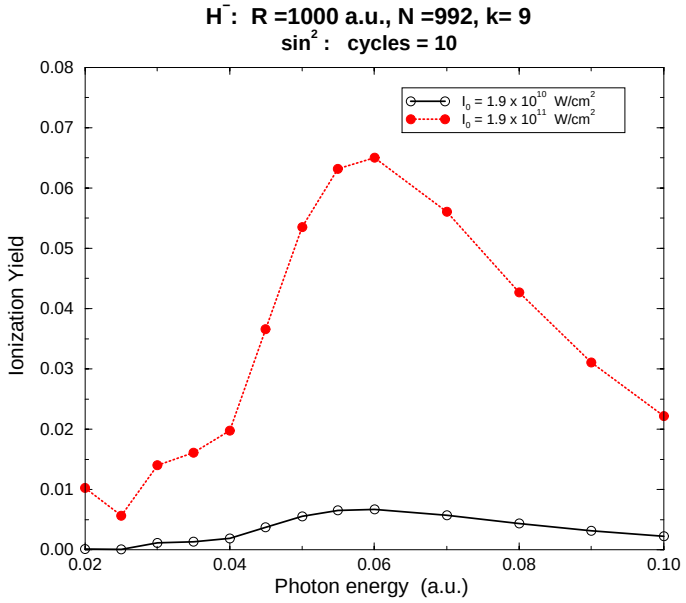

Figure 5.6: Ionization yield versus photon frequency.

excitation takes place during the rise of the pulse. Calculations of "weak"-field ionization which assume the intensity of the pulse constant (square pulse) are in good agreement with most of the available experimental data. On the other hand, non-perturbative time-dependent methods have inherent in their formalism the time-dependence nature of the laser field and a direct comparison with strong-field experiments (where the laser field has a pulsed shape) is possible. Nevertheless, in the limit of low intensities the results of the time-dependent methods, should be comparable with results obtained by perturbative approaches.

Defining an effective time τ_e^N corresponding to the duration of the laser pulse, a direct comparison is possible for the probability of ionization. From the rate ionization $W^{(N)}$, according to perturbation theory and for finite-time pulses we obtain the probability of N-photon ionization P_N, [48, 14]:

$$P_N = 1 - e^{\int_{-\infty}^{+\infty} dt \hat{\sigma}_N (I/\omega)^N} \tag{5.12}$$

The intensity dependence of a laser pulse is modelled as $I(t) = f(t)I_0$, with $f(t)$ the "profile" of the pulse with maximum value the unity and I_0 being the peak intensity of the pulse. Defining the effective time τ_e^N of the process as

$I_0 = 0.54 \times 10^{-6}$ a.u., cycles =10				
ω (a.u.)	P (eq.5.11)	P_1(eq.5.12)	P_2 (eq.5.12)	$P_1 + P_2$
0.03	0.0014	0.00134	0.00083	0.00217
0.04	0.00198	0.00188	0.00019	0.00207

Table 5.1: Perturbative and TDSE results for $\omega = 0.03, 0.04$ a.u. are compared.

$\tau_e^N \equiv \int_{-\infty}^{\infty} dt f^N(t)$, the probability of ionization, using equation (??), reads: $P_N = 1 - exp\left[-\hat{\sigma}_N(I_0/\omega)\tau_e^N\right]$ This formula is directly comparable with the ionization yield, obtained by the non-perturbative time-dependent methods in the low intensity limit. From the perturbative calculations, presented in a previous section, (see figures 3.3 3.6) we compute the relevant one- two and three-photon cross sections. In table (5.4) we present results obtained by the TDSE and LOPT method. Finally, for lower intensities, it is expected the rise of the nth-ATI peak to follow the perturbative predictions, namely nth-ATI peak $\sim I_0^n, n = 1, 2, ...$ In Fig.5.7, for photon energy $\hbar\omega = 0.82eV$ we plot this rising with the peak intensity for the first three ATI-peaks of the process. No surprises happen since the results gives, 1st-ATI peak $\sim I_0^{1.1}$ 2nd-ATI peak $\sim I_0^{1.9}$ and 3rd-ATI peak $\sim I_0^{2.9}$.

Pulse duration effects. Shortness of the laser pulse is essential, for the production strong fields (notice that $I \equiv \Delta E/\Delta S\Delta t$). Furthemore, short pulses give rise to new experimental approaches for the study of laser-atom dynamics.

An electron, ionized by a short laser pulse, is not accelerated by the ponderomotive potential since the field vanishes before the electron escapes from the focal region. Therefore the PES is not overwhelmed from this ponderomotive acceleration, thus detecting experimentally as photoelectron energy the energy at the instant of ionization. Therefore, an experiment with short laser pulses demonstrates the intensity dependence of the ionization probability in a direct way, making comparison with theoretical calculations straightforward.. It is well known, that a finite in time laser pulse is constituted by an infinite number of frequency modes of magnitude determined through the Fourier transform of the field. Roughly, the widths of $E(t)$ and $E(\omega)$ are governed by the relation $\Delta t\Delta\omega \sim 1/2\pi$. In the PES, this bandwidth nature of the field appears as a broadening (of order $\Delta\omega$) of the ATI peaks. For field strictly monochromatic the ATI peaks in the PES have a delta-function peak at the energies equal an integer multiple of the photon

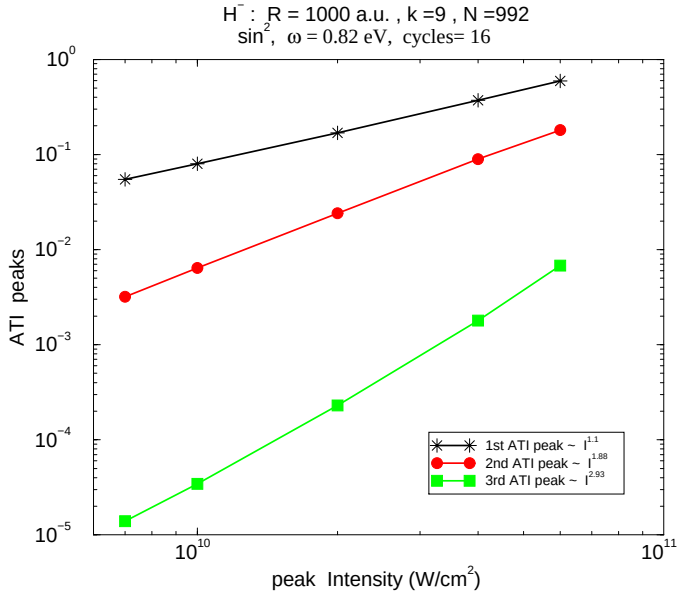

Figure 5.7: Intensity dependence of ATI peaks.

energy minus the binding energy (ignoring AC-Stark shifts and enhanced intermediated resonances which complicates the spectrum). In Fig.5.8 we present such calculations involving pulses that differs only in the duration time. It is obvious, the connection of the pulse duration (or equivalently the frequency bandwidth) of the pulse with the broadening of the ATI peaks. Notice also, the relevant position of the background signal (ionization yield) thus tending to the delta-function behavior of the PES. We also see, that the higher in height ATI peak corresponds to the longer pulse. This is reasonable, since the offered E/M energy is increased with increasing the pulse duration.

AC-Stark shift and channel closing. For weak fields, making a perturbative expansion of the binding energy gives [26]:

$$E_g(\omega, I) = E_g(0) - \frac{E_g^2(0)}{4}\left[\alpha(\omega) + \frac{1}{\omega^2}\right] \tag{5.13}$$

where $\alpha(\omega)$ is the dynamic polarizability[1]. The interaction of the field with

[1] The dynamic polarizability of an atomic state $|n\rangle$ in an electric field of amplitude E is obtained by $\alpha(\omega, n) = -\frac{1}{E}\partial S_n/\partial E$, where S_n is the level shift of the atomic states due to its interaction with the field [79].

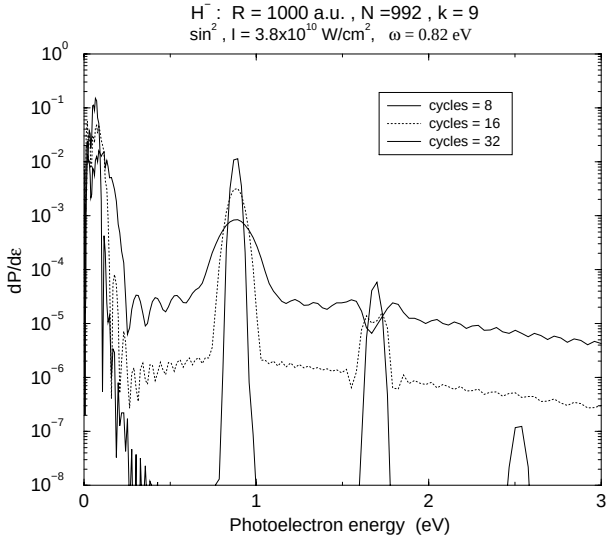

Figure 5.8: ATI peaks and pulse duration.

the atom, shifts the unperturbed energy of the atomic states. The first-order correction is constituted by two terms, the AC-Stark shift S_g and the ponderomotive potential $E_p = E_0^2/4\omega^2$. In general, the AC-Stark shift of an atomic state $|n\rangle$ interacting with a field of amplitude E_0 is given by [49]:

$$S_n = -\frac{E_0^2}{4}a(\omega, n) = -\frac{E_0^2}{4}\sum_i 2\omega_{in}\frac{|\langle n|\varepsilon\mathbf{r}|i\rangle|^2}{\omega_{in}^2 - \omega^2} \tag{5.14}$$

The ponderomotive shift is obtained as the limit of the $S_n(\omega \gg \omega_n)$, which is valid for high Rydberg states. For low frequencies the ponderomotive shift is the dominant one. In Fig.5.4 we present the dynamic polarizability of H^- as a function of the photon energy. This intensity-dependent shift (which is also signature of a non-perturbative behavior process) gives rise to an interesting phenomenon, namely, the "channel closure". Consider an ionization process with minimum number of required photons N, when the atom is unperturbed. Then, neglecting the AC-Stark shift, the first ATI peak is at photoelectron energy $E_e = N\hbar\omega - E_g(0)$. The ionization threshold, when the atom interacts with the field, moves upward. Eventually, with increasing intensity the ionization threshold will exceed the quantity $N\hbar\omega$, thus making ionization by a N-photon process impossible. The critical intensity

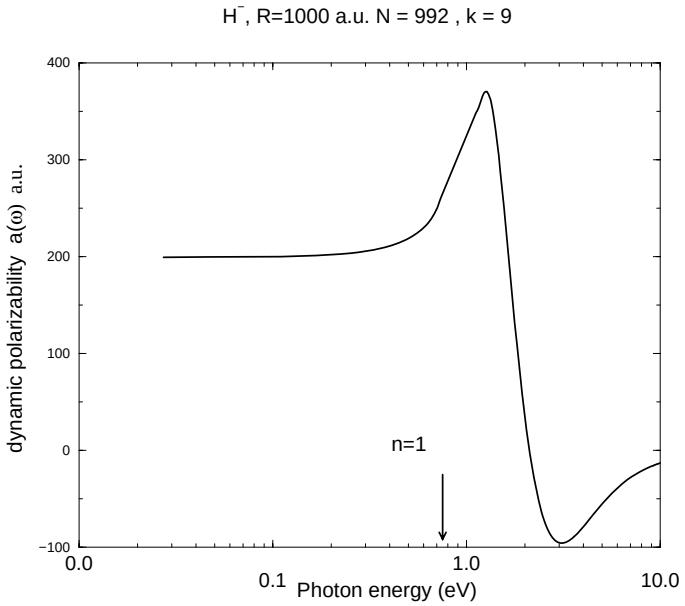

Figure 5.9: Dynamic polarizability.

I_{cr} where the N-photon channel closes, is given by the equation:

$$I_{cr} = 4\frac{E_g(0) - N\hbar\omega}{\alpha(\omega) + \frac{1}{\omega^2}} \tag{5.15}$$

5.5 Yukawa model potential and TDSE

This section is devoted to the minimal presentation of some results as a side part of the main project. We present the figures without a detail discussion on them. PES and yields have obtained with a model potential method. The potential used is the well-know Yukawa potential, mentioned in the first chapter of this Thesis. Figures are self-explanatory, since they include all the necessary information. A direct comparison of the The basic phenomena of non-perturbative process are also apparent in those figures.

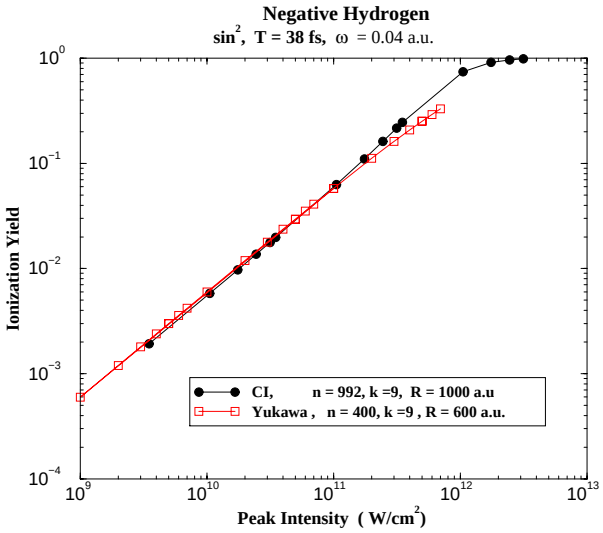

Figure 5.10: Ionization yield obtained using a CI method and the Yukawa model potential.

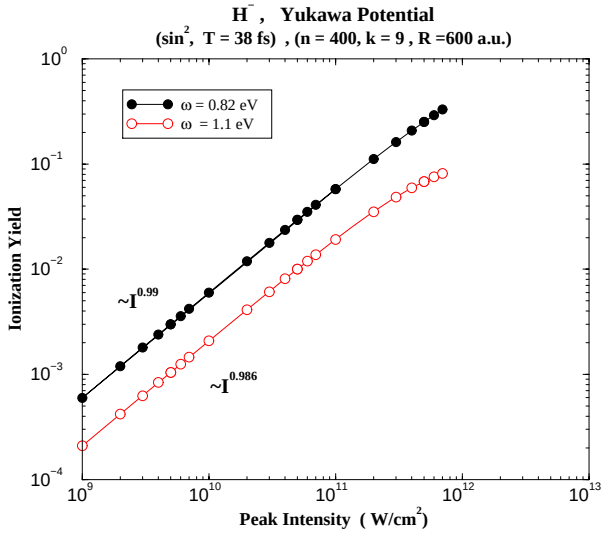

Figure 5.11: Ionization yield for two different photon energies obtained with the Yukawa model potential.

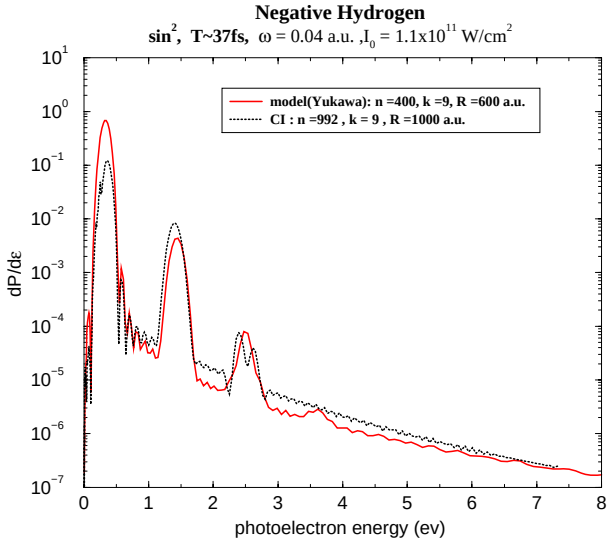

Figure 5.12: PES obtained with a CI method and the Yukawa model potential.

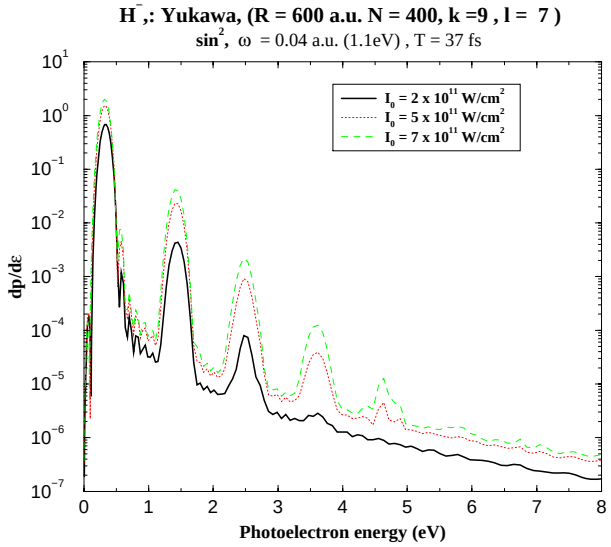

Figure 5.13: PES as a function of the peak intensity. The Yukawa model potential has been used for the atomic structure of H^-.

Conclusion

In summary, we have an elaborate picture of the strong-field behavior of a fundamental and rather unique two-electron system. Our results are very much within the scope of recent experimental activity [92, 80] providing at the same time predictions for the next phase of such experimental studies that could for the first time address the strong-field behavior of this system. The comparison of our results with other studies, on some aspects that have also been addressed by other authors, and the existence of non-trivial differences between different theoretical predictions point to a certain theoretical maturing of the problem, which in coordination with proven experimental possibilities may for the first time provide the stage for truly quantitative insights into one of the most elusive and yet very fundamental settings of strong field atomic behavior.

List of Figures

List of Tables

Bibliography

[1] H.H. Andersen, P. Balling, P.Kristensen, U.V. Pedersen, S.A. Aseyev, V.V. Petrunin, and T. Andersen. Positions and isotope shifts of the $h^-(^1p^0)$ dipole resonances below the $h(n = 2)$ theshold. *Phys. Rev. Lett.*, 79:4770, 1997.

[2] P. Balling, P. Krinstensen, H.H. Andersen, U.V. Petrunin, L. Prastegaard, H.K. Haugen, and T. Andersen. Vacuum ultraviolet spectroscopy of h^- in a heavy ion storage ring: The region near the h(n=2) threshold. *Phys. Rev. Lett.*, 77:2905, 1996.

[3] J.N. Bardsley, A. Szöke, and M. J. Comella. Multiphoton ionization from a short-range potential by short-pulse lasers. *J. Phys. B*, 21:3899, 1988.

[4] M. Bashkansky, P.H. Bucksbaum, and D.W. Schumacher. Asymmetries in above-threshold ionization. *Phys. Rev. Lett.*, 60:2458, 1988.

[5] Tomas Brage, Charlotte Froese Fischer, and Gregory Miecznick. Nonvariatonal, spline-galerkin calculations of resonance positions widths and photodetachment cross sections for h^- and he. *J. Phys. B*, 25:5289, 1992.

[6] B.H. Bransden and C.J. Joachain. *Physics of atoms and molecules.* Longman Scientific & Technical, 1983.

[7] J.T. Broad and W.P. Reinhardt. *Phys. Rev. A*, 14:2159, 1976.

[8] A. Burgess. The deternination of phases and amplitudes of wave functions. *Proc. Phys. Soc.*, 81:442, 1963.

[9] T.N. Chang. *Many-body theory of Atomic Structure*, chapter B-spline based Configuration-Interaction Approach for Photoionization of Two-electron and Divalent Atoms. World Scientific, Singapore, 1993.

[10] T.N. Chang. Widths of the doubly excited resonances of the two-electron atoms below the n=2 threshold. *Phys. Rev. A*, 47:705, 1993.

[11] T.N. Chang and Y.S. Kim. Theoretical study of the two-electron interaction in alkaline-earth atoms. *Phys. Rev. A*, 34:2609, 1986.

[12] T.N. Chang and X. Tang. Photoionization of two-electron atoms using a nonvariatonal configuration interaction approach with discretized finite basis. *Phys. Rev. A*, 44:232–238, 1991.

[13] T.N. Chang and X. Tang. Atomic-structure effects in multiphoton ionization of magnesium. *Phys. Rev. A*, 46:R2209–2212, 1992.

[14] D. Charalambidis, D. Xenakis, C.J.G.J. Uiterwaal, P. Maragakis, Jian Zhang, H. Schröder, O Faucher, and P. Lambropoulos. Multiphoton ionization saturation intensities and generalized cross sections from ati spectra. *J. Phys. B*, 30:1467–1479, 1997.

[15] L.A. Collins and A.L. Merts. Multiphoton detachment of negative ions in an intense radiation field. *Phys. Rev. A*, 45:6615, 1992.

[16] E. Cormier and P. Lambropoulos. Extrapolation method for the evaluation of above threshold ionization cross sections for the one- and two-electron systems. *J. Phys. B*, 28:5043–5055, 1995.

[17] E. Cormier and P. Lambropoulos. Optimal gauge and gauge invariance in non-prturbative time-dependent calculation of above-threshold ionization. *J. Phys. B*, 29:1667–1680, 1996.

[18] E. Cormier and P. Lambropoulos. Above-threshold ionization spectrum of hydrogen using b-spline functions. *J. Phys. B*, 30:77–91, 1997.

[19] M. Cortés and F.Martin. Photodetachment of h^- with excitation to h(n=2). *Phys. Rev. A*, 48:1227, 1993.

[20] R.D. Cowan. *The Theory of Atomic Structure.* Univ. of California Press, 1981.

[21] Michéle Crance. Multiphoton detachment from negative ions of halogens, angular distributions and excess photon absorption. *J. Phys. B*, 21:3559–3569, 1988.

[22] Martin Dörr, R.M. Potvliege, Daniel Proulx, and Robin Shakeshaft. Multiphoton detachment of H^- and the applicability of the Keldysh approximation. *Phys. Rev. A*, 42:4138, 1990.

[23] Carl de Boor. *A Practical Guide to Splines.* Springer and New York, 1978.

[24] Piero Decleva, Adriana Lisini, and Marco Venuti. Accurate ci expansion in a spline basis of the helium ground-state wave function. *Int. J. Quantum Chem.*, 56:27, 1995.

[25] Hugo W.van der Hart. Partial and total multiphoton detachment rates for h^- in a perturbative b-spline-based approach. *Phys. Rev. A*, 50:2508–2516, 1994.

[26] M Dòrr, J Purvis, M Terao-Dunseath, P G Burke, C J Joachain, and C J Noble. R-matrix floquet theory of multiphoton processes: V. multiphoton detachment of the negative hydrogen ion. *J. Phys. B*, 28:4481, 1995.

[27] G.W.F Drake and S.P. Goldman. Application of discrete-basis-set methods to the dirac equation. *Phys. Rev. A*, 23:2093, 1981.

[28] A. Chodos et al. *prd*, 9:3471, 1974.

[29] Autler et al. *Phys. Rev.*, 100:703, 1955.

[30] U. Fano. Effects of configuration interaction on intensities and phase shifts. *Phys. Rev.*, 124:1866, 1961.

[31] Charlotee Froese Fischer. *The Hartree-Fock method for atoms.* John Wiley & Sons, Inc, 1977.

[32] Charlotte Froese Fischer and Muhammad Idrees. Spline algorithms for continuum functions. *Computer in Physics*, May/June:53, 1989.

[33] M. Gailitis and R. Damburg. The influence of close coupling on the threshold behaviour of cross sections of electron-hydrogen scattering. *Proc. R. Soc. Lond.*, 82, 1963.

[34] M.L. Goldberger and K.M. Watson. *Collision Thoery.* Wiley, New York, 1964.

[35] I.P. Grant. Relativistic atomic structure calculations. *Comp. Phys. Comm.*, 17:149, 1979.

[36] R. Grobe and J.H. Eberly. Observation of coherence transfer by electron-electron correlation. *Phys. Rev. A*, 48:623, 1993.

[37] R. Grobe and S.L. Haan. *J. Phys. B*, 27:L735, 1994.

[38] Lars G. Hanson and P. Lambropoulos. Nondispersing wave packets in two-electron atoms: Atomic mode locking by loss modulation. *Phys. Rev. Lett.*, 74:5009, 1995.

[39] Lars G. Hanson, Jian Zhang, and P. Lambropoulos. Comment on "observation of continuum-continuum autler-townes splitting. *Phys. Rev. Lett.*, 77:202, 1996.

[40] Lars G. Hanson, Jian Zhang, and P. Lambropoulos. Manifestations of atomic and core resonances in photoelectron energy spectra. *Phys. Rev. A*, 55:2232, 1997.

[41] Y.K. Ho and A.K. Bathia. *Phys. Rev. A*, 48:3720, 1993.

[42] E.A. Hylleraas and B. Undheim. *Z. Phys.*, 65:759, 1930.

[43] W.R. Johnson, S.A. Blundell, and J. Sapirstein. Finite basis sets for the dirac equation constructed from b-splines. *Phys. Rev. A*, 37:307, 1988.

[44] W.R. Johnson, D.S. Guo, M. Idrees, and J. Sapirstein. Weak-interaction effects in heavy atomic systems. *Phys. Rev. A*, 32:2093, 1985.

[45] M. Yu. Kuchiev and V.N. Ostrovsky. Electron detachment from negative ions in bichromatic laser field. *J. Phys. B*, 31:2525–2538, 1998.

[46] Kenneth C. Kulander, Kenneth J. Schafer, and Jeffrey L. Krause. Time-dependent studies of multiphoton processes. Academic Press, Inc, 1992.

[47] P. Lambropoulos. Effect of light polarization on multiphoton ionization of atoms. *Phys. Rev. Lett.*, 28:585, 1972.

[48] P. Lambropoulos. Topics on multiphoton processes. *Adv. At. Mol. Phys.*, 12:67, 1976.

[49] P. Lambropoulos, P. Maragakis, and Jian Zhang. Two-electron atoms in strong fields. *Physics Report*, 305:203, 1998.

[50] P. Lambropoulos and X. Tang. Comment on "asymmetries in above-threshold ionization". *Phys. Rev. Lett.*, 61:2506, 1988.

[51] P. Lambropoulos and P. Zoller. Autoionizing states in strong laser fields. *Phys. Rev. A*, 24:379, 1981.

[52] Cecil Laughlin and Shih-I Chu. Multiphoton detachment of h^-. *Phys. Rev. A*, 48:4654, 1993.

[53] C. Lauglin and G.A. Victor. Model-potential methods. *Adv. At. Mol. Opt. Phys.*, 25(163), 1988.

[54] E. Lindroth. Photodetachment of H^- and Li^-. *Phys. Rev. A*, 52:2737, 1995.

[55] E. Lindroth, A. Bürgers, and N.Brandefelt. Relativistic effects on the H^- resonances converging to the $H(n = 2)$ threshold. *Phys. Rev. A*, 57:R685, 1998.

[56] Chih-Ray Liu, Bo Gao, and Anthony F. Starace. Variatonally stable treatment of two- and three-photon detachment of H^- including electron-correlation effects. *Phys. Rev. A*, 46:5985, 1992.

[57] D.W. MacArthur. unknown. *Phys. Rev. A*, 32:1921, 1985.

[58] Jacek Migdalek and Yong ki Kim. Core polarization and oscillator strength ratio anomaly in potassium, rubidium and caesium. *J. Phys. B*, 31:1927, 1998.

[59] C.E. Moore. Atomic energy levels. *Natl. Bur. Stand. Ref. Data Ser., Natl. Bur.Stand. (US. GPO, Washington D.C.)*, VII(35), 1971.

[60] H.G. Muller, G. Petite, and P. Agostini. unknown. *Phys. Rev. Lett.*, 61:2507, 1988.

[61] L. A. A. Nikolopoulos and P. Lambropoulos. Above-threshold Ionization of negative hydrogen. *Phys. Rev. A*, 56:3106–3115, 1997.

[62] David W. Norcross. Photoabsorption by cesium. *Phys. Rev. A*, 7:606, 1973.

[63] C.L. Pekeris. $1.^1S, 2.^1S$ and $2.^3S$ state of H^- and of He. *Phys. Rev.*, 126:1470, 1962.

[64] Daniel Proulx, Marcel Pont, and Robin Shakeshaft.
Multiphoton detachment, ionization, and simultaneous excitation of two-electron systems. *Phys. Rev. A*, 49:1208, 1994.

[65] Daniel Proulx and Robin Shakeshaft. Two- and three-photon detachment of H^- by a weak field. *Phys. Rev. A*, 46:R2221, 1992.

[66] J. Purvis, M. Dörr, M.Terao-Dunseath, C.J. Joachain, P.G. Burke, and C.J. Noble. Multiphoton ionization of h^- and he in intense laser fields. *Phys. Rev. Lett.*, 24:3943, 1993.

[67] William P. Reinhardt. L^2 discretization of atomic and molecular continua: moment, quadrature, and j-matrix techniques. *Comp. Phys. Comm.*, 17(1), 1979.

[68] J.J. Sakurai. *Advanced Quantum Mechanics*. Addison-Wesley Publishing Company Inc, 1967.

[69] J.J. Sakurai. *Modern Quantum Mechanics*. Addison-Wesley Publishing Company Inc, 1994.

[70] I Sánchez, H Bachau, and F Martin. Electron angular distribution in above-threshold two-photon detachment of h^-. *J. Phys. B*, 30:2417, 1997.

[71] I Sánchez, H Bachau, and F Martin. Asymmetry parameters in two-photon detachment of h^- below 1 ev. *J. Phys. B*, 49:2863, 1998.

[72] I. Sánchez, F. Martin, and H. Bachau. *J. Phys. B*, 28:2863–2873, 1995.

[73] J. Sapirstein and W.R. Johnson. Use of b-splines in theoretical atomic physics. *J. Phys. B*, 29:5213–5225, 1996.

[74] Armin Scrinzi and Bernard Piraux. Ionization and double excitation of helium by short intense laser pulses. *Phys. Rev. A*, 56:R13, 1997.

[75] Armin Scrinzi and Bernard Piraux. Two-electron atoms in short intense laser pulses. *Phys. Rev. A*, 58:1310, 1998.

[76] L.N. Shabanova and A.N. Khlyustalov. *Opt. Spectrosk.(USSR)*, (54):123, 1984.

[77] Robin Shakeshaft and X.Tang. Integral-equation approach to multiphoton ionization by intense fields. II. Application to H and H^-. *Phys. Rev. A*, 36:3193, 1987.

[78] Bruce W. Shore. Use of boundary-condition wavefunctions for bound states, continuum states, and resonances. *J. Phys. B*, 7:2502, 1974.

[79] I.I. Sobel'man. *Introduction to the theory of atomic spectra*. Pergamon Press Ltd, 1972.

[80] L. Præstegaard, T. Andersen, and P. Balling. *Phys. Rev. A*, Rapid communications, to be published, 1999.

[81] A. Stintz, Xin Miao Zhao, Charlie E.M. Strauss, W.B. Ingalls, G.A. Kyrala, David J. Funk, and H.C. Bryant. Resonant two-photon detachment through the lowest singlet d state in h^-. *Phys. Rev. Lett.*, 75:2924, 1995.

[82] X. Tang, T.N. Chang, P. Lambropoulos, S. Fournier, and L.F. DiMauro. Multiphoton ionization of magnesium with configuration-interaction calculations. *Phys. Rev. A*, R41:5265, 1990.

[83] Dmitry Telnov and Shih-I Chu. Electron angular distribution after above-threshold multiphoton detachment of h^- by 1064 nm radiation. *J. Phys. B*, 29:4401, 1996.

[84] T.N. Chang and Rong-qi Wang. Effect of positive-energy orbitals on the configuration interaction calculation of the h^- atom. *Phys. Rev. A*, 43:1218, 1991.

[85] M. Venuti and P. Decleva. Convergent multichannel continuum states by a general configuration interaction expansion in a b-spline basis: application to h^- photodetachment. *J. Phys. B*, 30:4839, 1997.

[86] Barry Walker, M. Kaluza, B.Sheehy, P. Agostini, and L.F. DiMauro. Observation of continuum-continuum autler-townes splitting. *Phys. Rev. Lett.*, 75:623, 1995.

[87] C.N. Yang. *Phys. Rev.*, 74:764, 1948.

[88] Wolfanng Zernik. Two-photon ionization of atomic hydrogen. *Phys. Rev.*, 135:A51, 1964.

[89] Jian Zhang and P. Lambropoulos. *Journal of Nonlinear Optical Physics and Materials*, 4:633, 1995.

[90] Jian Zhang and P. Lambropoulos. Non-perturbative time-dependent theory and ati in two-electron atoms. *J. Phys. B*, 28:L101, 1995.

[91] Jian Zhang and P. Lambropoulos. Time-dependent calculation of photoelectron spectra in mg involving multiple continua. *Phys. Rev. Lett.*, 77:2186, 1996.

[92] Xin Miao Zhao, M.S. Gulley, H.C. Bryant, Charlie E.M. Strauss, David J. Funk, A. Stintz, D.C. Rislove, G.A. Kyrala, W.B. Ingalls, and W.A. Miller. Nonresonant excess photon detachment of negative hydrogen ions. *Phys. Rev. Lett.*, 78:1656, 1997.